UNIVERSIDADE ESTADUAL DE CAMPINAS
Faculdade de Engenharia Química

Samuel Vitor Saraiva

Demulsifier dosage control in water-in-oil emulsion based on ultrasonic measurements

Controle de dosagem de desemulsificante em emulsão água em óleo baseado em medições ultrassônicas

Campinas
2024

Samuel Vitor Saraiva

Demulsifier dosage control in water-in-oil emulsion based on ultrasonic measurements

Controle de dosagem de desemulsificante em emulsão água em óleo baseado em medições ultrassônicas

Tese apresentada à Faculdade de Engenharia Química da Universidade Estadual de Campinas como parte dos requisitos para a obtenção do título de Doutor em Engenharia Química.

Thesis presented to the School of Chemical Engineering of the University of Campinas in partial fulfillment of the requirements for the degree of Doctor in Chemical Engineering.

Supervisor/Orientador: Prof. Dr. Flávio Vasconcelos da Silva

Este trabalho corresponde à versão final da Tese defendida por Samuel Vitor Saraiva e orientada pelo Prof. Dr. Flávio Vasconcelos da Silva.

Campinas
2024

Ficha catalográfica
Universidade Estadual de Campinas
Biblioteca da Área de Engenharia e Arquitetura
Rose Meire da Silva - CRB 8/5974

Saraiva, Samuel Vitor, 1994-
Sa71d Demulsifier dosage control in water-in-oil emulsion based on ultrasound measurements / Samuel Vitor Saraiva. – Campinas, SP : [s.n.], 2024.

Orientador: Flávio Vasconcelos da Silva.
Tese (doutorado) – Universidade Estadual de Campinas, Faculdade de Engenharia Química.

1. Controle de processo. 2. Desemulsificantes. 3. Transdutores ultrassonicos. I. Silva, Flávio Vasconcelos da, 1971-. II. Universidade Estadual de Campinas. Faculdade de Engenharia Química. III. Título.

Informações Complementares

Título em outro idioma: Controle de dosagem de desemulsificante em emulsão água-em-óleo baseado em medições ultrassônicas
Palavras-chave em inglês:
Process control
Demulsifier
Ultrasound transducers
Área de concentração: Engenharia Química
Titulação: Doutor em Engenharia Química
Banca examinadora:
Flávio Vasconcelos da Silva [Orientador]
Mauricio de Melo Freire Figueredo
José Henrique Araújo Lopes de Andrade
Thiago Vaz da Costa
Natan Augusto Vieira Bulgarelli
Data de defesa: 04-04-2024
Programa de Pós-Graduação: Engenharia Química

Identificação e informações acadêmicas do(a) aluno(a)
- ORCID do autor: https://orcid.org/0000-0002-4424-7668
- Currículo Lattes do autor: http://lattes.cnpq.br/4412620646554775

Folha de Aprovação da Defesa de Tese de Doutorado defendida por ***SAMUEL VITOR SARAIVA*** e aprovada em 04 de abril de 2024 pela Comissão Examinadora constituída pelos doutores:

Prof. Dr. Flávio Vasconcelos da Silva
Presidente e Orientador
FEQ/UNICAMP

Prof. Dr. José Henrique Araújo Lopes de Andrade
Universidade Federal de Alagoas - Campus Arapiraca

Prof. Dr. Thiago Vaz da Costa
Universidade Federal de Uberlândia - UFU
Videocoferência

Dr. Mauricio de Melo Freire Figueiredo
Universidade Estadual de Campinas

Dr. Natan Augusto Vieira Bulgarelli
Universidade Estadual de Campinas

A Ata da defesa com as respectivas assinaturas dos membros encontra-se no SIGA/Sistema de Fluxo de Dissertação/Tese e na Secretaria do Programa da Unidade.

Happy is the man who finds wisdom and the man who gains understanding. Her proceeds are better than the profits of silver, and her gain is greater than fine gold. She is more precious than rubies, and all the things you may desire cannot compare with her.

(Proverbs 3:13-15)

Aknowledgements

I am grateful to God for giving me the privilege of completing this stage of my professional career. He was always present to guide me through moments of doubt, challenges, and hopelessness.

I want to thank my family for their support, love, and endurance during the time of distance. I especially thank my parents, Raquel and Paulo Saraiva, and my beloved grandmother, Severina da Silva.

I would like to express my gratitude to my supervisors, Flávio Vasconcelos da Silva and Professor Ana Maria Frattini Fileti, for their guidance, friendship, and teaching throughout this work.

To my research colleagues who indirectly or directly contributed to this work, Darlan Bonetti, Carlos Adriano, Diane Otília, Tiago Ferreira, Caio Araújo, Raphael Santana, Felipe Sousa, and Caio Francescato, thank you for sharing your time, challenges, and knowledge with me.

I am also thankful for my friends outside the academic context, including Pockets, Abbacasa, Igreja do Nazareno, and JNI, for their mutual support. I would like to express my gratitude to Professor Frede de Oliveira, my friend and advisor.

I thank my beloved bride, Gabrielle Melo, for years of complicity.

Lastly, I want to acknowledge the financial support of Petróleo Brasileiro S.A. (Petrobras) and the Coordenação de Aperfeiçoamento de Pessoal de Nível Superior - Brazil (CAPES) - Financing Code 001 for their support in completing this work.

Resumo

A emulsificação na indústria de petróleo e gás há muito tempo apresenta desafios técnicos relacionados à garantia de escoamento. Uma vez que a emulsificação ocorre, a demanda de energia no sistema de bombeamento eleva-se devido à alta viscosidade do fluído. Um método para mitigar os efeitos da emulsificação é a adição de desemulsificantes. Esse químico pode ser dosados diretamente no fluxo, especialmente em estágios anteriores à separação de fases em tanques de separação. Quantificar o desemulsificante dosado requer uma avaliação da eficiência da desemulsificação. Adicionar pouco desemulsificante pode não alcançar a eficiência desejada, enquanto a adição excessiva pode levar a um efeito de overdose, além de ser dispendioso. Numerosos estudos na literatura relatam o uso de estratégias de controle de desemulsificação nas fases de separação de petróleo. No entanto, não foram encontradas estratégias de controle para controlar os padrões de escoamento na desemulsificação que ocorre no fluxo.

Nesse sentido, empregar uma estratégia de controle automático para dosar o desemulsificante no fluxo e controlar o padrão de escoamento resultante para garantir um escoamento menos viscoso seria de grande interesse. No entanto, desenvolver um sensor que quantifique/classifique adequadamente o escoamento é necessário para alcançar esse objetivo. Nesse contexto, os sensores ultrassônicos oferecem vantagens sobre outras técnicas de caracterização de emulsões, pois são sensores não intrusivos capazes de analisar amostras concentradas e opacas. Essas características tornam o ultrassom um sensor ideal para aplicação em fluxo. Portanto, este estudo teve como objetivo desenvolver um sensor ultrassônico para caracterizar o fluxo de emulsão e atuar como um classificador de desemulsificação, possibilitando a aplicação de uma estratégia de controle para dosar desemulsificantes automaticamente em linha. A classificação ocorre usando as propriedades acústicas da amostra e aplicando um sistema de controle fuzzy para identificar os padrões de escoamento que ocorrem durante a desemulsificação. Em seguida, a vazão ideal de desemulsificante é calculada e dosada automaticamente na tubulação.

Os principais resultados alcançados podem ser divididos em três pontos. Primeiro, foi possível caracterizar a dinâmica da desemulsificação no escoamento e como variáveis como temperatura, taxa de fluxo, cisalhamento e fração de água a influenciam. Em segundo lugar, observou-se que as propriedades acústicas, como velocidade do som, atenuação e impedância, eram altamente sensíveis a mudanças na morfologia da emulsão que ocorreram com a desemulsificação. Isso foi especialmente sensível quando a desemulsificação se intensificou e a fase segregada pôde ser vista no fluxo. Finalmente, essa sensibilidade permitiu a aplicação de um sistema de controle fuzzy para identificar os padrões de escoamento que ocorrem durante a desemulsificação e dosar o desemulsificante. O controle teve um desempenho adequado no sistema, mantendo o escoamento separado em um padrão de fluxo desejado. Esse controle foi avaliado em um circuito fechado (com recirculação de amostra) e em um circuito aberto.

Abstract

Emulsification in the oil and gas industry has long posed technical challenges concerning flow assurance. Once emulsification occurs, the pumping system's energy demand is elevated due to high viscosity. One method to mitigate emulsification's effects is by adding demulsifiers. These demulsifiers can be dosed directly into the flow, especially in stages preceding phase separation in separation tanks. Quantifying the dosed demulsifier requires assessing the demulsification efficiency. Adding too little demulsifier may not achieve the desired efficiency, while excessive addition may lead to an overdose effect, besides being costly. Numerous studies in the literature report the use of demulsification control strategies in the phases of oil separation. However, no control strategies were found for controlling flow patterns in the demulsification that occurs in the flow.

In this regard, employing an automatic control strategy to dose demulsifier into the flow and control the resulting flow pattern to ensure less viscous flow would be of great interest. However, developing a sensor that adequately quantifies/classifies the flow is necessary to achieve this goal. In this context, ultrasonic sensors offer advantages over other emulsion characterization techniques as they are non-intrusive sensors capable of analyzing concentrated and opaque samples. These characteristics make ultrasound an ideal sensor for flow application. Therefore, this study aimed to develop an ultrasonic sensor to characterize emulsion flow and act as a demulsification classifier, enabling the application of a control strategy to dose demulsifiers in-line automatically. The classification occurs by using the acoustic properties of the flow and applying a fuzzy control system to identify flow patterns occurring during demulsification. Then, the ideal demulsifier flow rate is automatically calculated and dosed in the system.

The main results reached can be split into three points. First, it was possible to characterize the dynamic of the demulsification in the flow and how variables such as temperature, flow rate, shear, and water fraction influence it. Second, it was observed that the acoustic properties, such as sound velocity, attenuation, and impedance, were highly sensitive to changes in emulsion morphology that occurred with the demulsification. This was especially sensitive when the demulsification intensified, and the segregated phase could be seen in the flow. Finally, this sensitivity enabled the application of a Fuzzy control system to identify flow patterns occurring during demulsification and dose the demulsifier. The control had a suitable performance in the system, keeping the flow separated in a desired flow pattern. This control was evaluated in a closed circuit (with sample recirculation) and an open circuit.

List of Figures

List of Tables

Nomenclature

Abbreviations

$argmax$	Function that returns the argument of the signal that has its maximum amplitude
$append$	Function that appends the element of the argument into a vector
max	Function that returns maximum values of the argument
min	Function that returns minimum values of the argument
FFT	Fast Fourier transform
$T - Pulser$	Pulser transducer
$T - Receiver$	Receiver transducer

Greek Symbols

α	Sound attenuation coefficient of the sample [Np/m]
γ	shear rate
ΔP	Pressure drop [Pa]
μ_i	Viscosity (i=emulsion, apparent, oil) [Pa.s]
μ_r	Relative viscosity [-]
μ^*	Complex viscosity
μA_i	Antecedents layer function [-]
ρ_i	The density of the sample i [kg/m^3]
σ_x	Stand deviation of x [-]
$\tau_c ross$	Cross-correlation time [s]
τ_{wall}	shear stress on the pipe wall
ϕ	Water fraction [-]
ϕ_{PIP}	Water fraction in phase inversion point
ω	Angular frequency

Latin Symbols

a	Parameters of the functions [-]
b	Parameters of the functions [-]
c	Parameters of the functions [-]
A_0	Emitter transducer excitation signal [vector]
$A_i^{'}$	Reflected echo with reference sample on the sensor (i=1,2) [-]
$A_1^{*'}$	First reflected echo with reference sample on the sensor [-]
A_i	Reflected echo with sample on the sensor [-]
A_1^*	The first echo received at the receiving transducer [-]
A_1^{air}	First reflected echo without a sample on the sensor [-]
A_{pulser}	Rceiver signal of the pulser transducer [-]
$A_{receiver}$	Rceiver signal of the receiver transducer [-]
$A_{zone:sample}$	Spectrum of the clipping pulser signal [-]
c	Sound speed in the sample [m/s]
c_w	Sound speed in the water at a specific temperature [m/s]
c_o	Sound speed in the oil at a specific temperature [m/s]
c_{rl}	Relative speed of the sound [m/s]
du	Output of the fuzzy system already applied the limits
du^*	Output of the centroid method of defuzzification
du_{min}	Minimum value for du
du_{max}	Maximum value for du
D_i	Diffraction coefficient of sound in the medium i [-]
D	Pipe diameter [m]
f_K	Sample echo frequency
f_m	Experimental friction factor
K	Relative echo amplitude in sample [-]
K_τ	Constant related the shear stress on the pipe wall and shear rate to non-Newtonian behavior
l_i	Length of delay line (i=1,3) and sample line (i=2) [m]
L	Pipe section length [m]
M_{du}	List of the past values of the du [-]
$\bar{M_{du}}$	Mean of the elements of the list M_{du} [-]
n	Number of samples (length of the time series) [-]
p_i	Signal clipping point in time (i=1,2)
R_{12}	Reflection coefficient between media 1 (wall) and 2 (sample) [-]
$R_{12}^{'}$	Reflection coefficient between media 1 (wall) and 2 (water) [-]
r_k	Result of rule implication k [-]
S_{du}	Velocity parameter of the controller
t	Actual time [s]

Latin Symbols, continuation...

t_{-1}	Time of the last action of the controller [s]
t_d	Delay time of the controller [s]
$u[-1]$	Last value of the actuation of the controller in the pump [ml/min]
u	Value of the actuation of the controller in the pump [ml/min]
v	Flow velocity [m/s]
x_c	volumetric fraction of continuous phase
x_d	volumetric fraction of dispersed phase
Z_i	Acoustic impedance in medium i [kg/m^{2}s]

Contents

Chapter 1

Introduction

Emulsions, defined as a metastable mixture of oil and water belonging to a class of colloidal systems, have broad applicability in industry, including their use in pharmaceutical, food, cosmetic, and other areas. The large number of applications of the emulsion in industry is due to its chemical characteristics. The emulsion formation makes it possible to create a homogeneous and kinetically stable mixture with hydrophobic and hydrophilic substances. So that one of these substances is dispersed within the other. Although in most industrial sectors, emulsion formation is desired to improve their products, in oil production in the petroleum industry, this formation is undesirable and costly (KOKAL, 2005).

Emulsions in the petroleum industry are present in all stages of production; their formation comes from the mixture of water and oil during the oil extraction process. The origin of this water can be geological or by injection. Water from geological sources is linked to the environmental circumstances prevailing when oil was formed (ASSUNCAO *et al.*, 2018). Injection origin, in turn, is related to the injection of water/steam into mature wells to improve oil recovery, maintaining pressure in the reservoirs (UMAR *et al.*, 2018). The most common emulsion in petroleum production is water-in-oil, while oil-in-water emulsion is found in the water clarification process (ABDULREDHA *et al.*, 2020).

The formation of emulsions in the oil industry occurs at points of turbulence and extreme mixing of oil with water, generally with salts and natural emulsifiers, such as asphaltenes, naphthenic acids, resins, and other organic compounds (KOKAL; AL-JURAID, 2000). Some of the main points of emulsion formation are present during the extraction of crude oil to the separation tank, including flow through reservoir rocks, lifting, usually by pumps, submerged

lines, valves, and others (UMAR *et al.*, 2018). This formation is unwanted and costly, both in productive and chemical terms (KOKAL, 2005).

In productive terms, for example, forming a kinetically stable emulsion increases the pumped fluid's viscosity. Consequently, the flow pressure drops, thus demanding a greater amount of energy. This fact increases operational costs in addition to causing technical problems regarding equipment sizing. Furthermore, in chemical terms, emulsions, especially oil in water, cause serious corrosion problems due to salts dissolved in the aqueous phase. In this context, there is an intense effort in academia and the oil industry to investigate this problem (ABDULREDHA *et al.*, 2020).

To mitigate the costly effect of emulsion formation, a technique widely employed in industrial practice involves the application of chemical demulsifiers. These chemical agents facilitate the destabilization of emulsions, thereby promoting the segregation of phases and effectively decreasing viscosity and pressure drop within the pipeline (WANG *et al.*, 2021). The efficacy of these agents in emulsion control is contingent upon the precise dosing point, as they can either facilitate emulsion breakdown or prevent its formation altogether.

With the dosage of the demulsifying agent, there will be a decrease in effective viscosity due to the formation of a more polydisperse emulsion or segregated flow, depending on the dosage rate of the chemical agent. It is worth noting that a high dosage rate, besides being economically burdensome, will induce the opposite effect desired, as the demulsifying agent at high dosage levels will act as an emulsifier, stabilizing the emulsion. This phenomenon is known as overdose (WANG *et al.*, 2021).

In this context, some variables that can be monitored to analyze the breakdown of the emulsion caused by the demulsifier in a flow are those related to detecting changes in the properties of the emulsion and flow. Among these variables, we can highlight the most used, the pressure drop (KOKAL; AL-JURAID, 2000; PLASENCIA *et al.*, 2013; BULGARELLI *et al.*, 2020), directly related to the change in flow patterns and effective viscosity. Moreover, variables related to the interactions of the flow with mechanical waves (sound characteristics) of the emulsion that can be used to characterize the flow pattern (FIGUEIREDO *et al.*, 2020), droplet size distribution (DSD) (POVEY, 2013; JIA *et al.*, 2019; SILVA *et al.*, 2020), and other properties such as droplet speed, expansion properties and others (FIGUEIREDO *et al.*, 2021; NORISUYE, 2017).

It is emphasized that for more precise control of the optimal dosage point of the demulsifier, the more intricate characteristics measured by complex sensors, such as the ultrasonic sensor, enabling detailed analysis of the emulsion, are required. It is worth noting that ultrasonic techniques are capable of non-intrusively examining opaque materials without the need for dilution (LI *et al.*, 2005; POVEY, 2013), qualifying them for online usage. The aforementioned points justify the use of ultrasonic sensors in the control loop for emulsion breakdown.

The central objective of implementing a control loop to dose the demulsifier is to maintain the process at the optimal dosage point. This optimal point is the minimum dosage rate required to achieve a specific viscosity flow, typically at the emulsion breaking point. It should be emphasized that viscosity, in this regard, is related to the pressure drop in the line and more intricately to changes in the characteristics of droplet distribution in the emulsion. The present proposal will focus on developing control strategies that meet these requirements.

It is noteworthy that, according to the literature review, there are numerous studies related to the analysis of chemical demulsification concerning process variables (temperature, agent dosage, residence time) and chemical aspects (mechanism of agent action, presence of dissolved solids, pH, type of demulsifier, droplet size distribution), as well as methodologies for demulsifier selection, as well as methodologies for demulsifier selection, as discussed for the reviewing done by Raynel et al. (2021). However, no studies were found related to the analysis of online control strategy applications for demulsifier dosing, whether based on ultrasonic sensor measurements or not. Therefore, the theme of the present doctoral proposal has an innovative focus, contributing to the literature for a more in-depth study of the application of demulsification control in real processes.

Chapter 2

Hypothesis and objective

The novelty of this work, in terms of technology, was solely using the ultrasonic sensor to characterize the flow and calculate the ideal dosage of demulsifier in the flow. It is worth noting that there is a patent application related to the device and the technique used here.

2.1 Hypothesis

The control based on the fuzzy system is efficient and can be used to manipulate the demulsification dosage, characterizing the demulsification using only the acoustic properties of the flow.

2.2 Objective

The main objective of this study was to investigate the application of control strategies for the demulsification process of water-in-oil emulsions based on ultrasonic measurements in a bench-scale circuit.

2.3 Specific objectives

To achieve the proposed overall objective, the following specific items were developed.

- Experimental setup of the bench-scale open circuit for studying demulsification in emulsion flow.

- Enhance and update the technical aspects of the ultrasonic sensor previously developed for improved characterization of emulsions.
- Development of an algorithm for monitoring and manipulating variables in open-loop and closed-loop process control, primarily related to the demulsification in the flow.
- Application and analysis of strategies encompassing non-linear controls for the studied process.

Chapter 3

Document division

The division of this document can be summarized in the flowchart presented in Figure 3.1. The list below presents a brief summary of the contents of each chapter and how they are connected.

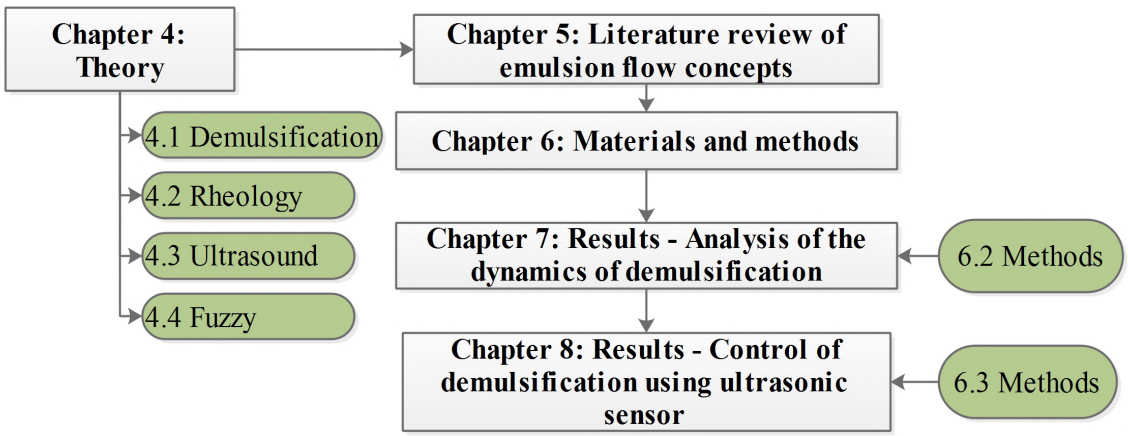

Figure 3.1: Flowchart of the document division.

- Chapter 4

  This chapter presents the theoretical foundation that is the basis for all analysis conducted in this work. The fundamental concepts about demulsification, especially in flow, rheological analysis, the ultrasonic sensor, and the fuzzy control system are covered.

- Chapter 5

This chapter presents a brief bibliographical and theoretical review of emulsion flow. In this chapter, the origin of the emulsion and the problems surrounding its formation in the petroleum industry were initially addressed. Phenomena that occur in flow, such as phase inversion and destabilization, are also presented. Finally, a review of techniques for characterizing the emulsion in flow was discussed, highlighting the advantages and disadvantages of each one, especially the ultrasonic technique.

- Chapter 6

  This chapter presents the material and methods used in the analysis. It is divided into two sections. In item 6.3, the methodology and materials used for demulsification dynamic analysis are presented. Similarly, item 6.4 refers to the methodology used in demulsification control analysis. The results and discussions for these two methodologies are presented separately in chapters 7 and 8, respectively.

- Chapter 7

  This chapter presents the results of the dynamics analysis of emulsion destabilization in the flow induced by adding a demulsifier. The focus of this chapter was to analyze the effect of variables such as temperature, flow rate, water fraction, and the presence of the shear pump in the flow on the dynamics of emulsion viscosity inferred by pressure drop transmitters.

- Chapter 8

  This chapter presents the results of applying the developed control strategy using fuzzy systems to dose the demulsifier in-line automatically. The acoustic properties of the flow from the ultrasonic sensor were used as monitored variables.

- Chapter 9

  This chapter presents the conclusion of the entire work according to the hypotheses tested and the objectives reached.

Chapter 4

Theory

4.1 Demulsification in flow

Researchers generally simplify the mechanisms of demulsification by the processes of flocculation followed by coalescence (AZIZI; NIKAZAR, 2015). Figure 4.1 illustrates the simplified demulsification process in the flow by dosing the demulsifier at a specific point. When the addition of the demulsifier starts, the first process begins. Flocculation occurs due to neutralizing the repulsive forces between droplets. The neutralization destabilizes the emulsion because of the replacement of emulsifiers by the demulsifier, reducing the interfacial tension of the droplets. Then, there is a formation of flakes. Coalescence occurs when these flakes merge and form large droplets.

The pressure drop in the flow can indicate the demulsification process. The larger the average droplet distribution, the lower the viscosity of the emulsion (PAL, 1996). The phase

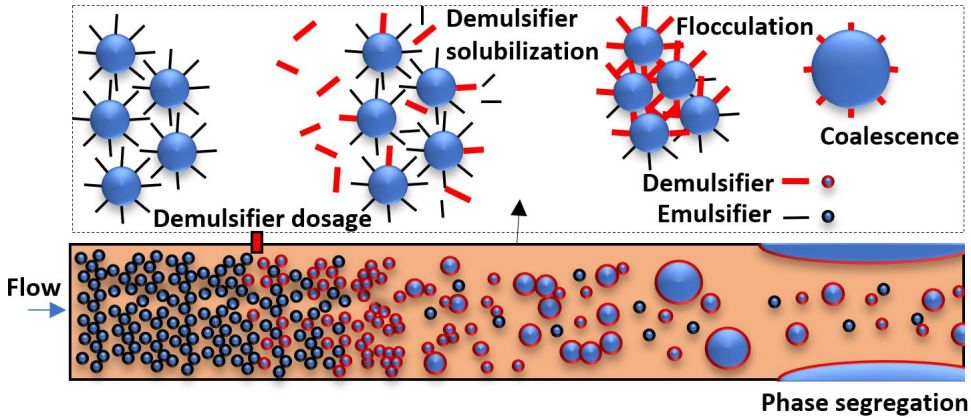

Figure 4.1: The representation of W/O emulsion demulsification using demulsifier dosage in a pipe flow.

segregation could happen depending on the amount of demulsifier added. The flow pattern, which depends on the velocity and phase's viscosity, is generally annular when the segregated phase flows in the pipe. This multiphase flow significantly decreases the viscosity. Depending on the opacity of the flow, this phenomenon can be seen with the naked eye (PLASENCIA J.; NYDAL, 2022).

The following factors influence the dynamic of demulsification.

- The flow velocity and stretches in the path influence the demulsifier solubilization velocity in the fluid once they can promote shear. At high flow rates, the intense mixing generated by the flow's energy breaks the emulsion into smaller droplets. Furthermore, sudden changes in the flow also promote mixing and increase emulsion formation, such as stretches with contractions (DOL *et al.*, 2018).

- Temperature and surfactant affinity influences the speed at which the demulsifier migrates to the droplet interface. High temperatures decrease the continuous phase's viscosity, increasing the collision frequency of droplets. Consequently, there is an improvement in the breakdown of the interfacial emulsifier film responsible for stabilizing the droplets. Therefore, the rate of coalescence rises (HJARTNES *et al.*, 2019; YONGUEP *et al.*, 2022). Despite this, some studies indicate increasing demulsification efficiency up to a specific temperature condition. These studies showed that increasing the temperature above 70°C had an insignificant effect on the demulsification efficiency (BALSAMO *et al.*, 2017; FORTUNY *et al.*, 2007).

- The amount of dispersed phase and the average droplet size influence the coalescence speed. Studies have shown that demulsification efficiency improves with increasing water content (AL-SABAGH *et al.*, 2011). The greater the volume of the dispersed phase, the smaller the distance between the droplets. Then, the faster the phase separation occurs (YONGUEP *et al.*, 2022).

The efficiency of demulsification could be affected by the re-emulsification phenomenon. This phenomenon occurs due to the shear caused by the flow, mainly when the flow is turbulent. Also, sections that promote intense fluid mixings, such as pumps and valves, could promote re-emulsion (VANKOVA *et al.*, 2007b). Depending on these factors, the amount of demulsifier added to achieve the phase segregation needs to be higher. It is worth noting that the limit for the amount of demulsifier is related to the area of the droplets that this

surfactant will act on. The excessive addition of demulsifier, in addition to being costly, is inefficient and can lead to the problem of overdose and the formation of surfactant agglomerates, which increases the viscosity of the system.

In the case of demulsification in the pipe, two flow patterns of liquid-liquid in horizontal pipe can be noticed. The patterns observed in this study are depicted in Fig. 4.2 and are inspired as per the nomenclature proposed by Barnes (1994). The first flow pattern, known as the Water-in-Oil (W/O) emulsion, represents the flow of only the emulsion. However, this flow pattern was subdivided into two flow patterns in this work. The first, shown in Fig. 4.2a, was the stable emulsion with tiny water droplets. It is named here as stable W/O emulsion (Ew/o stable). The flow in this pattern has a high viscosity. The second flow pattern appears when the droplet sizes grow and the emulsion phases are close to separating (Fig. 4.2b). It is named here as unstable W/O emulsion (Ew/o unstable).

The second flow pattern observed was the classical stratified flow. In this pattern, the denser phase flows at the bottom of the pipe, especially if the regime is laminar. This flow pattern is subdivided into two in this work. In the first, illustrated in Fig. 4.2c, the aqueous phase segregated is tiny and flows in the bottom of the pip. A part of the water remains emulsified in the emulsion that flows. This pattern occurs after the transition in the flow, which occurs with the gradual breakage of the emulsion. An intermittent flow pattern followed by stratification is observed at the moment of break. This pattern is named the stratified flow with little water content (S - litter water) in which there is a free liquid (water) and a dispersion in the other liquid. The second subdivided flow pattern is the aqueous phase case; Most of the water emulsioned is segregated (Fig. 4.2d). In this pattern, phase slip is more evident, i.e., the aqueous phase flows faster than the emulsioned one; it can be visualized by the naked eye. This flow pattern is named here as stratified with a lot of water content (S - very water content).

4.2 Rheological analysis

The mathematical relationship used to infer the apparent viscosity of the horizontal flow is presented in Equation 4.1. In this equation, the pressure gradient per meter is a function of the experimental friction factor (f_m) of Darcy, the mixture density (ρ), the flow velocity (v), and the pipe diameter (D).

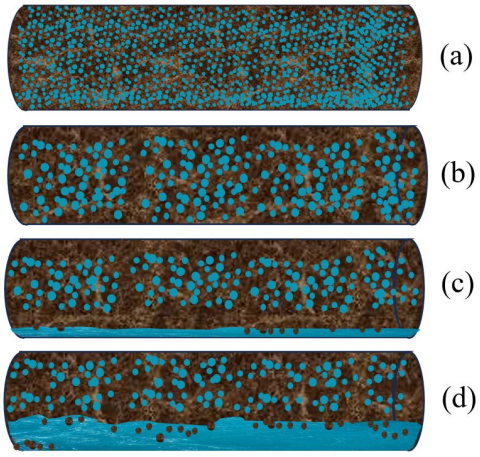

Figure 4.2: Flow patterns observed during observed demulsification: (a) Stable emulsion W/O (Ew/o stable), unstable emulsion W/O (Ew/o unstable), (c) stratified flow with little water content (S - littler water), and stratified with very water content (S - very water content).

$$\frac{dP}{dL} = f_m \frac{\rho v^2}{2D} \tag{4.1}$$

In which:

$$\rho = \rho_c x_c + \rho_d x_d \tag{4.2}$$

The subscripts c and d represent the continuous and dispersed phase, respectively. The x represents the volumetric fraction. Oil stands for continuous phase, while water stands for disperse phase. In the study, the flow regime was always laminar because of the slow velocity and the very high viscosity of the flow analyzed. According to the diagram of Moody, Equation 4.3 express the laminar regime friction factor as a function of Reynolds number (Re).

$$f_m = \frac{64}{Re} \tag{4.3}$$

Identifying the topology of the phases in the flow is unfeasible for a two-phase flow. To assume the phase arrangement as homogeneous is a reasonable simplification for working with this type of system.(PLASENCIA J.; NYDAL, 2022) adopted the apparent viscosity approach by considering homogeneous flow. This approach provides a direct relationship between the apparent viscosity and the pressure drop for a section of length (L), applying Equation 4.3 in 4.1. Integrating Equation 4.1 for a section of horizontal pipe, we have:

$$\int_{P_1}^{P_2} dP = \int_0^L \frac{64\rho v^2}{2ReD} dL = \int_0^L \frac{64\rho v^2 \mu_{apparent}}{2D\rho vD} dL \tag{4.4}$$

$$\mu_{apparent} = \frac{2D^2 \Delta P}{64vL} \tag{4.5}$$

Note that Equation 4.5 can be applied to calculate the apparent viscosity in the flow of the emulsion ($\mu_{apparent} = \mu_{emulsion}$) or pure oil ($\mu_{apparent} = \mu_o$). We used the relative viscosity given by Equation 4.6 in this work. In this equation, μ_o and $\mu_{emulsion}$ represent the viscosity of pure oil and emulsion at a given temperature, respectively. $\mu_{emulsion}$ was calculated using Equation 4.5 and μ_o using the experimental data present in Table A.2.

$$\mu_r = \frac{\mu_{emulsion}}{\mu_o} \tag{4.6}$$

The flow shear rate, which is a function of the flow speed, evaluates the rheology of the sample, especially the emulsion. Combined with viscosity, the shear rate checks whether the sample has Newtonian behavior. We calculate the shear rate through its relationship with the flow velocity, defined by Equation 4.7.

$$\sigma = \frac{2v}{D} \tag{4.7}$$

4.3 Ultrasound sensor

The sensor used in this work uses acoustic signal processing to extract the acoustic properties of the sample to characterize it. The sensor consists of a chamber in which the fluid flows upwards. This chamber called the sample line with length l_{wall}, is separated from the transducers by two parallel flat acrylic walls, called a delay line with length l_{wall}. Piezoelectric ultrasonic transducers are coupled to the delay line. The pair of transducers refers to the emitter transducer (TR-A) and the receiver transducer (TR-B). The electrical signal excites the emission transducer, which converts it into a sound signal. Both transducers capture the various echoes propagating in the cell, converting them into electrical signals (Fig. 4.3).

The sensor operation occurs in three steps. Firstly, the cell is emptied to digitize the signal reflected at the interface between the delay line and the air. The A_1^{air} echo is clipped and stored.

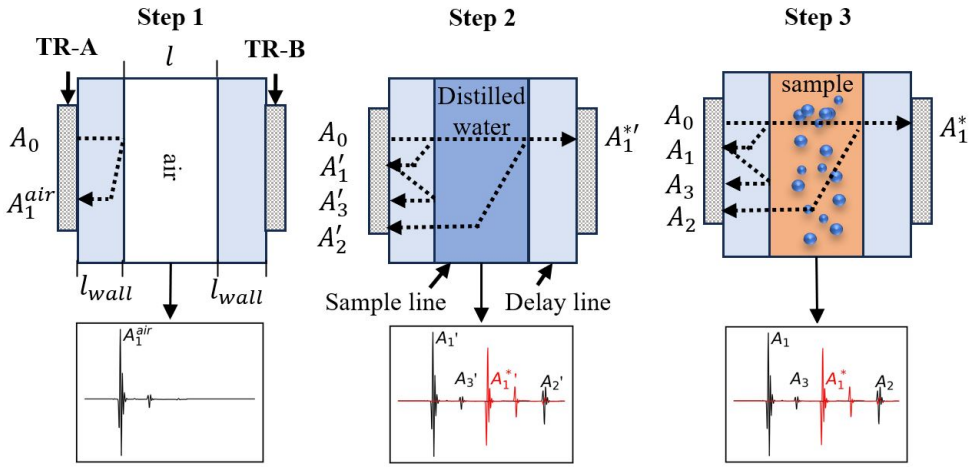

Figure 4.3: Illustration of the ultrasonic cell and its operation.

The second step, the cell is filled with a reference sample, in which the acoustic properties are known. The reference sample used was distilled water. The reflected echoes $A_1^{'}$ and $A_2^{'}$ and transmitted $A_1^{*'}$ are stored. After that, the sensor is used in real-time in the circuit to characterize the emulsion flow (Fig. 4.3).

The echoes $A_1^{'}$ and $A_2^{'}$ are utilized to calculate the length of the sample line. Although the sample line is fixed, it may undergo slight changes depending on the tightness of the transducers against the delay line. The cross-correlation between the echo $A_1^{'}$ and $A_2^{'}$ signals is used to calculate l through Equation 4.8 (Fig. 4.3). The sound velocity in water, c_w, found in the literature (KAYE; LABY, 1936) and $\tau_{cross:A_1'-A_2'}$ represents the cross-correlation time between the echoes $A_1^{'}$ and $A_2^{'}$.

$$l = \frac{c_w \tau_{cross:A_1'-A_2'}}{2} \tag{4.8}$$

The Fourier transform is applied to all echoes of sound signal and digitized to obtain the echoes in the frequency domain. With echoes in the frequency domain, their amplitude value is calculated using Equation 4.9

$$A_i = max\left(A_i(f)\right) \tag{4.9}$$

The properties of interest are the reflection coefficient, the sound attenuation in the sample, and the speed of sound. These properties are calculated using Equation 4.10, 4.11 and 4.12, respectively. Previous work demonstrates in detail the origin of these property equations (SILVA *et al.*, 2020; SARAIVA *et al.*, 2023). These properties can be used to

characterize the sample, as the physical properties and the morphological characteristics are intrinsically related, in the case of an emulsion (SILVA *et al.*, 2020).

$$R_{12} = -\frac{A_1}{A_1^{air}} \tag{4.10}$$

$$\alpha = \alpha^{'} + \frac{1}{l} ln \left\{ \frac{\left(1 - \left(A_1 / A_1^{air}\right)^2\right) A_1^{*'}}{\left(1 - \left(A_1^{'} / A_1^{air}\right)^2\right) A_1^{*}} \right\} \tag{4.11}$$

$\alpha^{'}$ represents the attenuation of the reference sample.

$$c = \frac{2l}{\tau_{cross:A_1-A_2}} \tag{4.12}$$

In the Equation 4.12, $\tau_{cross:A_1-A_2}$ represents the cross-correlation time between the echoes A_1 and A_2.

4.4 Fuzzy control

The fuzzy logic, pioneered by Zadeh (1965), is predicated upon defining the degree of membership of an element to a specific group. In contrast to Boolean logic, which asserts that an element either belongs or does not belong to a certain group, fuzzy logic entails a membership level. This logic introduces the concept of uncertainty, seeking to translate linguistic terms into mathematical functions. For instance, if we characterize a person as short or tall, in fuzzy logic, this person possesses a degree of pertinence to both the short and tall groups. They may be, for example, 30% tall and 70% short.

When applied to a control system, fuzzy logic offers several advantages. The fuzzy system can translate expert knowledge into a mathematical function suitable for implementation in a feedback system (EMAMI, 2010). Consequently, the fuzzy system adapts well to the nonlinearity of processes, particularly those with unknown dynamics.

One such fuzzy system applied in control systems was developed by Mamdani (1975). This control methodology has applications across various systems (CHEN; PHAM, 2000). In the subsequent section, we provide a concise overview of the Mamdani system, which serves as the foundation for the control system developed in this study. Figure 4.4 illustrates the fuzzy control system, segmented into layers of computations.

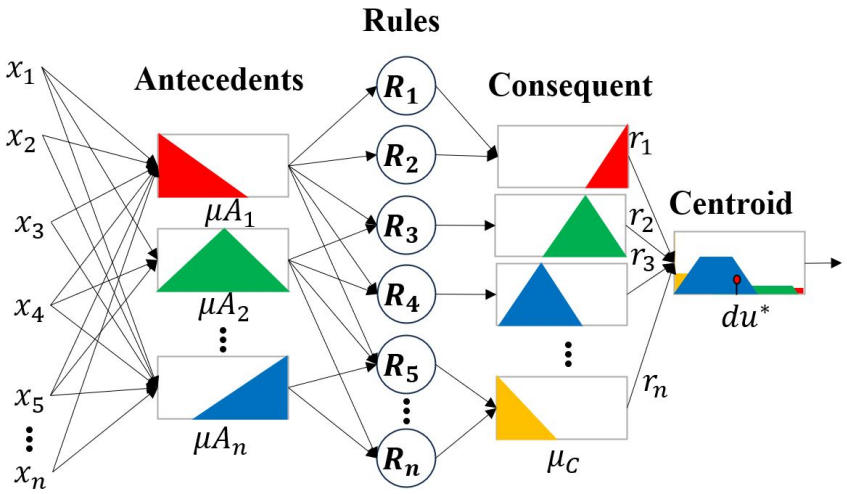

Figure 4.4: Fuzzy controller block: Fuzzy system.

- **Antecedents layer:** In this layer, in which fuzzification occurs, each node computes the degree of relevance of the input variables with the linguistic term associated with it. This calculation occurs through the membership function associated with a linguistic term. Several functions can be used in this association, such as ramp, triangular, trapezoidal, and Gaussian. Equation 4.13, 4.14, and 4.15 present the ramp, triangular and trapezoid functions, respectively, in which $\{a, b, c\}$ represent the parameters. These parameters, known as premise parameters, are essential in the adequacy of fuzzy sets.

$$\mu A_i(x) = max\left(min\left(\frac{x-a}{b-a}, 1\right), 0\right) \tag{4.13}$$

$$\mu A_i(x) = max\left(min\left(\frac{x-a}{b-a}, \frac{c-x}{c-b}\right), 0\right) \tag{4.14}$$

$$\mu A_i(x) = max\left(min\left(\frac{x-a}{b-a}, 1, \frac{c-x}{c-b}\right), 0\right) \tag{4.15}$$

- **Rules layer:** With the degree of pertinence of the linguistic variables to the system input data, it was possible to apply a set of rules. These rules aim to infer the degree of pertinence of the data to the consequent function associated with output terms linguistic of the fuzzy system. The two linguistic operators used to construct each rule are "and" and "or". The calculation of the result of these rules applied to the degree of belonging of the inputs to the antecedent functions are expressed by Equation 4.16 and Equation 4.17.

$$if\ \mu A_i(x)\ and\ \mu A_j(x),\ so\ r_k = \mu A_i(x) * \mu A_j(x) \tag{4.16}$$

$$if\ \mu A_i(x)\ or\ \mu A_j(x),\ so\ r_k = max\left(\mu A_i(x), \mu A_j(x)\right) \tag{4.17}$$

- **Consequent layer:** The results of the rules r_i are associated with the consequent's membership functions $\mu_C(r_i)$. The functions used in this layer are similar to the background layer.

- **Centroid:** With the result of the rules as a degree of relevance for each of the linquistic term of the consequent, defuzzification of the data is applied. The output of the defuzzification layer occurs by applying the centroid method (Equation 4.18) in the area formed by grouping the membership functions of the consequent μ_C related to their respective inputs r_i.

$$du *= \frac{\int \mu_C(r_i)\, r_i dr}{\int \mu_C(r_i)\, dr} \tag{4.18}$$

Chapter 5

Reviewer of oil emulsion flow: formation, rheology and characterization technics

The emulsion is formed by mixing two immiscible liquids so that one liquid becomes a dispersed phase in the other. In the formation of the emulsion, an amount of energy is required to promote it, which is thermodynamically non-spontaneous. After mixing, droplets of one phase become dispersed in the other. This phase is called the dispersed phase, and the other is called the continuous phase. The droplets remain dispersed until they come together and form the segregated phase again. This occurs because thermodynamically, the emulsion, without an emulsifier, is not kinetically stable (SILVA *et al.*, 2013; KABALNOV, 1998), and there is a spontaneous action of the phases to reduce the interfacial energy. In other words, there is a natural tendency for the emulsion (liquid-liquid system) to segregate and reduce the interfacial energy of the system.

When an emulsifier is present, the emulsion can become kinetically stable, depending on the time required for the phases to remain dispersed (KABALNOV, 1998). Besides this, some authors point out the complex system that forms thermodynamically stable emulsions (SILVA *et al.*, 2013; OKAZAWA; BRON, 1979), such as microemulsions. There are several techniques to determine the stability of the emulsion (MCCLEMENTS, 2007). External factors such as temperature, agitation, and the presence of salts also influence the stability of the emulsion.

The emulsion is found in several industrial areas. For some industrial sectors, the formation of this emulsion is desired and crucial in manufacturing their products. However, for the

oil and gas industry, emulsion formation is costly (UMAR *et al.*, 2018). There is a common challenge for all these areas when dealing with emulsion: its transportation. The emulsion is usually transported using pumping systems. In this system, high energy is demanded due to the viscous characteristic of the fluid. The emulsion is more viscous than the phases that make it up (BARNES, 1994).

In the literature, some works evaluate in detail the emulsion formation mechanism, stability, and techniques used to separate the phases (UMAR *et al.*, 2018; WANG *et al.*, 2021; YONGUEP *et al.*, 2022; MA *et al.*, 2022). Other works review the phenomena that can occur with the emulsion, such as phase inversion (MAFFI *et al.*, 2020). Recently, some work has explored phase inversion in flow (BULGARELLI *et al.*, 2020; TAN *et al.*, 2020; PRIETO *et al.*, 2019). Another very important phenomenon in the context of emulsion is destabilization. In this context, numerous studies evaluate existing techniques to promote phase segregation (YONGUEP *et al.*, 2022). However, no studies were found that address these techniques directly in the flow, only chemical demulsification (BULGARELLI *et al.*, 2021).

In this context, the objective of this chapter was to present a brief review of the emulsion concerning its formation, rheology, and characterization techniques to monitor the phenomena of phase inversion and destabilization. We address these topics specifically to describe these phenomena in flow.

5.1 Emulsion formation and stability in the flow

When an emulsion is formed, the size of the droplets is influenced by the amount of energy in the mixture. These droplets are stabilized due to the presence of emulsifiers that prevent coalescence. In flow, emulsion can be formed when two immiscible phases are present. These phases are mixed due to the flow and obstacles in the line, such as valves, pumps, and others (UMAR *et al.*, 2018; YONGUEP *et al.*, 2022).

The emulsion is classified according to the dispersed and continuous phases as O/W oil-in-water emulsion, W/O water-in-oil emulsion, or complex emulsion (TIAN *et al.*, 2022). W/O emulsions (Figure 5.1a), in which water is dispersed in the oil, are the most problematic regarding flow assurance, are mainly present in oil production, and have a high viscosity. O/W emulsions (Figure 5.1b), in which the oil is dispersed in the aqueous phase, are present in the post-extraction stages. These emulsions, also known in this context as produced water,

are subjected to processing to ensure adequate disposal. Furthermore, this emulsion is generally used to inject in wells. Finally, multiple emulsions are emulsions whose droplets of one phase are dispersed within another phase, which is yet then dispersed in another phase. This complex structure creates a multilayer of liquid phases. For example, we can see in Figure 5.1c oil in water in oil O/W/O. These emulsions are more difficult to find and are present when the emulsion is close to phase inversion (PLASENCIA J.; NYDAL, 2022; SARAIVA *et al.*, 2024).

The water present in the oil production line that promotes emulsion formation can have two origins. This water can be of geological origin or injection. The water of geological origin is present in the reservoir and is common in areas with aquifers. The injection origin comes from water used by the oil treatment unit to inject into generally mature wells to increase their pressure and guarantee oil production (UMAR *et al.*, 2018).

In the oil and gas industry, the formation of emulsions in pipes is harmful both in terms of production and in terms of maintenance of structures (KOKAL, 2005). The emulsions formed require more technical effort to guarantee flow and separate the phases in the pre-refining stage of the oil. Furthermore, the emulsion can promote greater deterioration of pipes and equipment due to corrosion promoted by the presence of chlorides dissolved in aqueous phase (UMAR *et al.*, 2018), especially if salts are present.

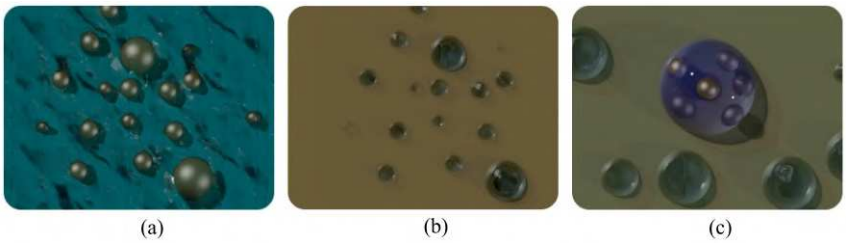

Figure 5.1: Classification of emulsions according to phases: Oil in water (a), Water in oil (b), oil in water in oil (c).

The emulsion is stabilized due to the presence of emulsifying agents. These chemical agents are surfactants that have a polar part and a non-polar part in their chain. The polar part adheres to the aqueous phase, and the non-polar part to the oily phase. When this surfactant adheres to the interface between the phases, it forms a layer that encompasses the drops, and due to its steric properties, this layer has a repulsive interaction with the layer of another drop (GOODARZI; ZENDEHBOUDI, 2019; KILPATRICK, 2012). In this way, the

droplets encapsulated by the emulsifier repel each other, preventing flocculation and coalescence.

Due to the chemical role of the emulsifier, it significantly reduces the interfacial tension of the drops due to changes in electrostatic and steric forces (GOODARZI; ZENDEHBOUDI, 2019). In petroleum, there are natural emulsifiers that play this role (KOKAL, 2005; WANG *et al.*, 2021), and the presence of salt can improve this stability. Some authors point out that the presence of salts tends to reduce the size of the droplets in the W/O emulsion, which contributes to the role of the emulsifier in stabilizing the emulsion (LIM *et al.*, 2015; BINKS, 2002). However, this effect is the opposite for O/W emulsion, i.e., the presence of salts increases the oil droplets (LIM *et al.*, 2015; BINKS, 2002; YONGUEP *et al.*, 2022; SULLIVAN; KILPATRICK, 2002). Binks (BINKS, 2002) discusses in detail the role of dissolved solids in emulsification. The emulsion stabilization mechanism promoted by the emulsifier can be divided into categories, some presented in the following list (NOUR, 2018).

- Electrostatic repulsion: This repulsion occurs when the interface absorbs ionic surfactants in O/W emulsion. These surfactants create electrical layers and prevent contact between drops.
- Steric repulsion: Common repulsion when the emulsifier is non-ionic. This effect is present in W/O emulsion. The emulsifier with polymeric molecules prevents contact between the drops due to their size.
- Marangoni effect: This effect redistributes the emulsifier at the interface to reduce the surface tension gradient, helping to stabilize the emulsion by reducing the concentration gradient of the emulsifier in the emulsion.

In flow, velocity plays an important role in emulsion formation. High flow velocities promote droplet deformation, weakening the interface and interfacial tension with the continuous medium. This promotes droplet breakage and the formation of smaller droplets (DOL *et al.*, 2018; KOBAYASHI *et al.*, 2002; YONGUEP *et al.*, 2022). This decrease in droplet size was also observed by Nina et al (VANKOVA *et al.*, 2007a). when analyzing high viscous emulsion in a turbulent flow.

5.2 Rheology of the emulsion

The Newtonian behavior of the emulsion is present only at low concentrations of the dispersed phase. As the water concentration increases, the emulsion exhibits non-Newtonian behavior. The emulsion has pseudoplastic characteristics, i.e., the viscosity decreases with the increase in the shear rate. This behavior is due to the packing of the drops (BARNES, 1994). Studies show this behavior begins to appear at 30% of the water fraction until reaching maximum packaging (KOKAL, 2005). Figure 5.2 presents an example of the behavior of the emulsion in relation to physical factors. Although these data refer to specific oils (KOKAL, 2005; LUO *et al.*, 2022), this behavior is generalized to several emulsions (LUO *et al.*, 2022).

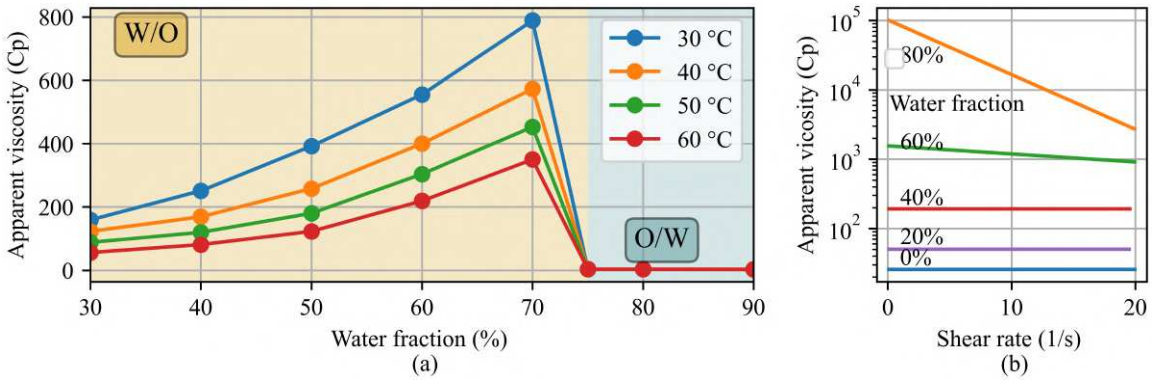

Figure 5.2: Influence of physical factors on the viscosity of W/O emulsions. Viscosity as function of temperature data of Oil#12 (LUO *et al.*, 2022) (a) and viscosity as function of shear hate from (KOKAL, 2005) (b).

When the emulsion presents non-Newtonian behavior, as shown in Figure 5.2, the shear stress on the pipe wall τ_{wall} can be expressed by the Eq. 5.1. In this equation, K is a constant, γ is the shear rate, and n is a constant. When $n = 1$ the fluid is Newtonian, $n > 1$, the fluid presents the pseudoplastic behavior, and $n < 1$ is the dilatant behavior. The W/O emulsion has pseudoplastic behavior (Figure 5.2b), in which the viscosity decreases with the shear rate. Note that Eq. 5.1 can be written as Eq. 5.2, in which μ_{app} is the apparent or effective viscosity of the emulsion.

$$\tau_{wall} = K\gamma^n \tag{5.1}$$

$$\tau_{wall} = \mu_{app}\gamma \tag{5.2}$$

Viscosity is related to several structural factors of the emulsion, the most common being the dispersed phase fraction ϕ. In the literature, several correlations define the emulsion's relative viscosity μ_r (Defined in Eq. 4.6) as a function of the water fraction and phase viscosities $\mu = f(\mu_o, \mu_w, \phi)$. Where μ_o and μ_w are the viscosities of oil and water, respectively. Some of these correlations are presented in Table 5.1.

Table 5.1: Correlations used to calculate the viscosity of the emulsion.

Model	Reference
$1 - 2.5\phi$	Einstein (EINSTEIN, 1906)
$1 - 2.5\phi \left(\frac{0.4 + \frac{\mu_d}{\mu_c}}{1 + \frac{\mu_d}{\mu_c}} \right)$	Taylor (TAYLOR, 1932)
$(1 - \phi)^{-2.5}$	Brinkman (BRINKMAN, 2004)
$1 + 2.5\phi + 7.349\phi^2$	Van (VAN, 1948)
$1 + 2.5\phi + 6.2\phi^2$	Batchelor (BATCHELOR, 1977)
$e^{h_1 + h_2 T + h_3 \phi + h_4 \phi T}$	Ronningsen (RONNINGSEN, 1995)
$\frac{1}{1-\phi} \left(1 + \frac{1.5\phi\mu_d}{\mu_c + \mu_d} \right)$	Vermeulen et al. (VERMEULEN *et al.*, 1955)

Other more complex correlations bring relative viscosity as a function of other additional factors, such as shear rate, temperature, and chemical characteristics of the oil. The correlation of Shi et al. (SHI *et al.*, 2018) (Eq. 5.3), for example, takes into account temperature (Eq. 5.4) and shear rate (Table 5.2)

$$\mu_r = 2.5 \frac{\mu_w/\mu_o + 0.4}{\mu_w/\mu_o + 1} e^f \tag{5.3}$$

$$f = a_1(a_2\phi + a_3\phi + a_4\phi + a_5\phi + a_5\phi)T^{a_7} \tag{5.4}$$

In addition to the effect of the concentration of the dispersed phase and the viscosities of the phases on the rheology of the emulsion (present in all correlations (PRIETO *et al.*, 2019)), other factors must be considered to understand better and estimate the viscosity of the emulsion. Factors such as droplet size distribution, the nature of the particles and their interactions, and deformability play a fundamental role in the rheology of the emulsion.

It is well known that the more monodisperse and tiny the droplet size distribution (DSD), the greater the viscosity (KOKAL, 2005; RICHARDSON, 1953). This observation occurs due to the increase in surface area in smaller drops; interactions between particles are greater.

Table 5.2: Table of constants of the Eq. 5.4.

Shear rate (s^{-1}) Coefficient	5	10	15-40
a1	1.5764e-7	-1.030998e-6	-1.97e-8
a2	119843.2033	-17270.07	-889486.8
a3	-8853.419167	1294.0452	66861.689
a4	302.0889531	-44.75888	-2318.999
a5	-3.780087983	0.5628887	29.172045
a6	0.014774289	-0.002202	-0.11409
a7	0.417199178	0.4194036	0.4203765

Ref: (SHI *et al.*, 2018)

Despite this, the droplet average increase requires a greater amount of emulsifier to stabilize it (BARNES, 1994).

When the emulsion is subjected to deformation, part of the energy used is recovered through its ability to deform elastically. This deformation, evaluated in terms of the elastic modulus $G^{'}$, is reversible. On the other hand, another part of the energy is dissipated as heat, this dissipation being related to an irreversible deformation, evaluated through the viscous modulus $G^{''}$. The relationship between these modules is given by Eq. 5.5, where ω is the angular frequency of the deformation and μ^* complex viscosity (MACOSKO, 1994).

$$\mu^* = \frac{G^{'}}{\omega} + \imath\frac{G^{''}}{\omega} \tag{5.5}$$

The particle interactions directly influence the emulsion rheology (FUHRMANN *et al.*, 2022). If the emulsion has a repulsive interaction between the particles, the drops tend to move apart, and there is a predominance of the elastic behavior of the emulsion. This means that the elastic modulus dominates over the viscous modulus. This predominance is only observed for low shear values (FUHRMANN *et al.*, 2022; FUHRMANN *et al.*, 2019). However, when the interaction is attractive, the drops form clusters, promoting flocculation. Increasing the shear rate for this emulsion promotes a rearrangement of the droplet structure in two stages. The first stage occurs with the disruption of interactions between particles due to increased movement. This means the emulsion behaves similarly to the repulsive ones (DATTA *et al.*, 2011). The second stage occurs with the increase in the shear rate, the rearrangement of the particles promoting flocculation, and the coalescence of some drops (ZHANG *et al.*, 2016).

The emulsion deformability refers to the drops ability to deform when a force is applied to them. This measurement is directly influenced by the chemical nature of the droplet and its interaction with its peers. Saiki and Prestidge (SAIKI; PRESTIDGE, 2005) analyzed the rheology of hard (viscoelastic) and soft (viscous) emulsions. They highlight that the effects of deformability on viscosity are more pronounced at a high dispersed phase content and shear rate.

5.3 Developed flow pattern

The flow pattern aspect of the stable emulsion is homogeneous due to the non-perception of different phases. However, when the emulsion destabilizes due to some phenomenon, it forms a liquid-liquid two-phase flow. When a liquid-liquid flows horizontally or vertically, different flow patterns are formed. In the literature, there are several flow classifications with different names (Figure 5.3); among the numerous, the most common classification for horizontal flow is the one developed by Trallero et al (TRALLERO *et al.*, 1997). and Tan et al (TAN *et al.*, 2020). For vertical flow, we highlight the pattern presented by Guo et al (GUO *et al.*, 2018). Figure 5.3 shows the liquid-liquid flow patterns in horizontal and vertical pipes.

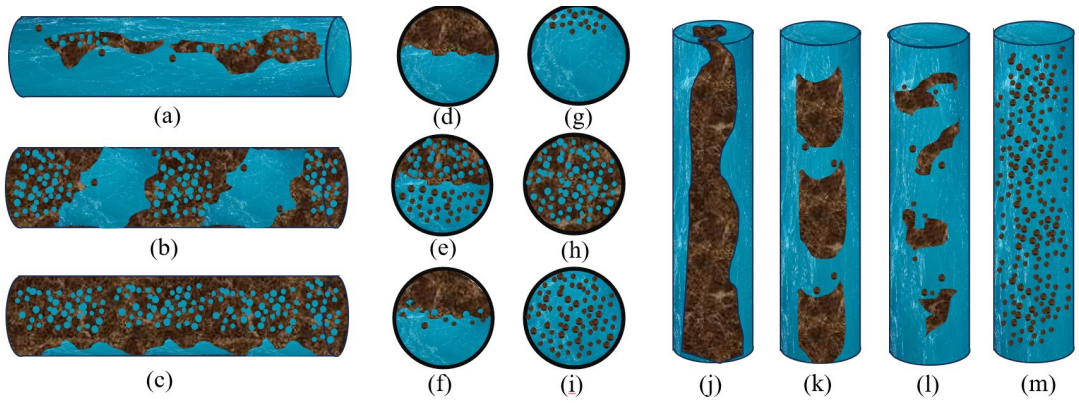

Figure 5.3: Flow partners of W/O flow: (a) Water semi-annular, (b) Intermittent flow of water, (c) Intermittent flow of separated water, (d) Stratified, (e) Dispersion of water-in-oil and oil-in-water, (f) Stratified flow with mixing at the interface, (g) Dispersion of oil-in-water, (h) Water-in-oil emulsion, (i) Oil-in-water emulsion, (j) Annular, (k) Slug, (l) Churn and (m) Dispersed. Flow partners (a)-(i) applied to horizontal flow and (a), (b) and (e)-(j) to vertical flow.

The semi-annular flow pattern occurs when the flow velocity is too small for the oily phase to remain continuous in the pipe core (Figure 5.3a).

The intermittent flow pattern presents the greatest pressure drop in the flow. It can be divided into two different patterns. The first is the intermittent with water, formed by water

and oil present throughout the tube (Figure 5.3b). In this pattern, the pressure drop presents more prominent oscillations due to these pockets of water and emulsion in the pipe. The second pattern is the intermittent with water layers, which is present when the oil fraction is high (Figure 5.3c).

The stratified flow pattern occurs horizontally in which the phase with different densities tends to flow in the different regions of the pipe. This pattern occurs at low flow velocity (Figure 5.3d). At high velocity, water can carry droplets of oil, and the interface between the phases presents disturbances, which sets up a pattern stratified mixing at the interface until reaching the dispersion pattern of water-in-oil and oil-in-water (Figure 5.3f and 5.3e).

The W/O and O/W emulsion flow patterns presents a homogeneous appearance for the stable emulsion and can be classified as oil-in-water and water-in-oil emulsions (Figure 5.3i and 5.3h). Vertically, the flow may also present an annular (Figure 5.3j), slug (Figure 5.3k), and churn pattern (Figure 5.3l).

5.4 Chemical demulsification

Chemical demulsification is the most used technique to separate the emulsion phases (RAYA *et al.*, 2020; YONGUEP *et al.*, 2022; WANG *et al.*, 2021). This technique involves surfactant agents that migrate to the interface of the dispersed and continuous phases, i.e., to the surface of the drops, replacing the emulsifier present. However, unlike the demulsifier, this molecule allows the drops to come closer together. When the drops approach, they form flakes and tend to coalesce, thus promoting phase segregation. This mechanism of replacing the emulsifier with the demulsifier is well-detailed by Wang et al (2021) and Ma et al. (2022).

Chemical demulsification, when applied to W/O emulsion, is known as the emulsion dehydration process. This process takes place through a few steps. Some authors point out two main steps. The first is flocculation, caused by decreased interfacial tension followed by sedimentation of the droplets. This sedimentation promotes coalescence and phase segregation (PENA *et al.*, 2004). However, in flow, sedimentation does not occur similarly. Due to the movement of the fluid, the drops tend to remain suspended. The main factors that affect the demulsification kinetics in the flow are listed in sequence.

- Diffusivity of the demulsifier in the flow: This diffusion occurs more quickly with increased temperature and better surfactant mixing. The velocity, flow regime, and

presence of disturbances in the flow that promote mixing influence the diffusion velocity (HJARTNES *et al.*, 2019; YONGUEP *et al.*, 2022).

- Demulsifier efficiency: This factor is related to the efficiency of the demulsifier in replacing the emulsifier at the droplet interface. This replacement mechanism promotes the suspension of the effect of the emulsifier and is detailed by (MA *et al.*, 2022).

- Drop flocculation: The weakening of repulsive forces promotes the approximation of the emulsion drops, and the flow velocity accelerates this process. Viscosity is another factor that influences this phenomenon.

- Drop coalescence: Authors point out that in flow, the destabilization of the emulsion occurs when the coalescence rate is higher than the breakage rate of the drops. This drop is inherent to the fluid movement promoted by the flow (HJARTNES *et al.*, 2019).

The flow pattern formed during demulsification depends on all the variables that influence the flow of oil and water. Factors such as phase viscosity, flow regime, and pipe diameter are important in forming the flow pattern. However, unlike mixing oil and water, W/O demulsification promotes the formation of segregated water and an unseparated emulsion. In a laminar regime, for example, we will have the formation of classic stratified flow. In the turbulent regime, no studies reported the analysis of demulsification, only emulsification. A possible cause for the lack of work on this topic is the difficulty in finding a suitable demulsifier and the high analysis cost due to the sample volume, mainly of the demulsifier, to be discarded. Another factor is the difficulty in reaching the turbulent regime due to the high viscosity of the emulsion.

5.4.1 Demulsification through other techniques

There are several demulsification techniques in addition to chemistry. These techniques can be classified as mechanical or physical, electrical, and thermal demulsification (YONGUEP *et al.*, 2022). Mechanical or physical demulsification involves devices that force the droplets to clump together and break their interface, promoting segregation. Examples of these devices are centrifugal separators (HAO *et al.*, 2013; KATO; KAWASAKI, 1987) or gravitational. Another technique, classified as physical demulsification that can be used is ultrasound. The

ultrasound promotes the agglutination of the drops due to the pressure gradient promoted by the mechanical wave (ISSAKA, 2015).

Electrical demulsification involves using an electric field in which current passes between electrodes. This electrical current promotes an oxidation-reduction reaction and polarization of the droplets, which increases the rate of coalescence (PENG *et al.*, 2016). Thermal demulsification, combined with another technique, combines both techniques to promote droplet coalescence. The temperature increases demulsification efficiency, decreasing the viscosity of the continuous phase (YONGUEP *et al.*, 2022).

In addition to these techniques, we can mention others, such as flotation (NIKOLOV M. RANDIE; WASAN, 1996). There is a improvement in efficiency in the use of these techniques, especially when combined with chemical demulsification (SUN *et al.*, 2017). Despite the efficiency of these techniques, they are not applied to flows in which environmental conditions are extreme, such as oil production.

5.5 Emulsion phase inversion in flow

Phase inversion in flow can occur in two ways. The first, called catastrophic phase inversion, occurs when there is an increase in dispersed phase until the phase inversion point (PIP) is reached. The second way, called transitional inversion, occurs due to the change in the interfacial tension of the droplets in the dispersed phases, anticipating the PIP. This occurs due to changes in the flow temperature or with the addition of surfactants that change the interfacial characteristic of the drops (PERAZZO *et al.*, 2015).

In flow, several works report that the phase inversion promotes an abrupt change in the pressure drop, which is translated into apparent/effectively viscosity (PLASENCIA J.; NYDAL, 2022). Authors point out that at the PIP, the viscosity reaches maximum values (MARTINEZ *et al.*, 1988; NäDLER; MEWES, 1997; IOANNOU *et al.*, 2005). Other authors point out the existence of an ambivalent region in the emulsion during phase inversion. In this region, there is the presence of both phases continuously, W/O and O/W emulsion, in the flow (PIELA *et al.*, 2006; LIU *et al.*, 2006). This region is known as the transition region. Despite this discussion about the existence of a transition region, the literature points to the existence of an exact point at which the phase inversion occurs. This point was observed experimentally and modeled by several authors through correlations (PRIETO *et al.*, 2019).

There are several correlations in the literature. These models were developed through adjustment with experimental data. Pietro et al (2019) reviews several correlations, highlighting that the best ones that fit the experimental data they used were those developed by Ngan (2010) based on Einstein (1906) and Taylor (1932) for very viscous oil and Ye et al (1964) and Verneule et al (1955) for less viscous oil. The Ngan graphic method plots the viscosity as a function of the dispersed phase for W/O and O/W emulsions (NGAN, 2010). The PIP is found by the intersection of these two curves, i.e., PIP obeys Eq. 5.6. In this equation, ϕ_{PIP} represents the PIP. Some models, such as those presented in Table 5.1, can represent the viscosity used in Eq. 5.6. The Ye et al (YEH *et al.*, 1964). model is presented in Eq. 5.7.

$$\mu_r(\phi_{PIP})|_{O/W} = \mu_r(\phi_{PIP})|_{W/O} \tag{5.6}$$

$$\phi_{PIP} = \frac{1}{1 + \sqrt{\frac{\mu_o}{\mu_w}}} \tag{5.7}$$

The factors influencing phase inversion in flow are temperature, viscosity, fluid velocity, flow regime, pipe diameter, and material (NGAN, 2010). These factors influence the value of ϕ_{PIP} and the flow pattern developed in the process.

The high temperature influences the viscosity of the emulsion, which anticipates the phase inversion point. However, as studied by Tan et al. (2020), this sensitivity is almost negligible when the oil phase has a high viscosity. Tan e al. (2020) points out that due to non-Newtonian behavior and the need for a greater shear force to promote the continuous phase transition, the effect of temperature on viscosity exceeds that for viscous oils. Therefore, other effects must be added to the flow for phase inversion.

The velocity influences in order to anticipate the phase inversion. De et al. (2010) point out the existence of a minimum velocity, at which the inversion can occur, corroborating the results found by Shi et al. (2018).

The high viscosity of the continuous phase anticipates the inversion point. According to Selker (1965), the tendency for a phase to become dispersed increases with increasing viscosity. This theory is corroborated by results found in several studies (TAN *et al.*, 2020). Another critical point is that high viscosity increases the bivalent region. This increase occurs because the coalescence rate decreases due to the longer film drainage time between

two drops (NORATO *et al.*, 1998). This theory explains why the transition region in phase inversion was shorter at 50C than at 30C in previous work (SARAIVA *et al.*, 2024).

During phase inversion, several flow patterns can be formed (flow pattern transition). These patterns depend on the velocity, pipe diameter, and phase viscosities. Tan et al. (2020) observed that in the inversion from W/O to O/W for a very viscous oil phase, generally, the flow pattern goes from an emulsion W/O pattern to a semi-annular and annular. At low velocities and minor diameters, the inverted W/O emulsion pattern presents intermittent water and intermittent with a separated water flow pattern (SARAIVA *et al.*, 2024).

5.6 Emulsion flow characterization techniques

There are many techniques to characterize emulsions (MCCLEMENTS, 2007). However, due to the challenges, fewer techniques are applied in the flow. In this context, although techniques can be used to infer important properties such as viscosity (BARNES, 1994), the essential characteristics of the emulsion are intrinsically related to its morphology. In other words, the droplet size distribution (DSD) and the flow pattern developed in case of destabilization. Monitoring the change in this variable during the phenomena mentioned in item 5.3 is of great importance for a better understanding of how the morphology of the emulsion is changed during these processes. The techniques found in the literature to measure DSD in-line are laser diffraction, laser reflection, ultrasound, microscopy, and particle video microscopy.

The focused beam reflectance measurement probe (FBRM) is a sensor that uses the laser reflection technique. This sensor measures the chord length distribution by scanning laser beams that reflect off the emulsion drops. DSD is inferred from the relationship with chord length. Some authors have used this sensor in emulsion characterization (PLASENCIA J.; NYDAL, 2022; BULGARELLI *et al.*, 2017; GREAVES *et al.*, 2008). Some studies show that the limitations of this technique lie in the calibration of the relationship between DSD and chord length distribution (GREAVES *et al.*, 2008).

The ultrasonic technique uses processed acoustic signals to infer, through physical wave propagation models, the DSD (CHALLIS *et al.*, 2005). This technique has advantages, including the possibility of analyzing opaque and concentrated emulsions; however, a significant amount of thermophysical properties of the phases is required. Silva et al. (SILVA

et al., 2020) analyzed the application of this technique to characterize concentrated sunflower oil emulsion flowing at low velocities, showing the accuracy of the technique when compared to laboratory analyses.

Microscopy is used in-line using equipment such as Canty Inc. DSD inference occurs through image processing collected in real-time (VENKATARAMANI; AICHELE, 2015). This technique has limitations with the opacity of the sample. Venkataramani and Aichele (VENKATARAMANI; AICHELE, 2015) used this technique to characterize diluted samples with water content less than 10%. The authors evaluated the effect of water content and flow velocity on DSD.

5.7 Conclusions and perspective

Ensuring emulsion flow continues to be a challenging area in the industry, especially in complex environments such as oil production. In industrial areas with less complex environments, such as the oil separation and processing stage, new technologies combined with the dosage of demulsifiers to destabilize the emulsion have gained notoriety. Techniques involving the use of electric field, ultrasound, microwave, and classic gravity have been developed, which reduces operational costs with demulsifiers.

However, in complex environments such as oil production, the application of these techniques to assure the flow is, for now, unfeasible due to the extreme conditions. Only the dosage of the demulsifier continues to be used. The evaluation of the efficiency of this technique in this context occurs by inference of the monitored variables, such as pressure. In addition, few studies evaluate how chemical demulsification occurs in the flow.

Our perspective is that more work involving the analysis of emulsion flow during destabilization promoted by various techniques, especially chemistry, will be carried out, and the results found will help those in the flow study area to understand better how this phenomenon occurs in flow in order to manipulate and control it. Moreover, in this context, it is hoped that this work will help researchers to have a more general understanding of this subject.

Chapter 6

Materials and methods

6.1 Materials

The material used to prepare the emulsion was high-viscosity naphthenic mineral oil (Energis, Brazil) and distilled water. The emulsifier used to produce a stable emulsion was Span 80 (Sigma Aldrich, France). The demulsifier used to evaluate demulsification was an amine-initiated polyol block copolymer (Dow Chemical Co, USA). This demulsifier was diluted in absolute ethyl alcohol at a concentration of 74.6 g/L and stored to be dosed into the flow using a peristaltic pump. Table A.3 and A.2 presents the curve of the oil density and viscosity as a function of the temperature. Table 6.1 presents the physical properties of the emulsion phases separated.

Table 6.1: Physical properties of the materials used.

Properties	Water	Oil
	40°C	
Sound velocity (m/s)	1528[&]	1398[$]
Density (kg/m^3)	992[&]	897*
Viscosity (N/m^2.s)	0.0006[&]	0.1248*
	50°C	
Sound velocity (m/s)	1542[&]	1376[$]
Density (kg/m^3)	988[&]	891*
Viscosity (N/m^2.s)	0.0005[&]	0.0683*

Obtained through [$]ultrasonic sensor, *experiments, and [&]the literature (KAYE; LABY, 1936).

6.2 Supervisory system

The supervisory system where the algorithm for monitoring acoustic properties and circuit variables was implemented was developed in open language (Python and C++). This system includes the computer communication environment with the programmable logic controller (sensors and actuators), the acoustic signal processing algorithm, and the fuzzy control algorithm. The manual with more details was attached in item A.1.3. It is worth noting that the program was registered with the intellectual property institute (INPI), with joint authorship from the researchers involved, Petrobras and Unicamp.

The Figure 6.1 depicts the snapshot of the supervisory system window. Within this window, it is possible to observe the indicators of the variables measured and manipulated within the circuit, the graph (on the right) displaying the historical data of the measurements, and additional application options. These supplementary options include the initiation of monitoring, the choice to save the data history, and the visualization options for both data history and manipulation of the manipulated variables (Pumps).

The USS1 button is associated with the ultrasonic sensor installed in the circuit. Upon activation, it will open the sensor configuration window (Figure 6.2). This application shows the monitor of the processing of ultrasonic data in more detail. The USS2 button pertains to another ultrasonic sensor that is not within the scope of this work.

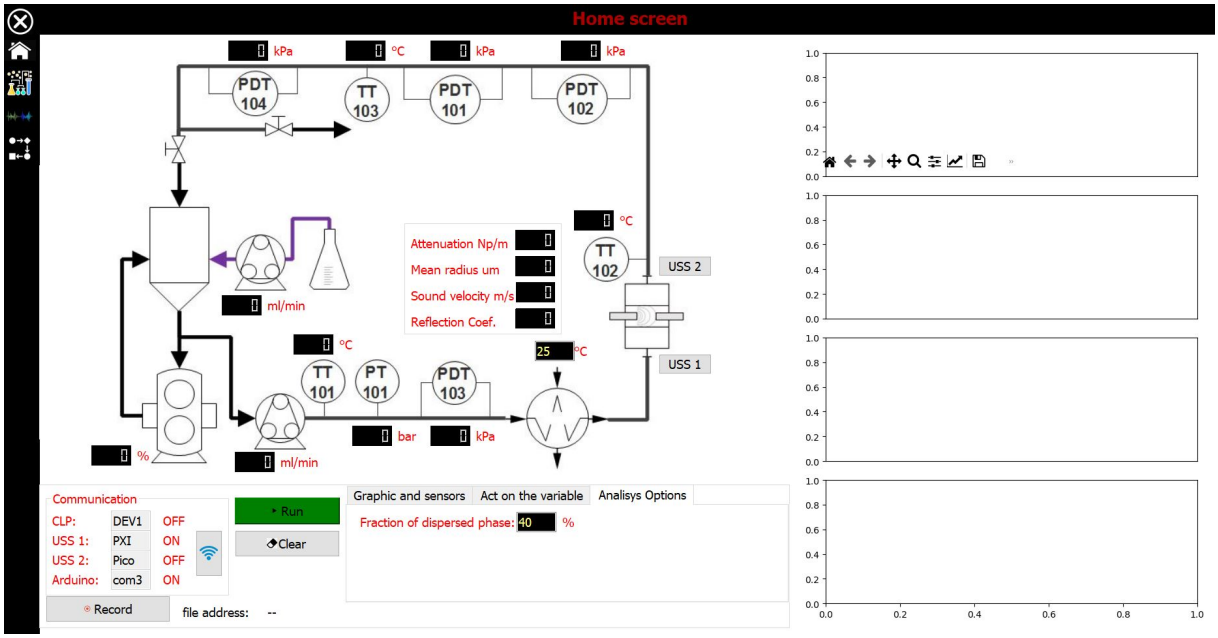

Figure 6.1: Supervisory system.

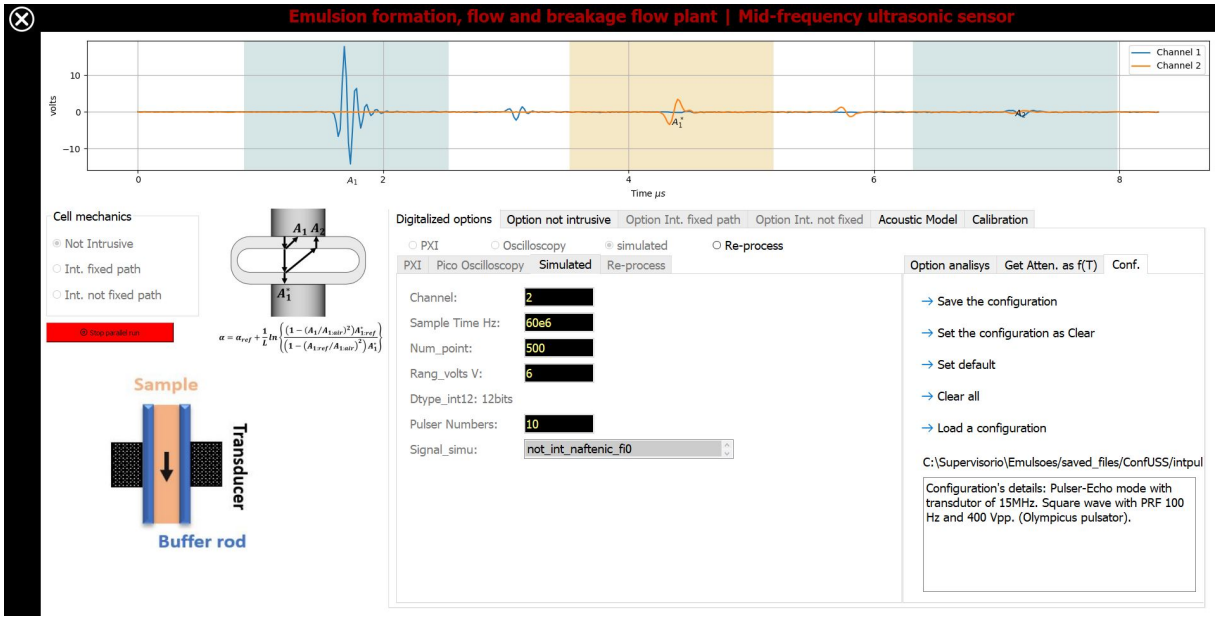

Figure 6.2: Supervisory system of the ultrasound sensor.

The supervisory system was developed in Python and comprises two main loops (Figure 6.3). The first loop involves reading, saving, and plotting the data history. The data pertains to the process variables monitored and manipulated through the PLC (programmable logic controller). Another monitored variable is the dosing pump, whose communication occurs via serial signal. The ultrasonic variables were monitored through another loop running in C++, necessitated by the requirement for faster processing of the ultrasonic signals.

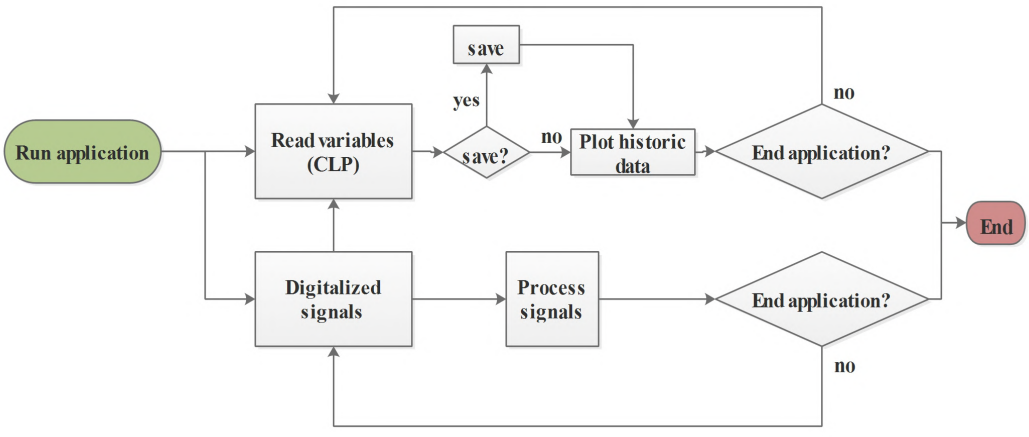

Figure 6.3: Supervisory system of the ultrasound sensor.

6.3 Materials and methods applied to demulsification dynamic analisys

This section describes the materials applied to the results of chapter 7.

6.3.1 Dynamic analysis

In the present work, we monitored the real-time response of the emulsion viscosity caused by a disturbance in the demulsifier dosage. In other words, the analyzed system was considered SISO (single-input, single-output). We chose a kinetic model of the first order to model the change in emulsion viscosity because this expression best fitted the dynamic data. The parameters of the model chosen were interpreted concerning the physics of the demulsification phenomenon.

Eq. 6.1 presents the function used to model relative viscosity response to input as the ramped fixed value function. The input function represents the demulsifier concentration. In Figure 6.4 and Eq. 6.1, K_p is the process gain (-/ppm), θ the system dead time (min), τ the process time constant (min), and $C(t)$ the demulsifier concentration (ppm). The function parameters of inputs A_C and φ represent the total amplitude of the function and the duration of the ramp, respectively. The variable $\mu_r(t < \theta)$ represents the stead-state of the relative viscosity before the disturbance promoted by the $C(t)$.

$$\mu_r(t) = \left\{ \begin{array}{c} \mu_r(t=\theta)\, for\ t \leq \theta \\ \frac{A_c K_p}{\varphi}\left(t + \tau e^{\frac{t-\theta}{\tau}} - \tau - \theta\right) + \mu_r(t=\theta)\, for\ \theta < t < \varphi \\ \frac{A_c K_p}{\varphi}\left(\tau e^{\frac{t-\theta}{\tau}} - \tau e^{\frac{t-\varphi}{\tau}} - \theta + \varphi\right) + \mu_r(t=\theta)\, for\ t \geq \varphi \end{array} \right\} \tag{6.1}$$

We used Eq. 6.1 to adjust the transfer function parameters in the demulsification dynamics using curve fitting implemented in Python based on the least squares method. Once adjusted, these parameters are used to interpret how variables such as temperature, flow rate, and others interfere with the studied phenomenon dynamics.

6.3.2 Emulsion preparation

Initially, we weighed the oil and the emulsifier in a vessel. Then, we homogenized this mixture. After that, the homogenizer remained on for 210 seconds while we gradually placed the water

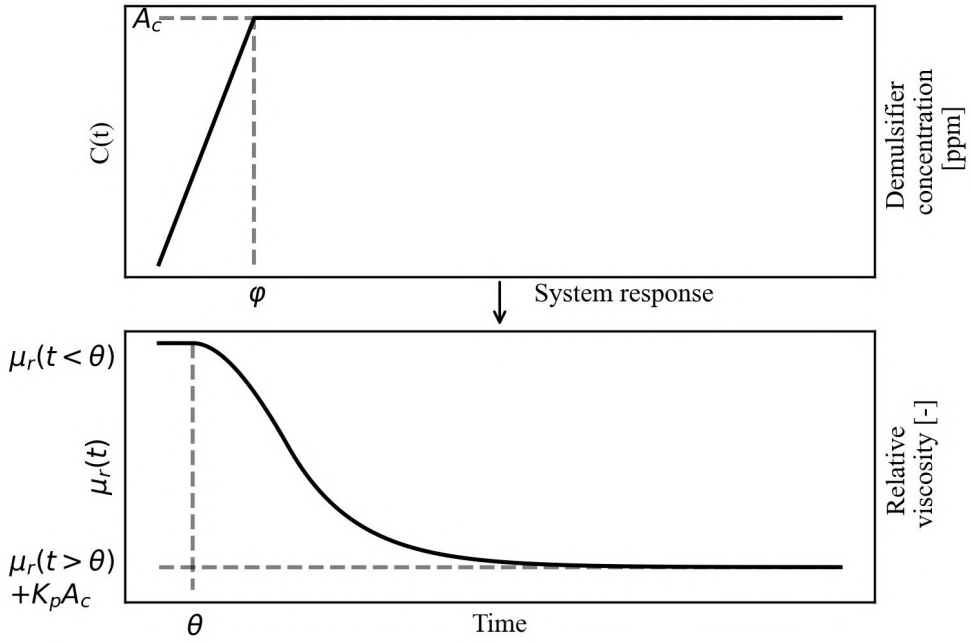

Figure 6.4: The representation of the applied ramp disturbance and the model response of the system.

in the vessel until reaching the desired dispersed mass fraction, and the whole sample formed a stable emulsion. We used a high-power industrial homogenizer (Semco, model ME-100, Brazil) set to 3330 rpm. This procedure was realized at room temperature.

6.3.3 Experimental setup

The setup consists of a tank (TK-101), two peristaltic pumps (P-101 and P-102), a gear pump (P-103), and pressure and temperature transmitters (Figure 6.5). In the close circuit, the emulsion flows through a PVC silicone tube of 8 mm with an internal diameter of 5.5 mm and 9 m in length. This tube diameter was chosen to reduce the emulsion residue generated.

The peristaltic pumps operated automatically, according to the flow information sent by the controller. The pumps had more than three rollers, which did not result in fluctuations in the pressure taps. In other words, the speed of the flow was maintained constant and without oscillations.

The P-101 pump doses the demulsifier into the TK-101 tank. The peristaltic pump P-102 moved the emulsion from the tank to the circuit. After pump P-102, the emulsion passes through temperature transmitter 1 (TT101), absolute pressure transmitter (PT101), and differential pressure transmitter 1 (PDT101). At this point, we used differential pressure and temperature measurements to characterize flow viscosity at the output of pump P-102. We

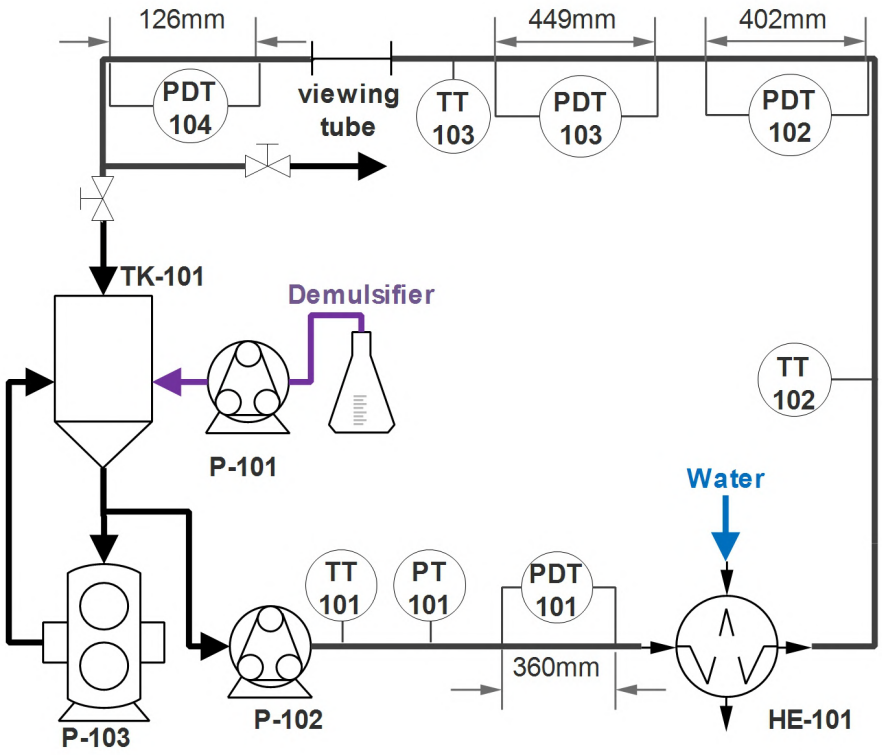

Figure 6.5: Schematic diagram of the experimental setup.

installed a gear pump (P-103) to homogenize the emulsion in the tank and simulate a high-shear obstacle in the flow. This pump recirculates the emulsion between pump P-103 and the tank, provoking the shear to the emulsion.

After PDT101, the fluid flows into the heat exchanger (HE-101) to achieve the desired flow temperature. Then, the emulsion passes through temperature transmitters (TT102 and TT103) and pressure drop transmitters (PDT102, PDT103, PDT104) and returns to the tank. The viscosity collection points (PDT101 to PDT104) aimed to monitor possible changes in the rheology of the emulsion during the flow. The flow distances between the PDT101-PDT102, PDT102-PDT103, and PDT103-PDT104 transmitters were 2, 4, and 2 m, respectively. We chose different measurement lengths due to the transmitters' sensitivity in measuring high-pressure values (Figure 6.5). The transmitters with greater capacity to measure high-pressure drops had more extensive lengths, such as the (PDT103) and (PDT102).

We placed a horizontal visualization section between temperature transmitter 3 and pressure drop transmitter 4 to observe the flow pattern during the emulsion destabilization. Before the tank, there is a bifurcation to take out small samples or to dispose of the material. Table A.1 describes the technical specification of each circuit item.

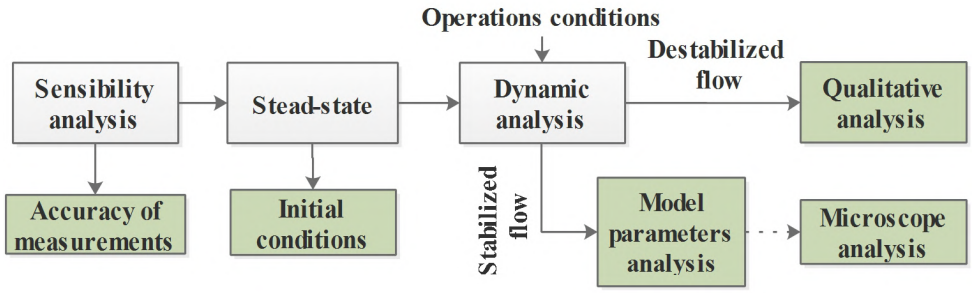

Figure 6.6: Flowchart of the presented results topics.

6.3.4 Experimental procedure

The schedule to perform the dynamic analysis of the demulsification process follows three procedures. In the first one, we analyzed the sensitivity of viscosity measurements by evaluating the accuracy of measurements made by pressure drop transmitters. The characterization of steady-state analysis for several different operating conditions was the second procedure. To conclude the procedure, we performed the dynamic analysis (Figure 6.6).

To analyze the sensitivity of the transmitters, we put pure oil at 22°C We compared the measurements presented by the transmitters with the viscosity measured by a rheometer. The oil viscosity was measured in cooperation with one laboratory at the Federal University of Rio de Janeiro. The data is available in item A.3.

We feed the closed circuit with 1.4 L of the emulsion to analyze the steady state. The emulsion circulated in the closed-loop circuit until it reached a steady state. This steady state is identified by monitoring all measured variables. After reaching the steady state, the variables are stored. We did this procedure for various operating conditions of interest. It is worth highlighting that the residence time in tank TK-101 remained below 1 minute. The fluid level in the tank was low enough to guarantee that even if the emulsion broke, it would not separate the phases in the tank.

For the dynamic analysis (Figure 6.6), similar to the steady-state analysis, the circuit was expected to reach the steady state under desired operating conditions. After reaching it, we started to dose the demulsifier with the pump P-101.

We calculated the amount of demulsifier added based on the dosing time to achieve the desired demulsifier concentration in the circuit. This time corresponds to the input ramp duration, as shown by the variable ϕ in Eq. 6.1 and Figure 6.4. The dosing time is equivalent to

the circuit's flow residence, and the dosing pump's flow rate is proportional to the demulsifier dosage in ppm.

The pump P-101 remains on for a time similar to the residence time of the fluid circulating in a closed-loop system, which was 28, 14, and 9.3 minutes for 40, 80, and 120 mL/min, respectively. This residence time is the time required for an emulsion package to leave the demulsifier dosing point to flow through the entire circuit and return to the dosing point again.

We adjusted the model (Eq. 6.1) to the dynamic data through an optimization algorithm based on the minimization of quadratic errors developed in Python.

Finally, to evaluate qualitatively (Figure 6.6) the flow pattern developed during the destabilization of the emulsion, an experimental run was elaborated with several dosages of demulsifier. We filmed a horizontal flow section throughout the experiment at 30fps.

6.3.5 Experimental matrix of dynamic analysis

In the steady-state analysis, we tested a wide range of operating conditions. We analyzed a larger range in volume flow rate ranging from 20 to 120ml/min, temperature between 22 and 50°C, and a dispersed phase fraction from 0 to 50% totaling 5 points of flow, 4 of temperature, and 5 of dispersed phase fraction, respectively. This wider range of the steady-state analysis was important in deciding which operating conditions to use in the dynamic analysis (Table 6.2).

For dynamic analysis, we chose the flow rates based on the sensitivity limits of the pressure drop sensors. The flow rates were 40, 80, and 120 ml/min. The pressure drop saturates the sensors at values above 120 ml/min. In addition, values above this threshold would lead the absolute pressure of the system (measured through the PT-101 sensor) to values above 6 bar. The high pressure might cause insecurity to the connections of the pipe used.

We selected three different fractions of the dispersed phase, namely 30%, 40%, and 50%, as these points correspond to the highest viscosity values. Additionally, preparing an emulsion with a water content exceeding 50% proved challenging due to its proximity to the inversion point. The fractions below 30% of water had a nonrepresentative viscosity to the issue we studied.

Table 6.2: Experimental matrix of dynamic analysis of demulsification.

	Circuit operating conditions			
Experimental runs	**Temperature (°C)**	**Volumetric flow (mL/min)**	**Dispersed phase fraction (%)**	**P-103 pump activation (%)**
1	30	80	40	0
2	40	80	40	0
3	50	80	40	0
4	40	40	40	0
5	40	120	40	0
6	40	80	30	0
7	40	80	50	0
8	40	80	40	20
9	40	80	40	40

To examine the influence of temperature on the process dynamics, we chose to analyze the emulsion at 30°C, 40°C and 50°C. The upper-temperature limit of 50°C was set considering the materials' resistance limitations used to construct the circuit.

Furthermore, we opted for three distinct levels of shear pump activation. The maximum limit of 40% was defined due to the significant interference with the circuit's temperature caused by values beyond this threshold, as the pump heats the fluid.

We performed the experimental runs with an average duration of 4 hours each. Table 6.2 presents the variables that were manipulated in the demulsification dynamics analysis.

6.3.6 Microscopic analysis

We examined the morphology of the droplets by light microscopy using an Axio Scope A1 microscope (Carl Zeiss, Gottingen, Germany) with an oil immersion objective lens at 100x magnification at room temperature. We took 2 samples referring to the experimental run with and without activating the pump to verify its influence on the average size of the drops. We collected the samples through aliquots removed from the circuit after they reached the steady-state under the desired operating conditions. We added Nile red dye to the sample to help distinguish the emulsion phases.

6.4 Materials and methods applied to demulsification control analysis

6.4.1 Preparation of the emulsion

26 L of emulsion were prepared with emulsion with 40% w/w water content and 8 L with 50% w/w water content. The emulsion was prepared in a batch series. In each batch, the oil and water were weighed separately. 2 L of emulsion was prepered, considering their specific mass (Table 6.1).The prepared emulsion was placed in the TK102 tank.

6.4.2 Experimental apparatus

The circuit consists of two tanks (TK101 and TK102) where the emulsion is stored. The TK101 tank can store 25 L of emulsion. The TK102 tank, with a capacity of 1 L, serves as a buffer tank, in which the level is manually controlled to keep the sample in circulation. Fig. 6.7 represents the circuit diagram built to analyze the control strategy.

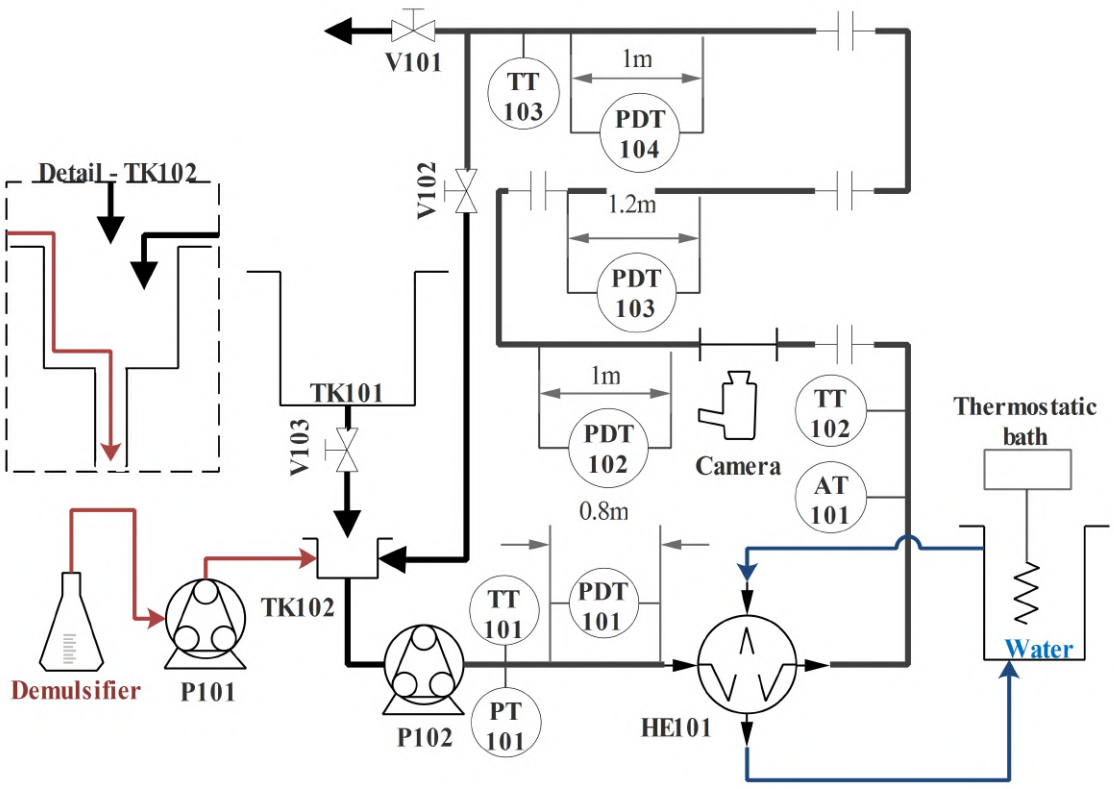

Figure 6.7: Experimental apparatus used to evaluate the controller.

The sample circulates in the circuit through the P102 pump. This pump is set to operate at a fixed flow rate. The circuit has several differential pressure transmitters in series (PDT101 to PDT104). These transmitters were used to infer the sample viscosity at various points in the circuit. The temperature transmitters (TT101 to TT102) were used to assist in the viscosity analysis and the emulsion characterization by the analysis transmitter (AT101).

The circuit temperature was controlled using a one-pass shell-tube heat exchanger (HE101). We use a bath that controls the temperature of the hot water and exchanges heat with the emulsion in the circuit. In addition to the heat exchanger, a thermal insulator was used in the pipes using a sponge rubber tube. The circuit has a length of 9 m of stainless-steel piping with a diameter of 12.7 mm. A 1 m section of acrylic piping was installed after the TT102 transmitter to film the flow. Filming was carried out at 30 fps.

The P101 pump was responsible for dosing the demulsifier in the circuit. The diluted demulsifier is dosed into the pipe located at the bottom of the TK102 tank, close to the suction of the P102 pump (Details in Fig. 6.7). The exit of the dosing tube was installed at this point to approximate the industrial operation in which the demulsifier is dosed directly into the line, already pressurized.

The two valves installed at the end of the circuit, after the TT104 transmitter, are intended to open or close the circuit. In the open circuit, valve V101 is closed, and valve V102 is open. The entire sample is discarded. In the closed circuit, however, valve V101 is open, and V102 is closed. The sample returns to the TK102 tank and remains circulating in the circuit. Aliquots were taken from the emulsion flowing through the sample outlet after valve V102. These samples were placed in 25 ml graduated cylinders.

The analysis transmitter (AT101) is the ultrasonic sensor coupled to the line. The device and the system (Fig. 6.8), detailed in previous works (SILVA *et al.*, 2020; SARAIVA *et al.*, 2023), comprises a pair of transducers TR-A and TR-B (Parametrics model V113). The ultrasonic signal digitization system comprises an oscilloscope system from PXI (National Instrument, PXI 12 bits) with a sampling rate of 60 MHz. The transducer excitation device (Olympus NDT, Parametrics 5077PR) emits and receives the reflected signal. The cell is composed of acrylic. The details of its construction and the software used to process the signals are present in the works of (SARAIVA *et al.*, 2024).

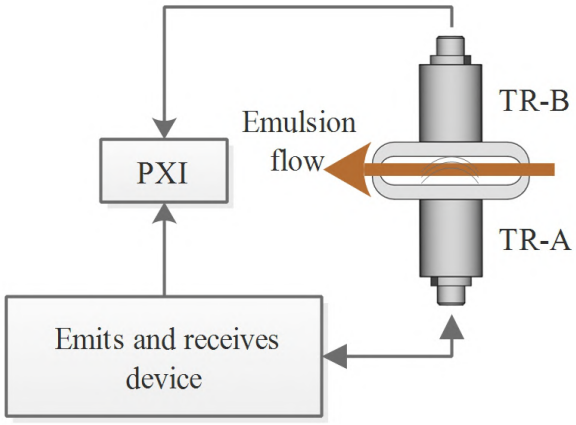

Figure 6.8: Illustration of the system that makes up the AT101.

6.4.3 Experimental procedure

The constructed circuit was operated in two different configurations: open and closed. The volumetric flow rate was set at 120 ml/min in all experimental runs. This flow rate was chosen due to the high viscosity of the oil. Flows greater than this increase the pressure in the system to values close to the safety limits of the connections. Therefore, this value represents the maximum capacity of the circuit and is ideal for observing the change in viscosity inferred by the differential pressure drop points.

Close circuit operation

In close-circuit operation, the emulsion was placed in the TK101 tank, and the pump P102 was activated. Valve V103 was opened until half of the maximum emulsion level in tank TK102 was reached. After reaching the level, the valve is partially closed to guarantee control at the level reached, i.e., the incoming flow is close to the outgoing flow. The emulsion passes through all the sensors until it reaches the end of the circuit. When the emulsion returns to the TK102 tank, valve V103 is closed. The emulsion remains circulating the circuit until it reaches a steady state. After the system reached the stationary state, when the monitored variables did not change, the experiment was started.

The closed circuit was used in two experimental procedures (Fig. 6.9). The first was developed to monitor chemical demulsification in closed-loop flow. The second was

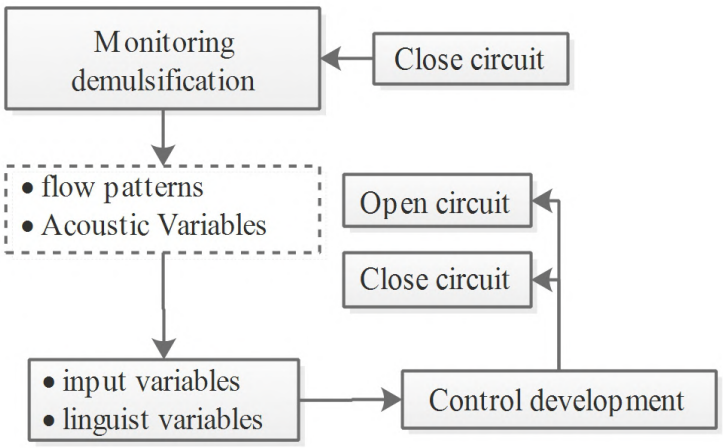

Figure 6.9: Flowchart of experimental procedures performed.

developed to apply the developed controller in the closed circuit. These procedures are described below.

- **Demulsification monitoring:** The P101 pump was activated to dose 0.3 ml/min of demulsifier into the flow. The dosage promoted by the P101 dosing pump gradually increased the concentration of the demulsifier in the circuit. The flow was analyzed qualitatively by filming and the aliquots removed and quantitatively by acoustic variables and viscosity monitored during the experiment (Fig. 6.9).

  The procedure used was to apply a continuous dosage in the circuit until the flow pattern stratified SW was established. We analyzed three experimental runs. The first condition referred to an emulsion with a water content of 40% w/w flowing at 40°C, the second to an emulsion with 50% of water at 40°C, and the last to an emulsion with 40% at 50°C. These analyses were used to choose the controller input variables.

- **Closed circuit demulsification control:** The controller evaluation procedure began analogously to the previous procedure. However, the controller is activated after the variables reach a steady state instead of the P-101 pump being set to a specific flow rate. This experiment evaluated the system dynamics with the controller and whether it acts appropriately, dosing the emulsifier until a desired flow pattern is reached.

Open circuit operation

In the open circuit operation, the emulsion was placed in the TK101 tank, the V103 valve was opened, and the P102 pump was activated. After reaching half the maximum level of the TK102 tank, valve V103 was partially closed to control the level reached. The emulsion flows through the circuit and returns to the TK101 tank. As the volume of this tank is large, i.e., the time for a sample to circulate is long (approximately two hours), the circuit presents the characteristics of an open circuit. When the monitored variables reached a steady-state, valve V101 was opened, the circuit output was removed from the TK101 tank to a disposal container, and the analysis was started. The open circuit was used to evaluate the demulsification control developed (Fig. 6.9). Therefore, the analysis begins with activating the automatic demulsifier dosage control through the P101 pump.

6.4.4 Control input variables

Six acoustic variables were used at the input of the fuzzy controller. The first four variables chosen were the dispersion of sound speed c, m/s (Eq. 4.12), reflection coefficient R_{12} (Eq. 4.10), acoustic attenuation α, np/m (Eq. 4.11), and relative echo amplitude in sample K. The dispersion was calculated through the standard deviation of the variables monitored over time. Eq. 6.2 presents the calculation of the standard deviation of the variables, with x being the acoustic variable.

$$\sigma_x = \sqrt{\sum_{i=1}^{n} |x_i - \bar{x}|^2 / n} \tag{6.2}$$

The constant n refers to the number of samples (length of the time series) to which the standard deviation calculation is applied. Therefore, the calculated standard deviation in monitoring refers to the 60 data points before the current time ($n = 60$).

The relative amplitude was calculated through the ratio between the maximum amplitudes of the pulse signal clipping (A_{pulser}) between 2 and 2.8 μs and the A_1 echo. During this period, the signal would naturally not present echoes (Fig. 4.3). However, due to the phase segregation promoted by demulsification, the signal is reflected in the sample between the interfaces of the segregated phases. Fig. 6.10 shows the cutout of the pulse signal (A_{pulser}), highlighting the sample zone between points p_1 and p_2.

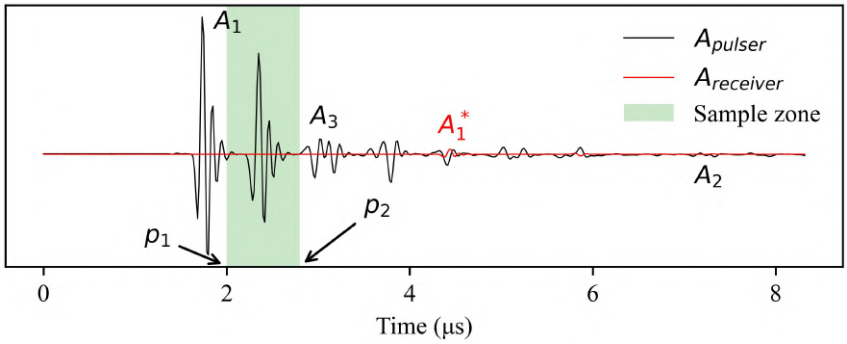

Figure 6.10: Clipping of the pulse signal where the echo appears in the sample.

Eq. 6.3 calculates the relative amplitude K. With the term $A_{zone:sample}$ calculated through Eq. 6.4, in which Fast Fourier Transform FFT is used to calculate the spectrum of the pulse signal A_{pulser} cut between p_1 and p_2. The $argmax$ function returns the frequency at which the amplitude of the signal spectrum reached the maximum value. In this way, the relative amplitude of the echo in the sample is only considered if its central frequency is greater than 2 MHz. This range eliminates the effect of possible noise in the sample zone, ensuring that only echoes will be considered.

$$K = \begin{cases} \frac{max\left(A_{zone:sample}\right)}{max(A_1)} & if\ argmax\left(A_{zone:sample}\right) \geq 2e6 \\ 0 & if\ argmax\left(A_{zone:sample}\right) < 2e6 \end{cases} \tag{6.3}$$

$$A_{zone:sample} = FFT\left(A_{pulser}\left[p_1, p_2\right]\right) \tag{6.4}$$

With the relative echo amplitude data in the sample, it was possible to calculate the sample echo frequency using Eq. 6.5. This frequency translates into the number of echoes in n times and was the fifth variable. In this case, n represents 60 samples. This sum considers whether or not echoes appear in the sample with values 1 and 0, respectively.

$$f_K = \frac{1}{n}\sum_{i=0}^{n} k_n \begin{cases} k_n = 1 & if\ K > 0 \\ k_n = 0 & if\ K = 0 \end{cases} \tag{6.5}$$

The last acoustic variable used as input into the control system was relative speed. Relative speed calculates how far the emulsion speed is from the oil speed c_o and water c_w, under the same temperature conditions T. This relative speed was calculated using Eq. 6.6. Using this variable, it was possible to mitigate the effect of temperature on the control system. It is well known that the speed of sound in the emulsion is temperature-dependent. Thus, the relative

speed calculation becomes more comprehensive, being able to characterize and standardize the flow at different temperatures. In Eq. 6.6, $\bar{c}$ represents the moving average of the speed of sound in the emulsion (Eq. 6.7). The n is the number of samples used in calculating the moving average.

$$c_{rl} = \frac{c_w(T) - \bar{c}}{c_o(T) - c_w(T)} \tag{6.6}$$

$$\bar{c} = \frac{1}{n} \sum_{i=0}^{n} c[i] \tag{6.7}$$

The input vector of the fuzzy control $\{x_1, x_2, .., x_n\}$ (Fig. 4.4), was therefore $\sigma_{R_{12}}$, σ_c, σ_α, σ_K, f_K, and c_{rl}.

6.4.5 Fuzzy control developed

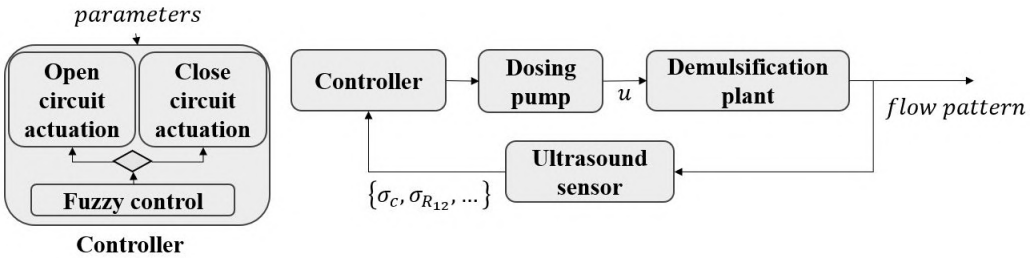

Figure 6.11: Illustration of the fuzzy control system implemented to act on the demulsifier dosage.

The implemented controller, illustrated in Fig. 6.11, is composed of the fuzzy controller block that represents the system illustrated in the diagram in Fig. 4.4. This diagram depicts a fuzzy control system designed to classify the demulsification in the flow by analyzing the flow patterns inferred through the ultrasonic input variables. Once the flow pattern is determined, the performance of the controller is calculated in the consequent layer, which returns the manipulated variable's variation. In this case, the manipulated variable is represented by u, which is the demulsifier flow variable operated by the pump P101. Similarly, $du*$ represents the increment to this variable after the control calculation.

After calculating the centroid (Fig. 4.4), $du*$ is denormalized to return the variable value on the standard scale du (Fig 6.12). The limits $\{du_{min}, du_{max}\}$ represent the maximum and minimum variation of the manipulated variable, considering the effort of the process actuator. -2 to 2 ml/min was considered the maximum and minimum variation.

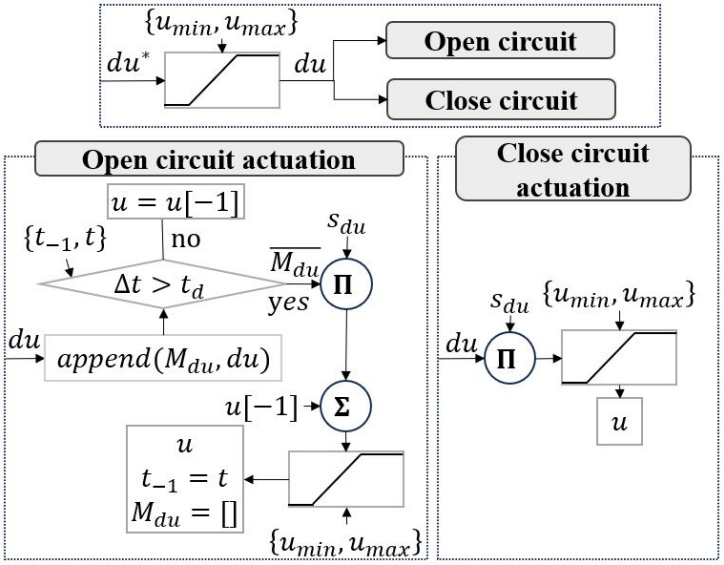

Figure 6.12: Actuation calculation block for open and closed circuits.

After calculating du, if the system operates in an open circuit, the value of du is allocated to the M_{du} list, stored in memory. If the system operates in a closed circuit, the value of du is multiplied by S_{du} and subjected to saturation of the actuator (Fig. 6.12).

The parameters t_{-1} and t represent the last and current actuation times, respectively. In the open circuit, after storage, if the elapsed time of the last actuation ($t - t_{-1}$) is greater than or equal to the controlled delay time t_d, the average of the list with the values of du ($\bar{M_{du}}$) is multiplied by the parameter S_{du} and added to the last actuation the control sent to the actuator $u[-1]$, resulting in the actuation value u. After this, the value of u is subjected to maximum and minimum saturation of the actuator $\{u_{min}, u_{max}\}$. This saturation is related to the dosing pump maximum and minimum flow values ranging from 0 to 2.5 ml/min. Finally, the M_{du} list is emptied, and the last actuation time receives the current time ($t_{-1} = t$).

The parameters S_{du} and t_d are related to the controller dynamics. The higher the S_{du} value, the faster the controller will act on the system. However, this rapid action can cause high fluctuations in the classification of flow patterns by the fuzzy system, leading to inefficient demulsification control. Very low values of S_{du} promote a very slow response of the controller in the system. Since it was impossible to build a model to simulate the application of the control and optimally tune these parameters due to the characteristics of the studied process, a value of 0.015 and 0.15 was stipulated for S_{du}, for the open and closed circuits, respectively. The delay time t_d was set at 20s. This parameter is important to minimize the frequency of

actuation changes and mitigate the effect of the system dead time since the dosing point is far from the ultrasonic sensor (Item 6.4.2).

Chapter 7

Results and discussion - Demulsification dynamic

7.1 Analysis of the sensitivity of the viscosity measurements

The analysis of the sensitivity of the transmitters was essential to ensure the accuracy of the viscosity measurements. We calculate the error between viscosity calculated through the pressure drop measurements of the transmitters and the rheometer measurement in Table 7.1. Viscosity is calculated by applying Equation 4.5. The viscosity data in Table 7.1 represent the mean and standard deviation of 5 viscosity measurements at ambient temperature 22°C and shear rate ranging from 5 to $30s^{-1}$. The oil viscosity values measured through the rheometer were 0.369, 0.228, 0.124, and 0.068 Pa.s for the 22, 30, 40, and 50°C, respectively (see supplementary material item A.3). We observed that within this margin, all sensors presented consistent readings with an error below 3.6%.

7.2 Analysis of the steady states of the flow

The steady-state analysis helps identify the initial conditions for dynamic analysis under various operating conditions. We established the initial steady state when all variables exhibited constant behavior. Consequently, these points defined the initial steady state in the dynamic function $\mu(t \leq \theta)$ in 6.1.

Table 7.1: Sensitivity of the viscosity measurements of the differential pressure transmitters with the measurements performed by the rheometer at an ambient temperature of 22°C.

Pressure differential transmitters	Viscosity measured (Pa.s)	Viscosity measured by the rheometer (Pa.s)	Error (%)
PDT101	0.368±0.005	0.369	1.67
PDT102	0.371±0.004		1.75
PDT103	0.366±0.009		3.64
PDT104	0.361±0.022		2.88

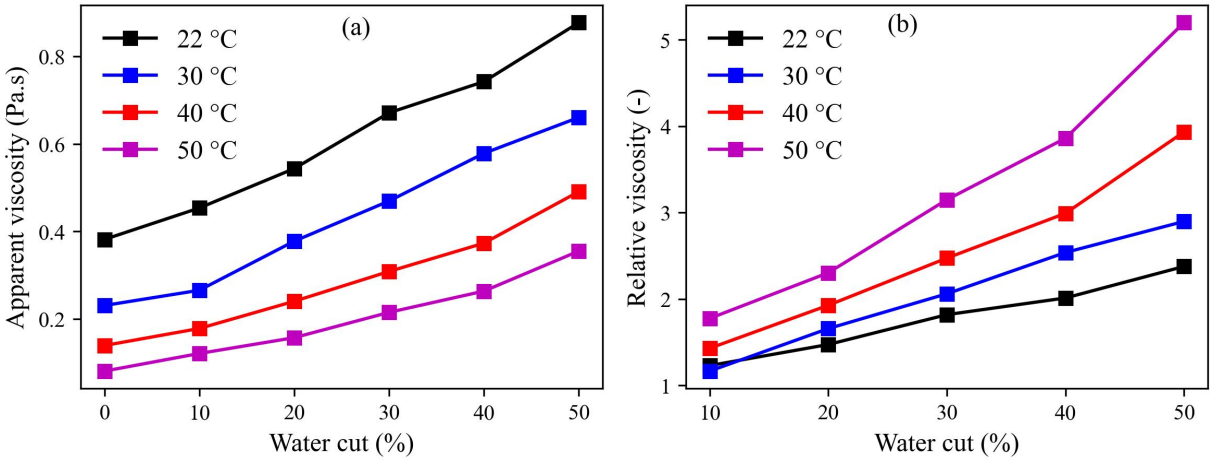

Figure 7.1: The steady state for (a) apparent viscosity and (b) relative viscosity of the emulsion flow for different water fractions and temperatures at 80 mL/min.

The steady-state analysis applied to the viscosity showed a behavior summarized in Figure 7.1, where each graph point represents the viscosity value for a steady state. In Figure 7.1a and Figure 7.1b, we made the measurements in terms of apparent viscosity (Equation 4.5) and relative viscosity (Equation 4.6), respectively. We performed these measurements using the differential pressure transmitter 2. Regarding the dispersed phase fraction (water cut), we needed to increase tension to promote their flow when we increased the fraction because of the increased viscosity.

The non-Newtonian behavior of the emulsion was another point observed. In Figure 7.2, the emulsion flows more easily as the shear rate increases. The shear rate was calculated using Equation 4.7. This behavior characterizes a pseudoplastic fluid and is more evident for emulsions with a highly dispersed phase content. These measurements were important in analyzing the dynamics of demulsification at various volumetric flows.

The final steady-state analysis focused on examining the impact of the shear pump (gear pump P-103) on viscosity. We tested different shear pump activation levels and presented the

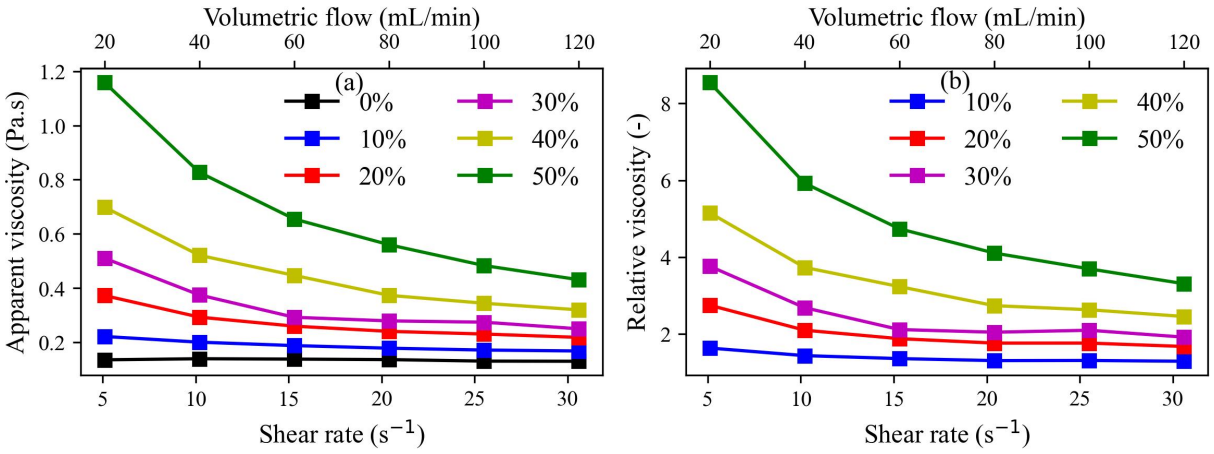

Figure 7.2: Emulsion (a) apparent viscosity and (b) relative viscosity for different shear stress and water fraction at 40°C.

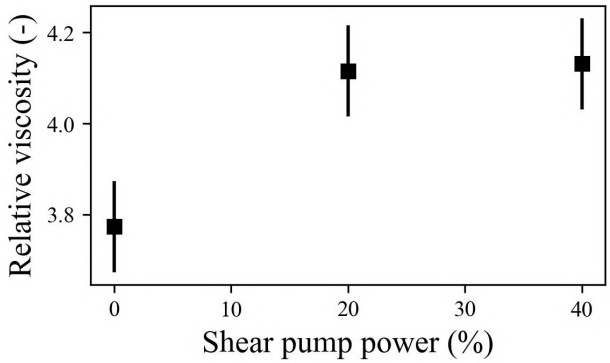

Figure 7.3: Steady-state relative viscosity of the emulsion flowing at a volume flow rate of 80 mL/min and 40°C under varying levels of shear pump activation.

results in Figure 7.3. The graph shows the increase in emulsion relative viscosity when we raised the level of pump activation. However, the increase was not significant for different levels of pump activation. The relative viscosity values for 20 and 40% were within the same margin, considering the error of 0.1 in the measure (calculated through the error data in Table 7.1). Despite that, the effects of these two measures on dynamic analyses were significant. In general, we observed that the gear pump promotes a high shear in the emulsion, significantly decreasing the drop size and increasing the fluid viscosity.

7.3 Dynamic analysis

The first few minutes in the experimental run were necessary for the system to achieve a steady state. After reaching this state, we started the demulsifier dosage. The dynamic analysis began at this point. We applied two different ramp inputs of demulsifier dosage in order to verify

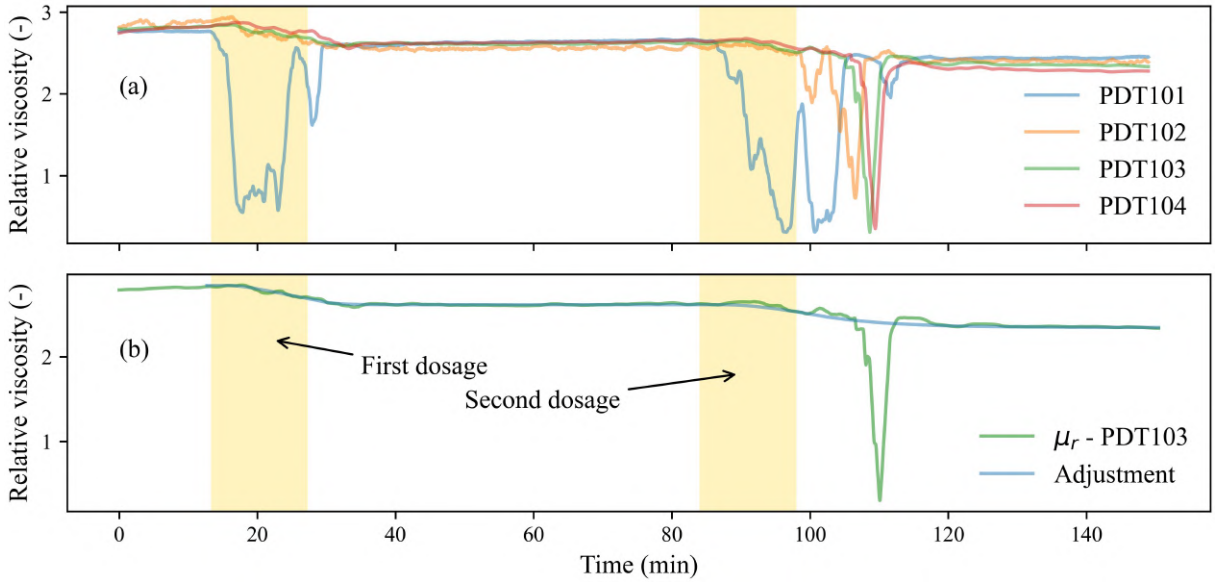

Figure 7.4: Graphical representation of the data collected for the experimental (a). Adjustment of the first-order transfer function in the demulsification dynamics for changes in demulsifier concentration (b). Curve refers to the experimental run 2 - (Table 6.2).

the non-linearity of the process in relation to its gain. Therefore, we dosed the emulsifier at a constant rate until it reached the desired amount of demulsifier. The first ramp ended at 100 ppm and the second at 200 ppm, resulting in a total of 300 ppm at the conclusion of the analysis. Figure 7.4a presents the data collected while analyzing the flow dynamics of experimental run 2 (Table 6.2). After collecting the time series, the data were fitted to the model proposed in Equation 6.1. We submitted the entire set of experimental runs to adjust to this model. Figure 7.4b shows the application of the adjustment to the viscosity dynamics. We analyzed model parameters considering the effect of different operating conditions in the following items.

It is worth highlighting in Figure 7.4 that the abrupt fall and oscillation in the relative viscosity, especially for PDT101, occurs because its transmitter is close to the dose point. As the demulsifier is dosed at a point, its concentration close to that point is high. However, as the flow carries it, it tends to homogenize.

7.3.1 Effect of operating conditions on the process gain

The process gain represents how much the relative viscosity changed due to demulsifier concentration. We start from a steady state, so we apply the first and then the second doses. There is a gain related to each dosage. The summarization of the effect of operating conditions on the process gain is in Figure 7.5 for the first and second dosages.

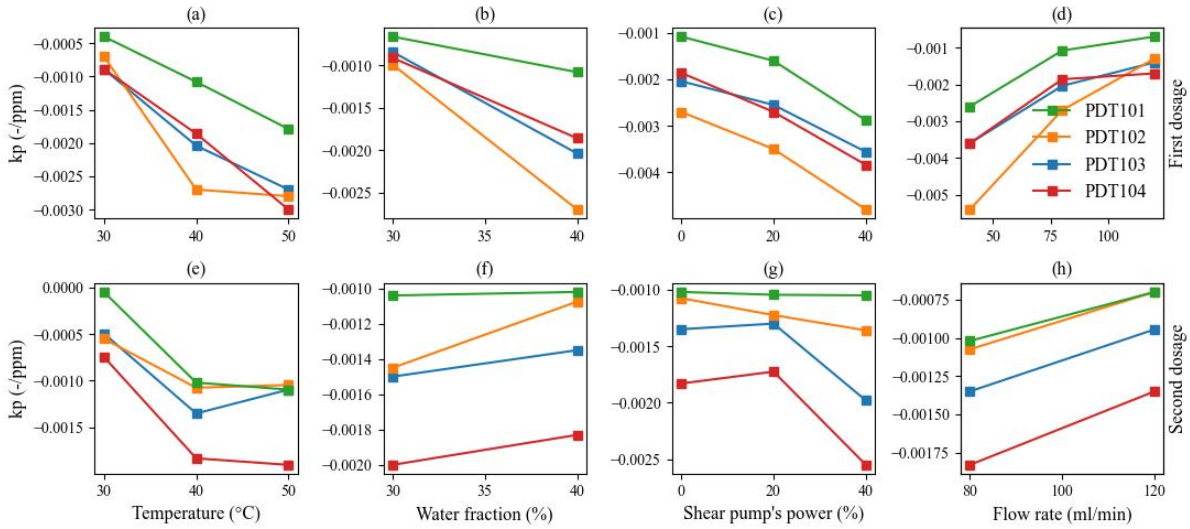

Figure 7.5: Effect of operating conditions on the process gain. The first and second row represents the first (100ppm) and second dosages (200ppm), respectively.

The pressure transmitters perceive the drop in viscosity according to the distance between the dosing point at the tank and differential pressure measuring points. Thus, the demulsification efficiency in relative viscosity followed the order PDT101 < PDT102 < PDT103 < PDT104. The PDT104 was located farther from the tank, so the demulsifier diffused more effectively and had more time to act during the flow. Therefore, the longer the demulsifier resides in the emulsion, the better its effectiveness. This result corroborates the observations made by some studies (KOKAL, 2005; RAJAK *et al.*, 2016; YONGUEP *et al.*, 2022). However, for some operational points for the first dosage (Figure 7.5a, Figure 7.5b, Figure 7.5c, and Figure 7.5d), PDT102 presented a more significant gain than PDT103 and PDT104. This behavior occurred because the PDT102 was installed after the heat exchanger (Figure 6.5). This increase in temperature implied an acceleration in the demulsification process promoted by the increase in temperature. Between PDT102 and PDT103, a re-emulsification may have occurred due to the distance and the natural decrease in temperature. It is worth noting that the effect of temperature on viscosity was compensated because the analysis was done in terms of relative viscosity. Furthermore, we observed that the values of gains tended to be smaller as we added demulsifier (Figure 7.5). In other words, the process gain was more expressive in the first dosage than in the second.

Figure 7.5a and Figure 7.5e show the effect of temperature on the process gain for the first and second dosages of the demulsifier. At high temperatures, there is a decrease in the continuous phase's viscosity, which increases the demulsification efficiency. When the

continuous phase's viscosity decreases, the demulsifier has a better diffusion. This proportionality tends to be maintained up to a specific temperature, as observed in tests in the literature (BALSAMO *et al.*, 2017).

The higher the water fraction in the emulsion, the higher its viscosity (Figure 7.1). For the first dosage, the higher the water concentration, the greater the system gain with the addition of the demulsifier (Figure 7.5b). As the emulsion with a high water content drops are already close to each other, the demulsifier's action is more significant in terms of reducing viscosity; that is, it is more efficient. In the second dosage (Figure 7.5f), despite the process gain being slightly lower at 40% water fraction than at 30%, the sum of the gains from the first and second dosages were much greater at 40%. The analysis performed with water fraction values of 50% destabilized the emulsion.

The shear promoted by the gear pump created an ascendent trend toward the process gain in modulus and pump activation for the first dosage (Figure 7.5c). The initial relative viscosity of the system with the pump activated at 20 and 40% were close (Figure 7.3). However, the drop in viscosity with the addition of the demulsifier was more significant with the higher pump activation level. For the second dose (Figure 7.5g), the gains for the gear pump at the turned-off state and active state at 20% were very close, except for the differential pressure transmitter 2. Similar to the 40% water fraction analysis, the overall process gain is higher for the highest shear pump's power. The greatest drop in viscosity for the high-shear system is due to the reduced droplet size promoted in this system. The smaller the droplets, in other words, the finer the DSD, the higher the emulsion viscosity will be. In this highly viscous system, the addition of the demulsifier will promote a more pronounced decrease in viscosity.

The microscopy analysis offers valuable insights into the emulsion's morphology. In Figure 7.6, we compared experimental runs 2 and 9. The first row of Figure 7.6 demonstrates the natural tendency for droplets to grow with the amount of demulsifier in the flow, as evidenced by the average droplet sizes for the initial, first (100ppm), and second (300ppm) dosages. When the shear pump was activated, we observed a reduction in average droplet size, as seen in the second row of Figure 7.6. This finding corroborates the circuit viscosity analysis, which shows that the emulsion relative viscosity increases when the gear pump is on due to the added shear reducing the droplet sizes.

Finally, volume flow rate highly influenced process gain (Figure 7.5d and Figure 7.5h). The relationship between the flow rate and the process gain is inversely proportional. We observed

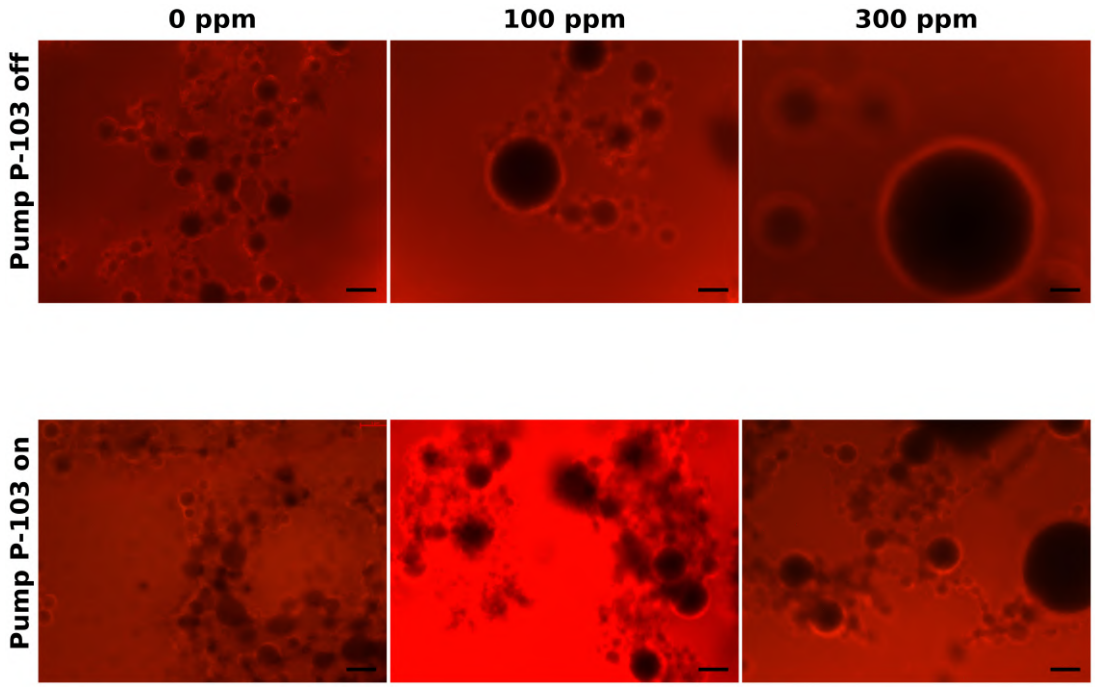

Figure 7.6: Microscopy analysis of samples from experimental runs 2 and 9 (Table 6.2). Sample referring to the original emulsion, the first and second dosing with the shear pump on with power on and at 40%. We used Axio Scope A1 light microscope (Carl Zeiss, Germany) with a scale of 5 μm.

this behavior for both the first and the second dosage. The cause of this behavior is the re-emulsification of the fluid due to the shear promoted by high flow rates. Furthermore, there is a forces balance between the demulsification and re-emulsification processes. While the diffusion of the demulsifier through the flow favors demulsification, high flow rates favor the re-emulsification process. The second dosage applied to the emulsion flowing at 40 ml/min destabilized the emulsion.

7.3.2 Effect of operating conditions on the process time constant

The process time constant represents the time required for the monitored variable (relative viscosity) to reach approximately 64% from its initial to the final value, indicating the speed at which the process reaches a new steady state. In our system, the time constant is associated with the various operational conditions studied and the position of the transmitters, as shown in Figure 7.7. For all results, the longer the distance between the dosing point and the transmitters, the greater the time constant value. As explained in the last section, the competition between demulsification and re-emulsification is more

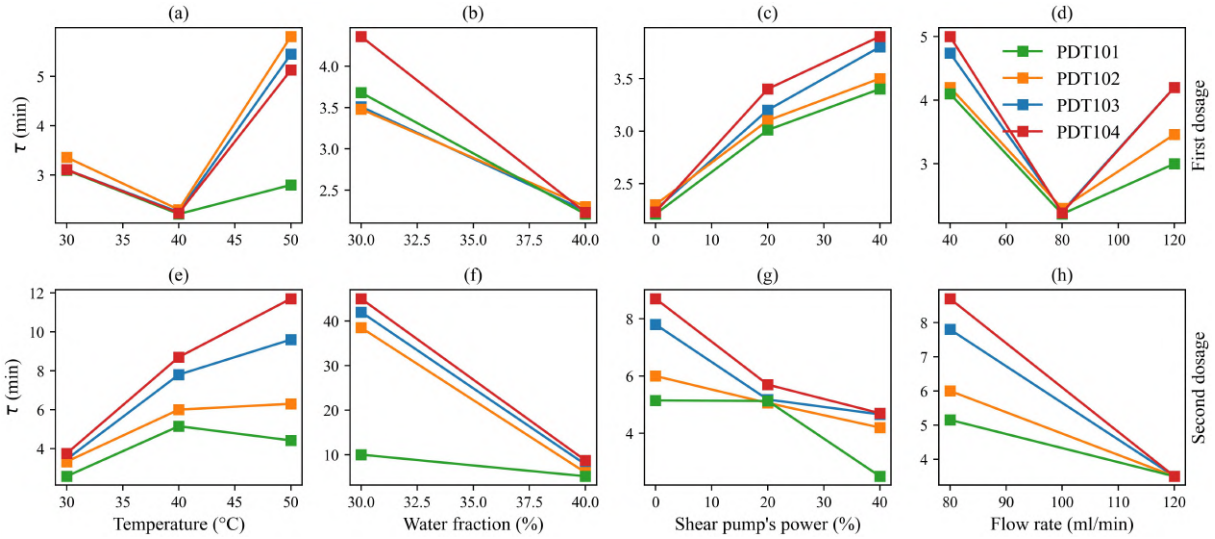

Figure 7.7: Effect of operating conditions on the process time constant. The first and second row represents the first and second dosages (100ppm) and the second dosages (200ppm), respectively.

accentuated along the flow. In this case, the time for the viscosity to reach a stationary value is longer.

We summarize the effect of temperature on the process time in Figure 7.7a and Figure 7.7e. We expected an inversely proportional behavior between the temperature and process time because the higher the temperature, the greater the diffusion speed of the demulsifier in the emulsion.

However, we noticed that only the temperatures of 30°C and 40°C at the first dosage exhibited this behavior. The time constant increased for the other temperature pairs in both dosages, and we attributed this observation to the analysis presented for temperature and process gain in the last section. Specifically, the observed process gains were two to three times greater for 40°C and 50°C than 30°C (Figure 7.5a), indicating a significant change in the emulsion's morphology. Despite the temperature increase accelerating the demulsifier's diffusion speed, the emulsion's rheological changes were highly pronounced, leading to a longer time required to reach a new steady state in the process.

Furthermore, we can infer that the decrease in the demulsification time constant due to the higher diffusion speed of the demulsifier between 30°C and 40°C for the first dosage is more substantial than the decrease between 40°C and 50°C. This lesser influence on the process at higher temperatures aligns with findings in the literature, suggesting that temperature influences demulsification efficiency to a certain extent (BALSAMO *et al.*, 2017).

Process time constant proved inversely proportional to the two dosage steps concerning the water fraction (Figure 7.7b and Figure 7.7f). As the water fraction increases, the droplets will be closer together despite the increase in surface area. This proximity enhances the rate of droplet flocculation and coalescence, thereby increasing the desemulsification rate. However, in terms of time constant, despite the action of the demulsifier being faster in the system with a more dispersed phase, the change promoted by the demulsifier was much more significant (Figure 7.5c). This implied that the time for this change (going from one steady state to another) in viscosity to occur was longer, even though the action of the demulsifier was faster.

For the gear pump effect, the time constant followed the tendency to increase with higher pump power values for the first dosage (Figure 7.7d). In this case, the higher time constant for highly sheared emulsions by the pump (20% and 40%) is due to the longer demand for the surfactant to act in tiny droplets. Despite the agitation caused by the pump promoting faster solubilization of the dosed surfactant, the effect of the surfactant on the flow is slower. The time required for the transmitters to sense the coalescence of the drops in the flow is longer since the sheared droplets are tiny. In the second dosage, although the time constant was higher than in the first dosage, this one did not show the same tendency (Figure 7.7g). In other words, the homogenization effect due to a higher flow rate was more pronounced than the re-emulsification promoted by the flow.

Regarding the volumetric flow, the greater the volumetric flow, the faster the homogenization of the surfactant in the medium. However, a high volumetric flow promoted a re-emulsification due to the shear of the fluid itself. Figure 7.7d shows this balance of forces. There is a natural tendency to increase the speed of action of the demulsifier between 40 and 80 ml/min. This increase is due to better solubilization of the chemical in the flow. However, for a flow rate of 120 ml/min, the homogenization speed of the demulsifier, although more significant, does not affect the time constant proportionally due to the re-emulsification promoted by the flow. For the second dosage (Figure 7.7h), despite the re-emulsification promoted by the flow, as the drops were already larger, the action of the demulsifier was faster.

7.3.3 Effect of operating conditions on process dead time

Dead time refers to the time required for disturbances in the process, in this case, surfactant dosage, to be perceived by the transmitters. Figure 7.8 shows the behavior of the system dead

time value for each installed transmitter. The process dead time in each transmitter followed the order of the bigger distance between the dosing point and the measurement location.

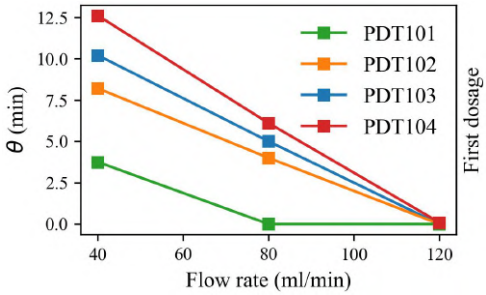

Figure 7.8: Process dead time adjusted for all experimental runs.

7.4 Dynamic behavior of destabilized flow

Destabilization occurred as the dosage of the demulsifier increased, resulting in larger drop sizes and promoting phase segregation. Consequently, the flow rheology sensors detected an abrupt change in viscosity at these points. Two experimental runs demonstrated flow destabilization. The first instance was observed during the second dosage of the demulsifier in experimental run 4 (Table 6.2). At this particular stage, the flow rate of 40 mL/min could not maintain the emulsion's cohesion, unlike higher flow rates, mainly due to the low shear level present in the emulsion.

The second occurrence of destabilization happened in experimental run 7. At this point, the emulsion, containing 50% water content, was nearing the phase inversion point for the amount of emulsifier. Consequently, the added demulsifier acted rapidly, and despite the shear generated by the flow, the segregated phases could not re-emulsify. These two points did not exhibit adjustable dynamics when analyzed through a function.

After the dosage of the demulsifier, the emulsion presented an unstable relative viscosity, as shown in Figure 7.9a. As this emulsion flows in the circuit, the surfactant better homogenizes, and the emulsion's viscosity, inferred through pressure drop, returns to values close to the segregated phases (water). However, the transmitter PDT101 indicates that the emulsion broke when we finished feeding the demulsifier. As the flow is not turbulent and does not have high shear points, destabilization occurs through the appearance of segregated phase pockets in the viewing pipe. Pockets of water, oil, and emulsion pass through the sensors, causing an abrupt measurement oscillation.

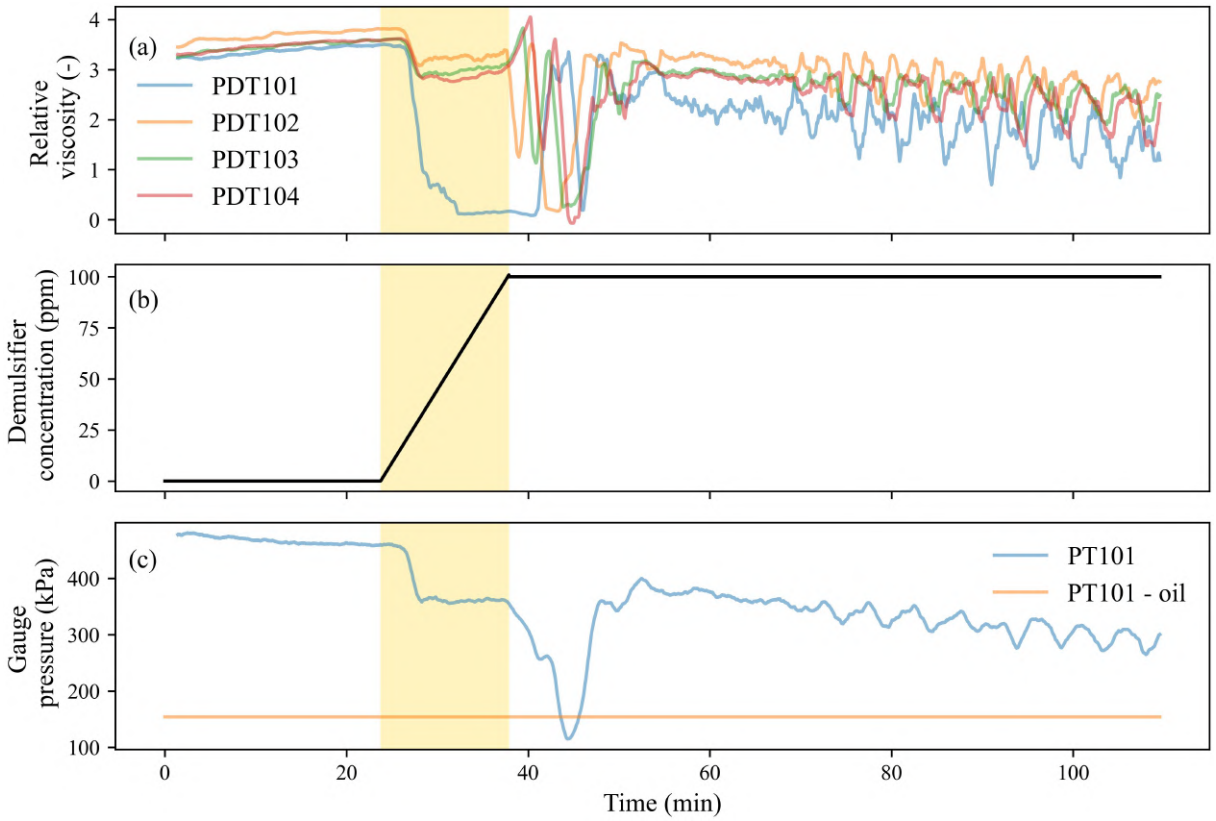

Figure 7.9: Graphical representation of the experimental run 7 that presented a destabilization in the flow after the first dosage of the demulsifier.

The PT101 absolute pressure sensor shows evidence of flow destabilization. After adding the demulsifier, we observed that the flow showed a drastic drop in pressure to values below the flow with pure oil (Figure 7.9c). Shortly after this severe drop due to the internal shear promoted by the flow, a re-emulsification of fluid sections occurred, and the system pressure increased. However, as it is a laminar flow, there are formations of pockets of segregated phases and emulsion, promoting downward oscillations observed in the PT101 graph in the time above 50 min in Figure 7.9c.

7.4.1 Developed flow pattern

During the filming process, we encountered challenges in obtaining useful information due to the white and opaque nature of the emulsion under study. The emulsion displayed a homogenous appearance throughout most of the flow, making it difficult to observe the phase formation that typically characterizes multi-phase flows. Upon adding the demulsifier, we observed a noticeable change in the emulsion's color; it transitioned from a milky white to a light-yellow hue. This color change indicated that the demulsifier initiated the

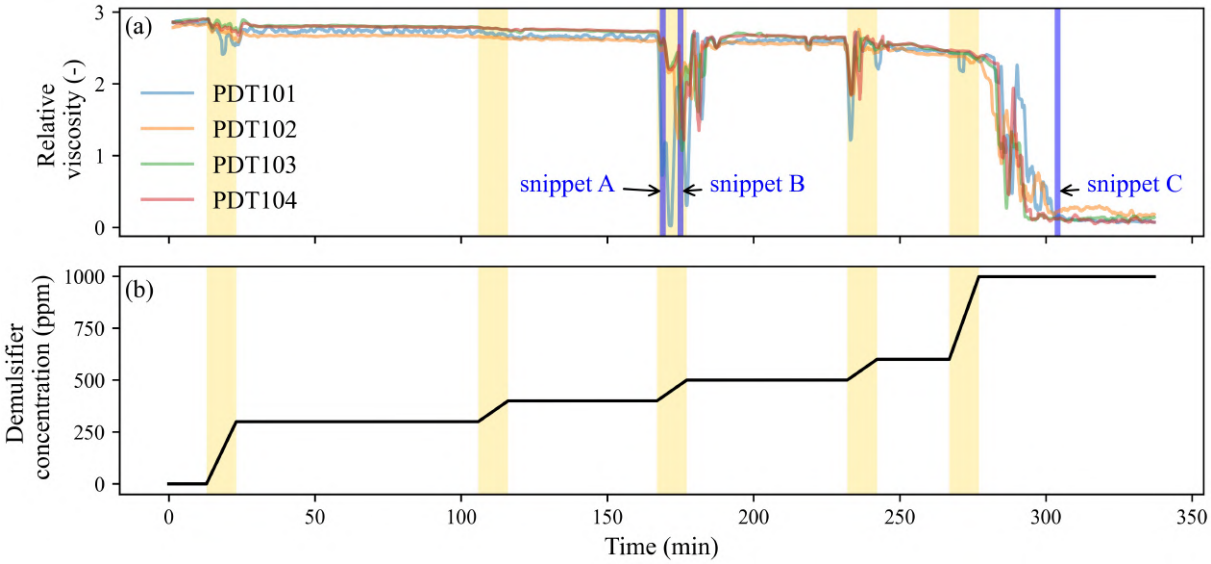

Figure 7.10: Dynamic viscosity data for experiments run 2 with consecutive dosages to evaluate the flow pattern.

breakdown of the emulsion, leading to the separation of the individual phases. As a result, we gained better visibility into the flow dynamics, allowing us to observe the phase formation that the homogeneity of the emulsion had previously obscured.

We followed the emulsion destabilization process in Figure 7.10. The two first dosages did not interfere with the homogeneity of the emulsion. The third dosage of the demulsifier destabilized the emulsion. We presented some frames of this process as indicated in snippet A in Figure 7.11. Under these conditions, the demulsifier dosed was solubilized in some parts, promoting phase segregation. This flow pattern presents similarities with the multiphase flow of very viscous W/O emulsion in water found in the literature (BANNWART *et al.*, 2004). After a short time, the flow showed the appearance of small pockets of W/O emulsion followed by water in the dispersed phase, as shown in snippet B in Figure 7.11. These pockets generated large oscillations in the pressure sensors (Figure 7.10) and emerged due to the laminar flow. The low flow rate did not promote enough fluid mixing to keep the demulsifier homogeneously solubilized in the flow. Consequently, it promoted the appearance of pockets of segregated water where it acted.

The observed pattern in the flow comprised a stratified region primarily composed of the segregated aqueous phase, while the oil and the remaining W/O emulsion flowed in the top region of the tube. This flow pattern significantly decreased the overall viscosity, resembling values similar to a flow comprising only the aqueous phase. This behavior aligns with findings reported in the existing literature (PLASENCIA J.; NYDAL, 2022; BANNWART *et al.*,

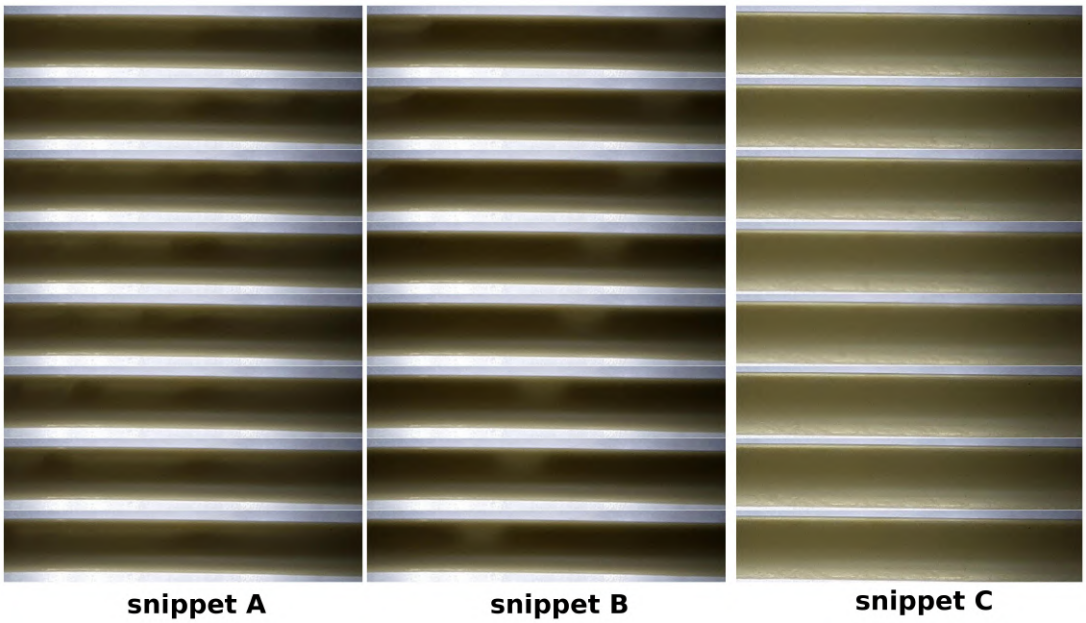

Figure 7.11: Filming frames (30fps) of the horizontal section of the pipe during the destabilization of the flow promoted by the demulsifier.

2004). Throughout the flow, phase segregation occurred, causing the emulsion to become more translucent. This phenomenon facilitated better light transmission from a source behind the flow, resulting in a clearer and unobstructed view of the observed phenomenon, as depicted in snippet C in Figure 7.11.

7.5 Conclusion of the chapter

In this study, we employed a first-order dynamics model to investigate chemical demulsification in flow. The model parameter analysis allowed us to comprehend how various operational conditions influence the dynamics of the in-line demulsification process, with each factor showing nuanced effects.

The gain in demulsification efficiency with temperature occurs up to a certain extent. In comparison, the demulsification efficiency decreases and becomes more challenging as the dispersed phase fraction decreases. The gear pump effect acted in the morphological properties of the emulsion; at the same time, it promoted the solubilization of the demulsifier; however, the mixture characteristic of the shear applied had a major influence on increasing the demulsification efficiency. The analysis of flow rates indicated that improving the demulsification action requires a delicate balance between demulsification

and re-emulsification processes. Higher flow rates improved the solubilization speed, but the relative viscosity reduction was smaller and slower for these values.

Moreover, our investigation into emulsion destabilization allowed us to observe the boundaries where the model accurately captured the phenomenon's behavior. We identified the formation of pockets of segregated phases in the flow, leading to absolute pressure and relative viscosity oscillations. While the visual observation of the formation was not entirely clear, the annular flow pattern became visible when we added enough demulsifier to establish the destabilization flow pattern.

As one of the pioneering studies on the dynamics of demulsification in flow, we believe the tests and evaluations carried out here will significantly contribute to a better understanding of chemical demulsification in the oil industry. The insights gained from this research will aid in optimizing demulsification processes, ultimately enhancing oil production and transportation efficiency.

Chapter 8

Results and discussion - Control strategy

8.1 Demulsification monitoring

8.1.1 Qualitative analysis

The qualitative analysis of demulsification in the flow was observed by filming the flow in the visualization section (Figure 6.7), which formed four distinct flow patterns (Figure 8.1). These patterns are classified numerically in this work according to the following list.

Flow Pattern 1: This flow pattern appears homogeneous with a white color. Although the viscosity of the emulsion changes with the addition of the demulsifier and an increase in the average droplet size, it is not possible to observe the flow movement. We can refer to Figure 4.2a for this flow pattern.

Flow Pattern 2: The flow appears homogeneous, but the color of the emulsion changes to yellowish. This change is due to the instability caused by the increase in droplet size. The oily phase becomes more visible, and the sample has better light passage. This flow pattern is close to phase segregation. We can refer to Figure 4.2b for this flow pattern.

Flow Pattern 3: In this flow pattern, phase segregation occurs due to an increase in the amount of demulsifier. It's slightly noticeable in the flow, and the aqueous phase flows in tiny filaments close to the pipe wall. We can refer to Figure 4.2c for this flow pattern.

Flow pattern 4: The flow has the same characteristics as flow pattern 3. However, more intense phase segregation occurs due to increased demulsifier concentration. As the flow is

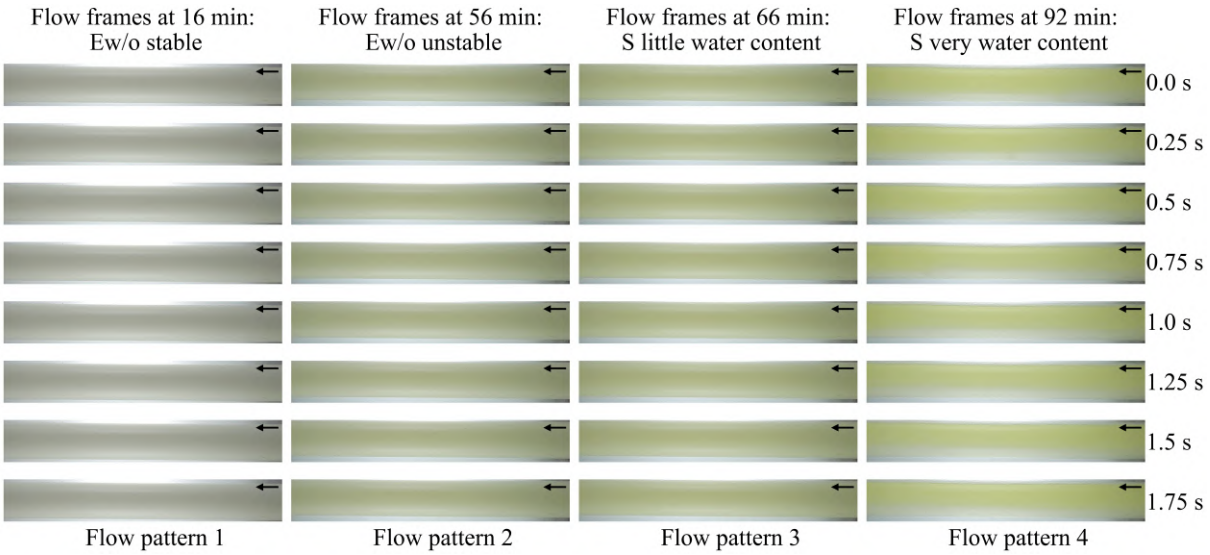

Figure 8.1: Flow patterns developed during chemical demulsification. Excerpts from the footage of the analysis of the breakdown of the 40% emulsion at 40°C in a closed circuit.

laminar at a low velocity, the segregated aqueous phase flows in regions close to the pipe bottom at a higher velocity than the oil phase. These differences in the flow velocities of the phases are due to the lower water viscosity in relation to oil. The friction promoted by the oil phase with the pipe wall is greater than that promoted by the aqueous phase, so the aqueous phase flows with greater ease and velocity (Figure 8.1). This flow pattern is similar to that shown in Figure 4.2d.

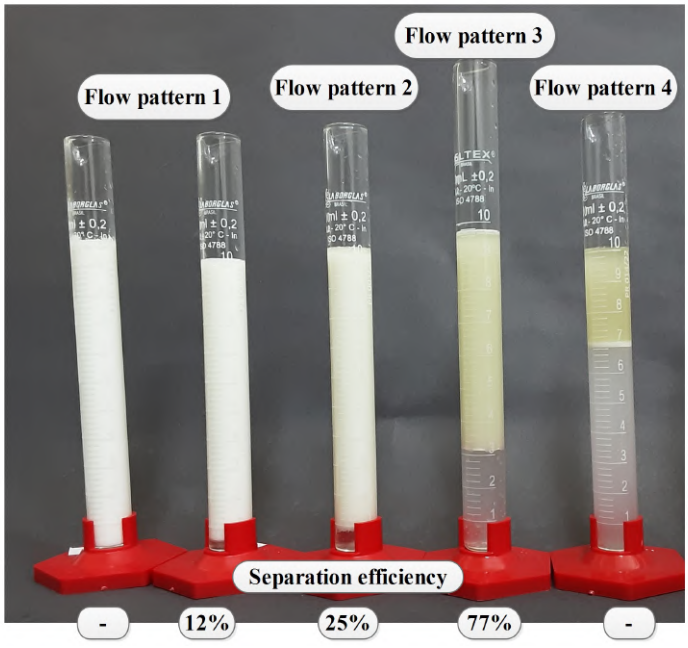

Figure 8.2: Aliquots of 10 ml taken during the closed-loop flow analysis.

Figure 8.2 shows aliquots removed during the closed circuit demulsification operation. In this figure, it was possible to observe that flow pattern 1 has a small segregation of the phases due to the action of the small amount of demulsifier. This segregation could only be observed through the decrease in relative viscosity. In flow pattern 2, there was a slight change in the color of the sample, which was observed more clearly in the flow. The quantity of water (segregated phase) was greater than in flow pattern 1. In flow pattern 3, the segregated phase was more significant, reaching values close to 30% v/v. Note that the emulsion was prepared with a water content of 40% w/w, which is 39% v/v in volumetric terms.

In flow pattern 4, as the phases slipped more intensely, the volume of the segregated aqueous phase was greater in proportion to the amount of water in the prepared emulsion. This amount of segregated water is evidence that phase slippage occurred in the flow, with the velocity of the aqueous phase being greater than that of the oil phase. As the circuit was closed and the level of phase segregation was very high, this implies a localized oil accumulation in the circuit. The possible location of this accumulation was in tank TK102, which, despite having a low residence time (less than 1 minute), provided the ideal system for separating the phases of the stratified flow that circulated in it. Notably, flow pattern 4 can only be achieved when the circuit is closed due to these characteristics of potential phase separation in the tank.

8.1.2 Quantitative analysis

The quantitative analysis of demulsification in the closed circuit was carried out by monitoring the variables during the process. The Figure 8.3 shows the monitoring, in which the variable μ_r represents the relative viscosity calculated by Equation 4.6 and u the demulsifier dosage in the circuit, which occurs by pump P101 (Figure 6.7). The other variables are the acoustic properties defined in the item 6.4.4.

As the demulsifier concentration increased in the circuit with the start of dosing at 16 min, the relative viscosity inferred by the four transmitters decreased. The most significant drop occurred in the PDT101 transmitter, installed close to the dosing point (Figure 6.7). This gradual decrease in interference is due to the demulsifier's action in increasing the droplets size.

When demulsification intensified due to the high concentration of demulsifier in the flow in 60 min, the ultrasonic variables showed a high dispersion. During this time, the flow pattern

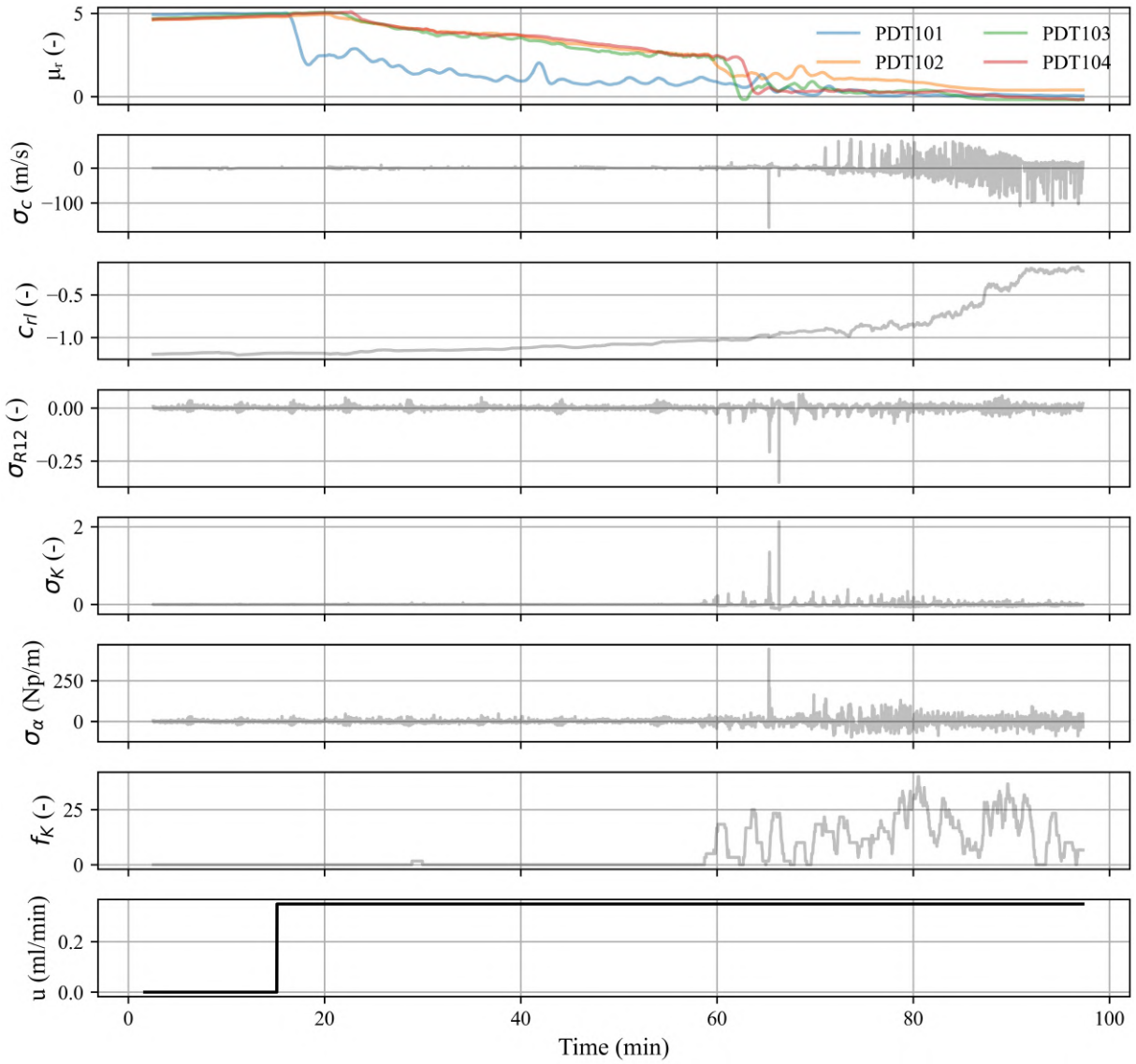

Figure 8.3: Monitoring acoustic variables during emulsion flow with a water content of 40% w/w during chemical demulsification in a closed circuit at 40°C. Controller input acoustic variables in gray.

changed (Figure 8.1). With the increase in demulsifier concentration after 70 min, the flow pattern changed again, and the ultrasonic variables showed a more pronounced dispersion.

The changes observed in the flow in 60 min were unclear in the flow photos; only with a detailed look at the footage is it possible to see thin phase-segregated filaments at the bottom of the tube. However, viscosity monitoring highlights that the flow pattern transitioned from homogeneous to stratified, becoming intermittent. The intermittent pattern is inferred by the oscillations in viscosity displayed by the transmitters. These oscillations highlight the passage of fluid potions with different viscous characteristics, which we infer to be potions of the destabilized emulsion.

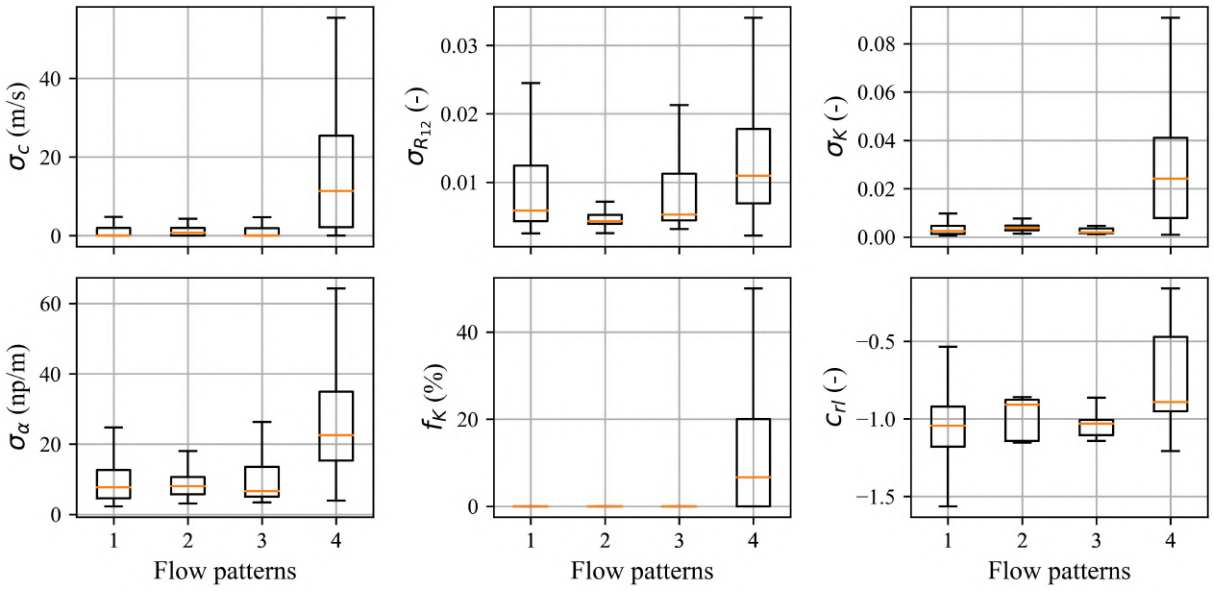

Figure 8.4: Classification of ultrasonic variables during chemical demulsification monitoring.

With the monitoring data, we apply the equations to calculate the input variables of the fuzzy controller. Through filming in qualitative analysis (item 8.1.1), we divided the data set according to the observed flow pattern. Figure 8.4 presents the classification of ultrasonic variable data collected in the experiments, applying Equation 6.2, 6.5, and 6.6. These data averages and dispersion information were used to build the basis of the membership functions of the input variables in the fuzzy system to control chemical demulsification.

8.2 Parameters set on the controller

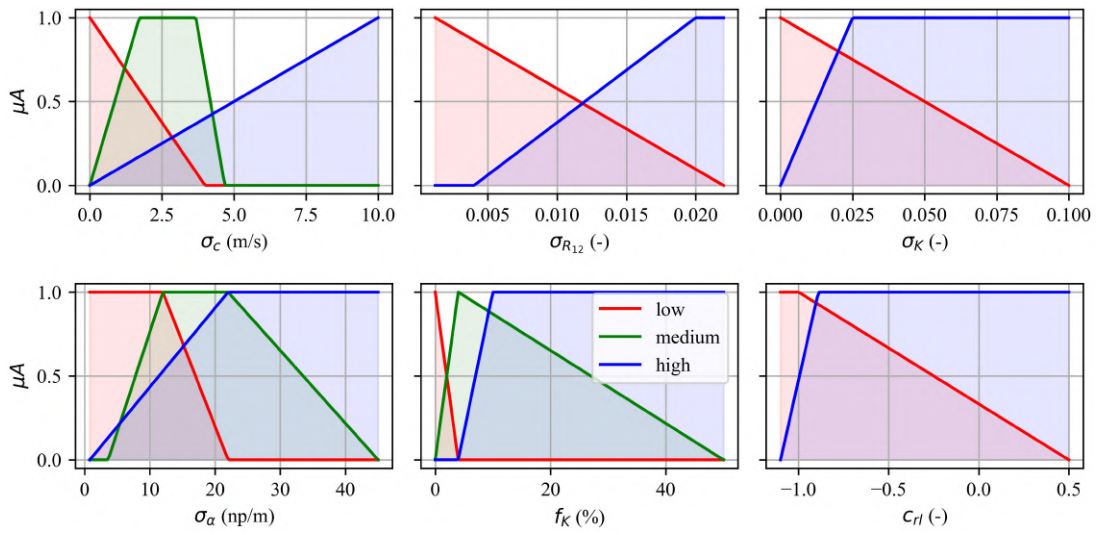

Figure 8.5: Membership functions of the antecedent layer of the fuzzy control system.

The developed controller aimed to maintain the specific flow pattern. In this case, flow pattern 3 was chosen. In this pattern, unlike flow patterns 1 and 2, the demulsifier fulfills its role of promoting phase segregation, reducing the viscosity of the flow with a smaller amount of demulsifier. The flow pattern 4 is not desired, as the aqueous phase flows faster than the oil phase, and the amount of demulsifier dosed is high.

Figure 8.5 presents the antecedent membership functions related to each system input variable. The number of membership functions of the acoustic variables and their parameters a,b,c were adjusted according to the data in Figure 8.4. The choice of these parameters was elaborated according to the observed regions of the possible classification of the data regarding to the flow pattern. For example, we can observe from the dispersion of the data that σ_K can be divided into two groups. The first group covers patterns 1, 2, and 3, with data scattered between 0 and 0.01 and some points outside the distribution reaching 0.1. The second group covers flow pattern 4 with a distribution between 0 and 0.43 and an average of 0.025 (Figure 8.5). Therefore, this variable was assigned two membership functions (low and high) referring to the degree of belonging of the data to one of these two observed groups (Figure 8.5).

Table 8.1: Fuzzy control system rules.

σ_c	σ_{R_12}	σ_α	σ_K	f_K	c_{rl}	Consequent
low	low	low	low	low	low	flow pattern 1
low				low	low	flow pattern 1
low	low	low	low	medium	low	flow pattern 2
medium	low	high	high	high	high	flow pattern 3
high	high	high	high	high	high	flow pattern 4
high					high	flow pattern 4

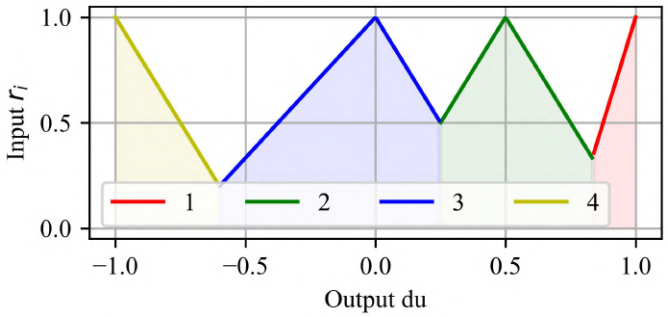

Figure 8.6: Membership functions of the consequent of the fuzzy control system.

Table 8.1 presents the set of rules implemented in the system. In the table, the operator between the columns is 'and'. For example, if $\sigma_c = low$, $f_K = low$, and $c_{rl} = low$, we

are in flow pattern 1. When more than one rule classifies the data as an equal flow pattern, the 'or' operator is applied between these rules. The 'and' and 'or' operators are expressed mathematically by Equation 4.16 and 4.17.

The membership functions of the consequent were chosen according to the observed flow patterns (Figure 8.6). Triangular functions were used for each pattern. The output universe of the consequent layer extends from the minimum value to the maximum of the control actuation du. Figure 8.7 illustrates the complete fuzzy system, according to the example presented in section 4.4.

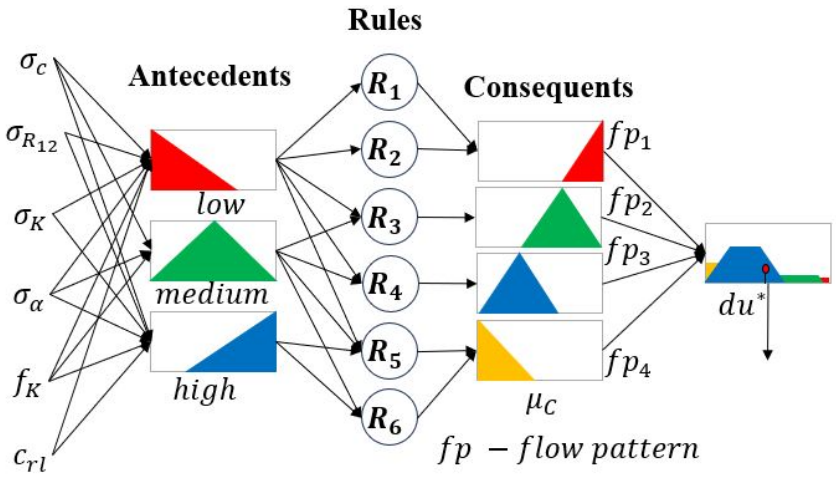

Figure 8.7: Fuzzy control system with acoustic variables as the input.

8.3 Control applied in closed circuit

The first test of the developed controller was its application in a closed system at 40°C with a 40% w/w emulsion. In this case, the amount of demulsifier was accumulated in the circuit. Its objective was to achieve a concentration of the demulsifier in the circuit where phase segregation occurs without reaching the flow pattern 4. In other words, the system reaches and remains in flow pattern 3.

Figure 8.8 shows the monitoring of the closed circuit variables with the control action on the demulsifier dosage variable. We can observe that initially, after being activated in 28 min, the controller responds to the system with a fixed demulsifier flow rate in the circuit. This flow is calculated according to the value assigned to the S_{du} parameter. The higher S_{du}, the higher the flow values the dosing pump can achieve. The value assigned to S_{du} was 0.15, which implies a maximum actuation in this system of 0.25 ml/min, close to the actuator minimum

saturation. This low dosage value, promoted by S_{du}, was chosen to monitor changes in the circuit in more detail, with the controller acting until phase segregation is achieved.

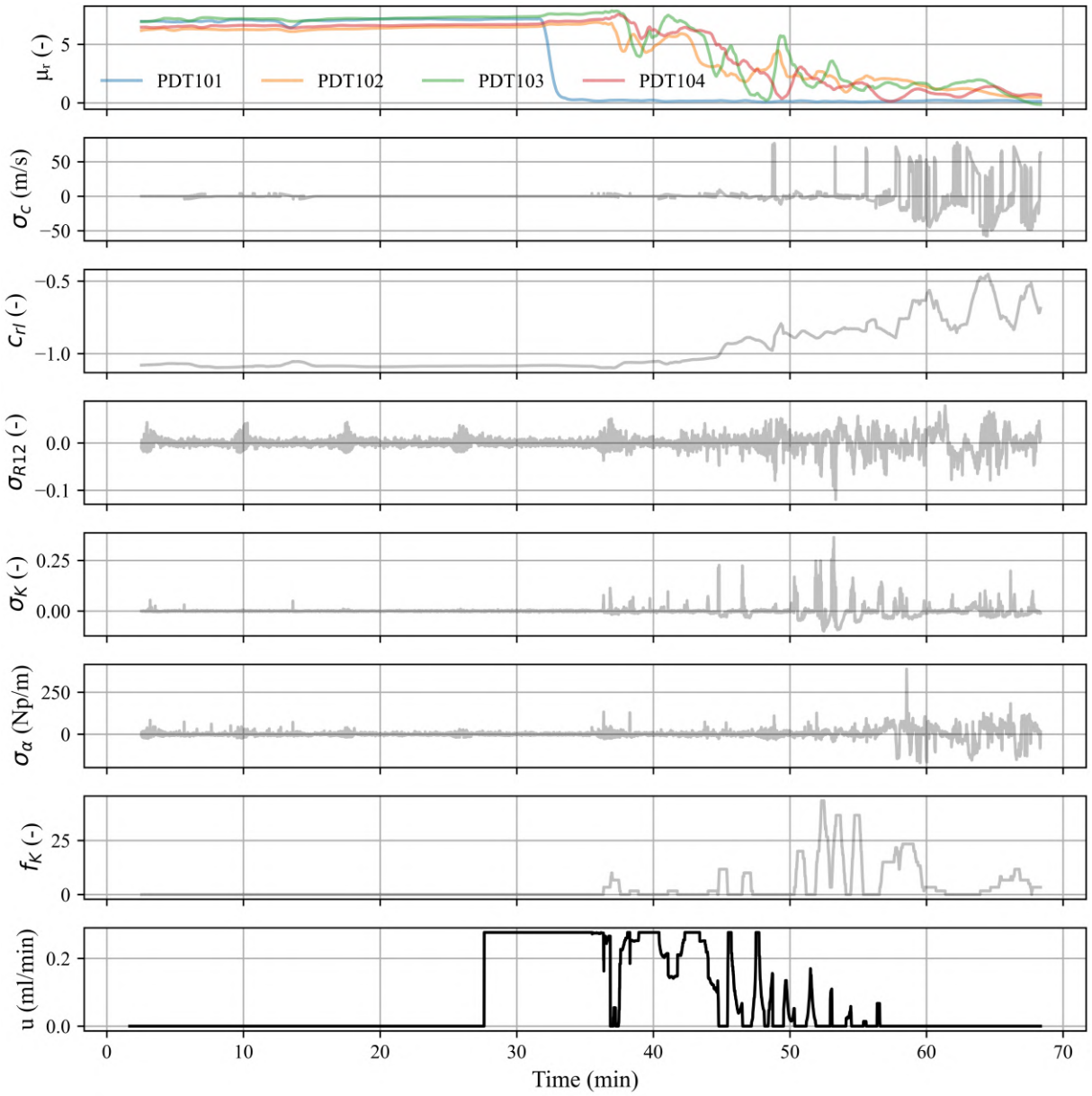

Figure 8.8: Monitoring the closed circuit variables during fuzzy control during flow demulsification. Controller input acoustic variables in gray.

As the demulsifier concentration increased in the circuit, after activating the control in 28 min, the relative viscosity of the emulsion dropped significantly in the region close to the PDT101 transmitter in 32 min. However, due to the flow characteristic of promoting a mixture of the fluid itself, the demulsifier homogenizes in the flow, and this drop in viscosity does not propagate throughout the entire circuit. Only when 38 min is reached does demulsification intensify to the point of being perceived by transmitters PDT102 to PDT104. In the region

close to 45 min, the amount of demulsifier in the circuit becomes more significant, which promotes a more intense oscillation in the controller performance. In this region, the fuzzy system identifies that the flow is segregated. After 55 minutes, the fuzzy system identifies that the flow is completely segregated and deactivates the demulsifier dosage to avoid reaching a flow pattern 4.

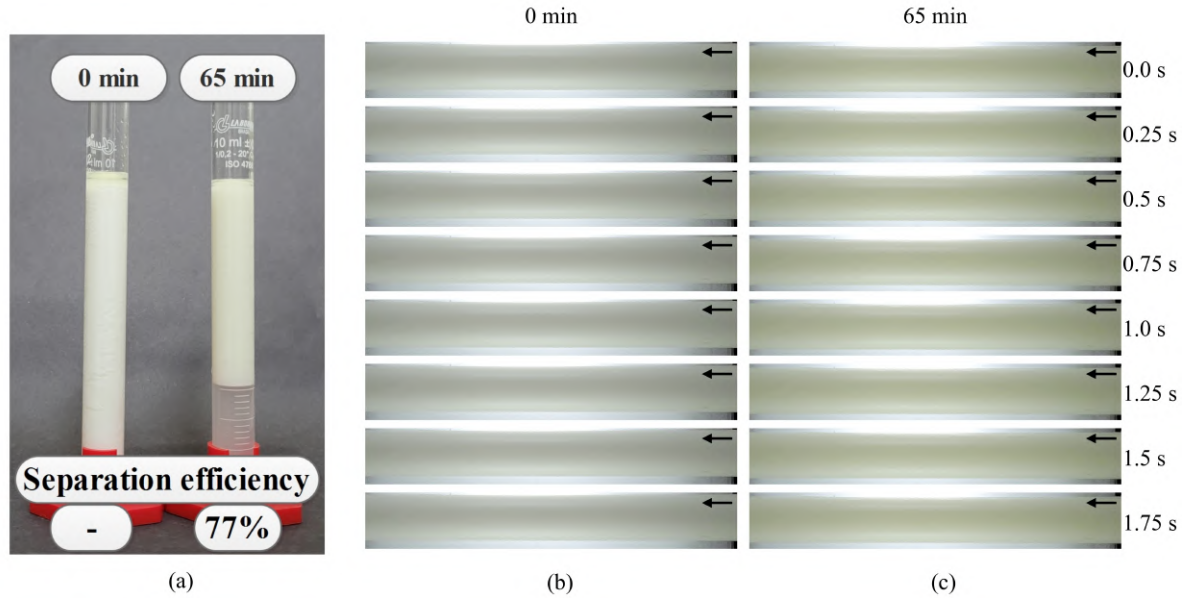

Figure 8.9: Aliquots of 10 ml taken from the analysis before and after the controller action (a) and frames from the cropped footage of the flow pattern at the initial time (b) from the analysis after the controller action (c).

Figure 8.9a shows the aliquots removed from the analysis before and after the controller action. It reveals the control's effectiveness in achieving adequate phase segregation in the circuit. Note that the sample had a water content of approximately 40% v/v, which resulted in an efficiency of 77% in phase separation. The footage of the initial and final flow patterns are shown in Figure 8.9b and 8.9c. In this section, there was an apparent change in the color of the flow. Furthermore, in the final flow pattern, it was possible to observe the segregated phase flowing close to the pipe bottom, with a profile similar to flow pattern 3, defined in Figure 8.1.

8.4 Control applied in open circuit

In the open circuit, it is not possible to reach flow pattern 4, in which oil accumulates in the circuit. In this sense, the objective of the control was to adequately dose the demulsifier so that the flow remains segregated (flow pattern 3) without an excessive amount of demulsifier. In

other words, after reaching flow pattern 3, the control maintains the dosage stable, regulating its performance according to the disturbances made in the process.

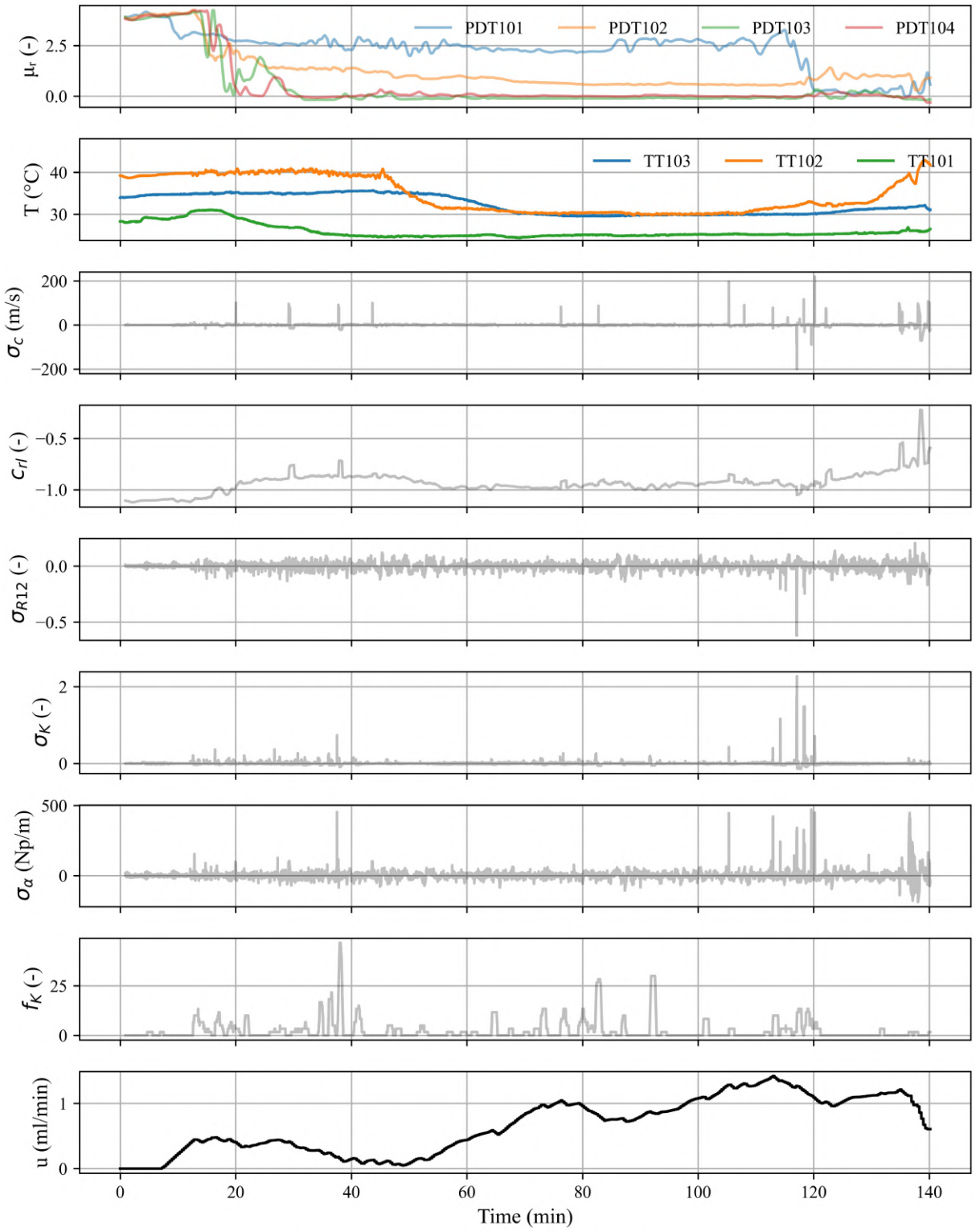

Figure 8.10: Monitoring open circuit variables during fuzzy control during flow demulsification. Controller input acoustic variables in gray.

In the open loop, the final calculation of the fuzzy controller action is illustrated in Figure 6.12. The values of the control delay time t_d and the damping parameter S_{du} were 20s and 0.015, respectively.

Figure 8.10 shows the monitoring of circuit variables during the action of the fuzzy controller initialized in 7 min. In the figure, it can be seen that, at the beginning, the fuzzy system identified the flow patterns Ew/o stable (flow pattern 1), activating the actuator until it reached 0.47 ml/min. After that, the flow fluctuates slightly around this value. This indicates that during this period, the controller identified a phase segregation. Although the aliquot removed at 17 min (Figure 8.11) does not show clear segregation, the significant drop in viscosity in this region indicates that the flow has segregated.

In 30 minutes, the demulsifier flow decreases until the value reaches 0.1 ml/min in 45 minutes. This indicates that the controller identified the flow pattern 4 and acted by reducing the amount of demulsifier dosed. The aliquot taken at 46 min (Figure 8.11) shows that the flow was very close to flow pattern 4 since the aqueous phase separated from the emulsion almost exceeded its water content, reaching a high value of separation.

Within 46 min after removing the aliquot, a disturbance was introduced. This disturbance was the decrease in flow temperature from 40 to 30°C. Due to this decrease, the viscosity of the emulsion increases (see how temperature influence the oil viscosity in the item A.3), and there is a need for a greater amount of demulsifier to break down the emulsion. The controller identified this need and increased the demulsifier flow rate to 1 ml/min in 80 minutes. During this rise, an aliquot was removed at 69 min (Figure 8.11). This rate proves that there is a decrease in the efficiency of the demulsifier in relation to 46 min. However, the stratified flow pattern remains during the controller action. At 112 min, another aliquot was removed, and in its analysis, we saw that the flow pattern remained similar to 69 min.

After removing the aliquot at 112min, the next disturbance occurred with the change in the water content of the emulsion from 40% w/w to 50% w/w. We observed a tendency for the demulsifier flow rate to increase to a point close to 1.4 ml/min in 113 min. However, this change did not occur due to the disturbance caused by the sample exchange. When observing the relative viscosity, we see that only after 115 minutes was the presence of the emulsion with a higher water content noticed by the system. Note that the higher the water fraction, the lower the demulsifier required to promote phase segregation. The control noticed this lesser need for the demulsifier, which reduced the amount dosed into the system to 1 ml/min

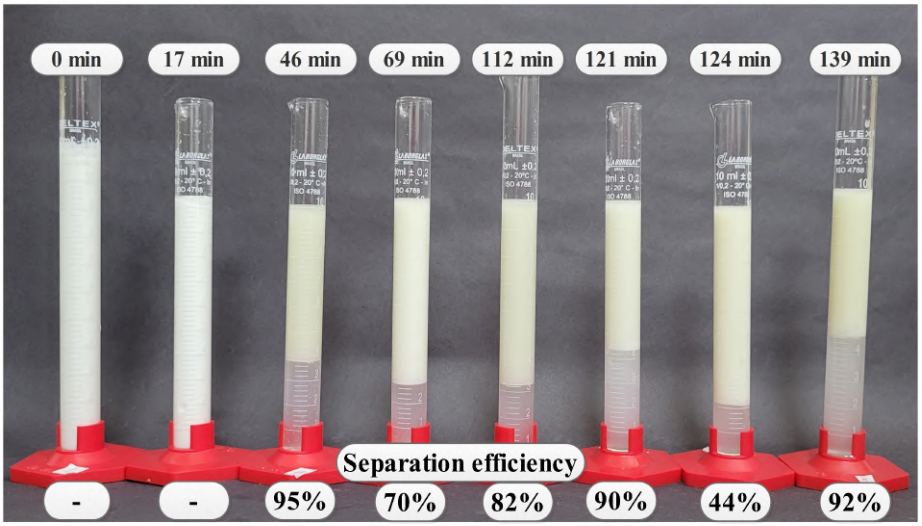

Figure 8.11: Aliquots of 10 ml removed from the analysis during the controller action in the open circuit.

in 120 min. The analysis of the aliquot removed in 124 min (Figure 8.11) highlights that the flow remained segregated.

After removing the aliquot, the last disturbance occurred at 124 min, with the temperature increasing to 40°C. This increase in temperature was noticed by the fuzzy system only after 135 min, which classified the flow pattern as SW with great water content, i.e., it had a high degree of pertinence to the flow pattern 4, initiating a sudden decrease in the flow rate of the dosed demulsifier. The last aliquot removed at the end of the experiment in 139 min (Figure 8.11) shows that the flow pattern was very close to phase slip, which made sense with the controller action in reducing the dosage.

Figure 8.12 shows three sections of footage of the flow during three moments when an aliquot is removed. During most of the experiment, the flow pattern remained similar to the time of 69 min. In this pattern, the phases are segregated, and the aqueous phase flows in the bottom region of the tube. In the figure, it is possible to see the formation of this bottom region that divides the aqueous and emulsion phases. For some specific points, the level of phase segregation became more intense. At these points, as we can see in the figure, at 121 minutes, the interface between the phases presented a malleable curvature in the flow. This characteristic indicates that the flow pattern increases the stratified water content, and the fuzzy identified it as having a certain degree of pertinence to flow pattern 4. The other specific point was at the end of the experiment at 139 min, in which a flow pattern similar to that at

69 min was observed; however, it had a more voluminous aqueous phase. This occurred due to emulsion breakdown with a higher water content than the emulsion that flowed in 69 min.

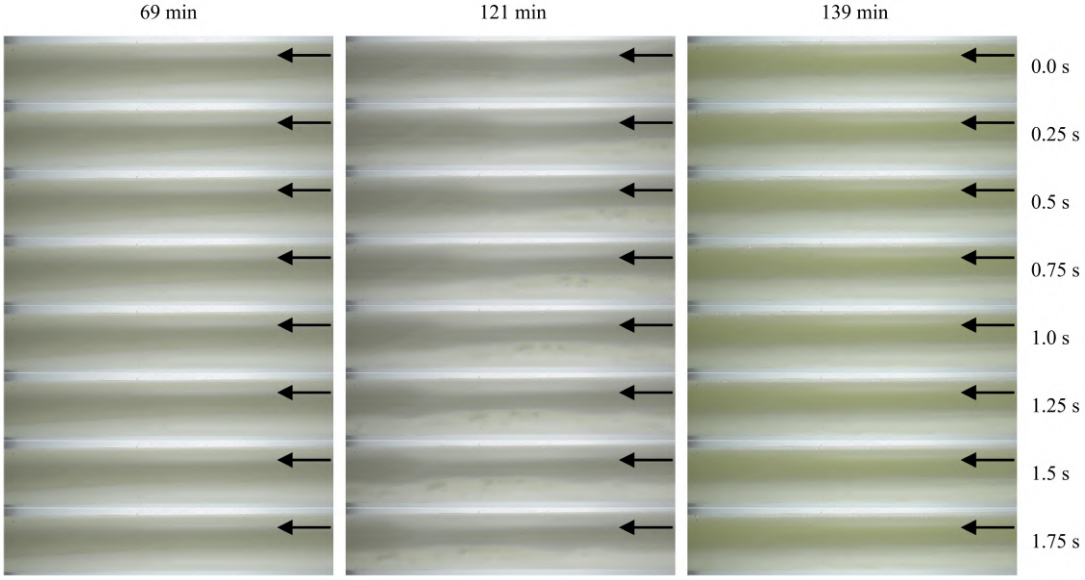

Figure 8.12: Frames of cropped footage of the flow patterns during the action of fuzzy control in the open circuit.

8.5 Conclusions of the chapter

In this study, we developed a control strategy using the processing of ultrasonic signals from the sensor coupled to the flow. The sensor was built to capture the echoes that pass through the emulsion and reflect at the sensor interface with the flow, considering the high attenuation of the emulsion. With signal processing, it was possible to define six important acoustic variables that demonstrated sensitivity to emulsion destabilization. These variables served as input into a fuzzy system that classified the flow into four patterns: water-in-oil stable emulsion, water-in-oil unstable emulsion, stratified with low and great water content. The control was thus applied to maintain the stratified with low water content flow pattern.

A set of experiments was carried out to define the input variables of the fuzzy system. These experiments showed that the variable standard deviation demonstrated sensitivity to the demulsification of the emulsion in the flow, mainly the sample echo frequency. These variables demonstrated that ultrasonic signals were sensitive in identifying emulsion destabilization.

We applied the control strategy developed to closed-circuit flow, in which the emulsion was continuously re-circulated. In this experiment, the control proved to be efficient, as it managed to achieve segregation, the objective of dosing the demulsifier until the emulsion destabilizes

and forms a segregated phase. To do this, the controller activated the dosing pump until this happened. After that, the controller deactivated the dosing pump.

The last application of the control was in an open circuit, in which the emulsion did not re-circulate. In this experiment, two perturbations were applied to the system. One was the change in flow temperature, and the other was the change in the water content of the emulsion. The control performed adequately in this system, keeping the flow segregated at all times. This performance was observed through the aliquots removed during the experiment and the drainage filming.

In summary, the control strategy developed here presented adequate performance in controlling chemical demulsification to ensure flow. In this sense, the results open new perspectives for applying non-intrusive sensors with fuzzy controllers in a control loop in the demulsification process in the flow.

Chapter 9

Conclusion

The chemical demulsification of emulsion composed of naphthenic oil in the flow was studied. This oil was chosen due to its rheological characteristics, similar to high viscosity petroleum. This study was conducted quantitatively by monitoring process variables, such as viscosity and acoustic properties, during demulsification and qualitatively by evaluating the flow pattern formed. The influence of variables such as temperature, flow rate, and water content on the dynamics of this process was established.

An ultrasonic sensor was constructed to operate in transmission-reception mode to characterize the concentrated emulsion. The developed sensor was an update of the sensor previously developed in the research group (see supplementary material in item A.1). The update was aimed to mitigate the effect of preferential paths and increase the amplitude of the transmitted echo in the sample, as the echo is crucial in emulsion analysis.

The developed ultrasonic sensor was coupled to a circuit operating in both closed and open systems. The ultrasonic properties of the emulsion derived from the ultrasonic signal, were monitored during the chemical demulsification occurring in the flow. These variables showed sensitivity to changes in emulsion morphology and were used to classify the flow pattern emerging during this process.

A system based on a fuzzy controller was used to classify the flow pattern developed based on the monitored ultrasonic variables: sound velocity, reflection coefficient, attenuation, and the emergence of reflected echoes in the sample. With this classification, an algorithm was developed to dose the demulsifier automatically. The developed control proved efficient in maintaining the desired flow pattern during demulsification in closed and open circuits.

9.1 Future work

For future work, the following points are recommended:

- Restructure the circuit so that the demulsifier is dosed in the pressurized pipeline;
- Evaluate/improve the control algorithm with dosing at different points upstream of the ultrasonic sensor;
- Evaluate/improve the control algorithm for use in a larger experimental-scale circuit;
- Evaluate/improve the control algorithm using the ultrasonic sensor, which utilized only one transducer in order to be applied to a larger pipe;
- Evaluate/improve the control algorithm for emulsion flow with air.

Bibliography

ABDULREDHA, M. M.; Siti Aslina, H.; LUQMAN, C. A. Overview on petroleum emulsions, formation, influence and demulsification treatment techniques. *Arabian Journal of Chemistry*, v. 13, n. 1, p. 3403–3428, 2020. ISSN 1878-5352.

AL-SABAGH, A. M.; KANDILE, N. G.; EL-GHAZAWY, R. A.; Noor El-Din, M. R. Synthesis and evaluation of some new demulsifiers based on bisphenols for treating water-in-crude oil emulsions. *Egyptian Journal of Petroleum*, v. 20, n. 2, p. 67–77, 2011. ISSN 1110-0621.

ASSUNCAO, M. V. D.; VIEIRA, M. M.; ALMEIDA, M. R. The influence of oil well on the water generation from the potiguar basin / brazil. *Acta Scientiarum. Technology*, Universidade Estadual de Maringa, v. 40, n. 1, p. 38403, abr. 2018. ISSN 1806-2563.

AZIZI, K.; NIKAZAR, M. Characterization of chemical demulsification of oil in water emulsion: Comparison between a kinetics model and laboratory experiments. *Petroleum Science and Technology*, Taylor & Francis, v. 33, n. 1, p. 8–14, 2015.

BALSAMO, M.; ERTO, A.; LANCIA, A. Chemical demulsification of model water-in-oil emulsions with low water content by means of ionic liquids. *Brazilian Journal of Chemical Engineering*, Brazilian Society of Chemical Engineering, v. 34, n. 1, p. 273–282, Jan 2017. ISSN 0104-6632.

BANNWART, A. C.; RODRIGUEZ, O. M. H.; CARVALHO, C. H. M. de; WANG, I. S.; VARA, R. M. O. Flow patterns in heavy crude oil-water flow. *Journal of Energy Resources Technology*, ASME International, v. 126, n. 3, p. 184–189, set. 2004. ISSN 1528-8994.

BARNES, H. A. Rheology of emulsions: a review. *Colloids and Surfaces A: Physicochemical and Engineering Aspects*, v. 91, p. 89–95, 1994. ISSN 0927-7757. A selection of papers presented at the First World Congress on Emulsions.

BATCHELOR, G. K. The effect of brownian motion on the bulk stress in a suspension of spherical particles. *Journal of Fluid Mechanics*, v. 83, n. 1, p. 97–117, 1977.

BINKS, B. P. Particles as surfactants: similarities and differences. *Current Opinion in Colloid & Interface Science*, Elsevier BV, v. 7, n. 1-2, p. 21–41, mar. 2002. ISSN 1359-0294.

BRINKMAN, H. C. The Viscosity of Concentrated Suspensions and Solutions. *The Journal of Chemical Physics*, v. 20, n. 4, p. 571–571, 12 2004. ISSN 0021-9606.

BULGARELLI, N.; BIAZUSSI, J.; CASTRO, M. de; VERDE, W.; BANNWART, A. Experimental study of phase inversion phenomena in electrical submersible pumps under oil/water flow. *J. Offshore Mech. Arct. Eng.*, v. 142, p. 041402, 2020.

BULGARELLI, N.; BIAZUSSI, J.; PERLES, C.; VERDE, W. M.; CASTRO, M. D.; BANNWART, A. Analysis of chord length distribution in phase inversion of water-oil emulsions at electrical submersible pump outlet. In: *9th World Conference on Experimental Heat Transfer, Fluid Mechanics and Thermodynamics. Iguazu Falls, Brazil*. [S.l.: s.n.], 2017.

BULGARELLI, N. A. V.; BIAZUSSI, J. L.; VERDE, W. M.; PERLES, C. E.; CASTRO, M. S. de; BANNWART, A. C. Experimental investigation on the performance of electrical submersible pump (esp) operating with unstable water/oil emulsions. *Journal of Petroleum Science and Engineering*, v. 197, p. 107900, 2021. ISSN 0920-4105.

CHALLIS, R.; POVEY, M.; MATHER, M.; HOLMES, A. K. Ultrasound techniques for characterizing colloidal dispersions. *Reports on Progress in Physics*, v. 68, p. 1541, 2005.

CHEN, G.; PHAM, T. T. *Introduction to Fuzzy Sets, Fuzzy Logic, and Fuzzy Control Systems*. [S.l.]: CRC Press, 2000.

DATTA, S. S.; GERRARD, D. D.; RHODES, T. S.; MASON, T. G.; WEITZ, D. A. Rheology of attractive emulsions. *Physical Review E*, American Physical Society (APS), v. 84, n. 4, out. 2011. ISSN 1550-2376.

DE, B.; MANDAL, T.; DAS, G. Experimental studies on phase inversion in a small diameter horizontal pipe. *Chemical Engineering Research and Design*, Elsevier BV, v. 88, n. 7, p. 819–826, jul. 2010. ISSN 0263-8762.

DOL, S. S.; WONG, S. F.; WEE, S. K.; LIM, J. S. Experimental study on the effects of water-in-oil emulsions to wall shear stress in the pipeline flow. *Journal of Applied Fluid Mechanics*, v. 11, n. 5, p. 1309–1319, 2018. ISSN 1735-3572.

EINSTEIN, A. Eine neue bestimmung der moleküldimensionen. *Annalen der Physik*, v. 324, n. 2, p. 289–306, 1906.

EMAMI, M. S. Fuzzy logic applications in chemical processes. *J. Math. Comput. Sci*, v. 1, n. 4, p. 339–348, 2010.

FIGUEIREDO, M. de M. F.; CARVALHO, F. de C. T.; FILETI, A. M. F.; SERP, A. L. Flow pattern classification in water-air vertical flows using a single ultrasonic transducer. *Experimental Thermal and Fluid Science*, v. 119, p. 110189, 2020. ISSN 0894-1777.

FIGUEIREDO, M. de M. F.; CARVALHO, F. de C. T.; FILETI, A. M. F.; SERP, A. L. Dispersed-phase velocities for gas-liquid vertical slug and dispersed-bubbles flows using an ultrasonic cross-correlation technique. *Flow Measurement and Instrumentation*, v. 79, p. 101949, 2021. ISSN 0955-5986.

FORTUNY, M.; OLIVEIRA, C. B. Z.; MELO, R. L. F. V.; NELE, M.; COUTINHO, R. C. C.; SANTOS, A. F. Effect of salinity, temperature, water content, and ph on the microwave demulsification of crude oil emulsions. *Energy & Fuels*, v. 21, n. 3, p. 1358–1364, 2007.

FUHRMANN, P. L.; BREUNIG, S.; SALA, G.; SAGIS, L.; STIEGER, M.; SCHOLTEN, E. Rheological behaviour of attractive emulsions differing in droplet-droplet interaction strength. *Journal of Colloid and Interface Science*, v. 607, p. 389–400, 2022. ISSN 0021-9797.

FUHRMANN, P. L.; SALA, G.; STIEGER, M.; SCHOLTEN, E. Clustering of oil droplets in o/w emulsions: Controlling cluster size and interaction strength. *Food Research International*, v. 122, p. 537–547, 2019. ISSN 0963-9969.

GOODARZI, F.; ZENDEHBOUDI, S. A comprehensive review on emulsions and emulsion stability in chemical and energy industries. *The Canadian Journal of Chemical Engineering*, v. 97, n. 1, p. 281–309, 2019.

GREAVES, D.; BOXALL, J.; MULLIGAN, J.; MONTESI, A.; CREEK, J.; SLOAN, E. D.; KOH, C. A. Measuring the particle size of a known distribution using the focused beam reflectance measurement technique. *Chemical Engineering Science*, Elsevier BV, v. 63, n. 22, p. 5410–5419, nov. 2008. ISSN 0009-2509.

GUO, J.; YANG, Y.; ZHANG, S.; ZHANG, D.; CAO, C.; REN, B.; LIU, L.; XING, Y.; XIONG, R. Heavy oil-water flow patterns in a small diameter vertical pipe under high temperature/pressure conditions. *Journal of Petroleum Science and Engineering*, v. 171, p. 1350–1365, 2018. ISSN 0920-4105.

HAO, M.; BAI, Z.; WANG, H.; LIU, W. Removal of oil from electric desalting wastewater using centrifugal contactors. *Journal of Petroleum Science and Engineering*, Elsevier BV, v. 111, p. 37–41, nov. 2013. ISSN 0920-4105.

HJARTNES, T. N.; SøRLAND, G. H.; SIMON, S.; SJöBLOM, J. Demulsification of crude oil emulsions tracked by pulsed field gradient (pfg) nuclear magnetic resonance (nmr). part i: Chemical demulsification. *Industrial & Engineering Chemistry Research*, v. 58, n. 6, p. 2310–2323, 2019.

IOANNOU, K.; NYDAL, O. J.; ANGELI, P. Phase inversion in dispersed liquid-liquid flows. *Experimental Thermal and Fluid Science*, v. 29, n. 3, p. 331–339, 2005. ISSN 0894-1777. Third European-Japanese Two-Phase Flow Group Meeting.

ISSAKA, S. A. Review on the fundamental aspects of petroleum oil emulsions and techniques of demulsification. *Journal of Petroleum & Environmental Biotechnology*, OMICS Publishing Group, v. 06, n. 02, 2015. ISSN 2157-7463.

JIA, N.; SU, M. xu; CAI, X. shu. Particle size distribution measurement based on ultrasonic attenuation spectra using burst superposed wave. *Results in Physics*, v. 13, p. 102273, 2019. ISSN 2211-3797.

KABALNOV, A. Thermodynamic and theoretical aspects of emulsions and their stability. *Current Opinion in Colloid & Interface Science*, Elsevier BV, v. 3, n. 3, p. 270–275, jun. 1998. ISSN 1359-0294.

KATO, S.; KAWASAKI, J. A new technique for the mechanical demulsification of o/w emulsions. *Journal of Chemical Engineering of Japan*, v. 20, p. 232–237, 1987.

KAYE, G.; LABY, T. *Tables of physical and chemical constants and some mathematical functions*. [S.l.]: Longmans, Green, 1936.

KILPATRICK, P. K. Water-in-crude oil emulsion stabilization: Review and unanswered questions. *Energy & Fuels*, American Chemical Society (ACS), v. 26, n. 7, p. 4017–4026, jun. 2012. ISSN 1520-5029.

KOBAYASHI, I.; YASUNO, M.; IWAMOTO, S.; SHONO, A.; SATOH, K.; NAKAJIMA, M. Microscopic observation of emulsion droplet formation from a polycarbonate membrane. *Colloids and Surfaces A: Physicochemical and Engineering Aspects*, Elsevier BV, v. 207, n. 1-3, p. 185–196, jul. 2002. ISSN 0927-7757.

KOKAL, S. Crude oil emulsions: A state-of-the-art review. *SPE Production & Facilities - SPE PRODUCTION FACILITIES*, v. 20, p. 5–13, 2005.

KOKAL, S.; AL-JURAID, J. Quantification of factors affecting emulsion stability. v. 52, p. 41–42, 2000.

KUSHIBIKI, J.; ARAKAWA, M. Diffraction effects on bulk-wave ultrasonic velocity and attenuation measurements. *The Journal of the Acoustical Society of America*, v. 108, n. 2, p. 564–573, 2000.

LI, M.; WILKINSON, D.; PATCHIGOLLA, K. Comparison of particle size distributions measured using different techniques. *Particulate Science and Technology - PARTICULATE SCI TECHNOLOGY*, v. 23, p. 265–284, 2005.

LIM, J.; WONG, S.; LAW, M.; SAMYUDIA, Y.; DOL, S. A review on the effects of emulsions on flow behaviours and common factors affecting the stability of emulsions. *Journal of Applied Sciences*, Science Alert, v. 15, n. 2, p. 167–172, jan. 2015. ISSN 1812-5654.

LIU, L.; MATAR, O. K.; LAWRENCE, C. J.; HEWITT, G. F. Laser-induced fluorescence (lif) studies of liquid-liquid flows. part i: Flow structures and phase inversion. *Chemical Engineering Science*, v. 61, n. 12, p. 4007–4021, 2006. ISSN 0009-2509.

LUO, H.; WEN, J.; JIANG, R.; SHAO, Q.; WANG, Z. Modeling of the phase inversion point of crude oil emulsion by characterization of crude oil physical properties. *ACS Omega*, v. 7, n. 43, p. 39136–39146, 2022.

MA, J.; YAO, M.; YANG, Y.; ZHANG, X. Comprehensive review on stability and demulsification of unconventional heavy oil-water emulsions. *Journal of Molecular Liquids*, Elsevier BV, v. 350, p. 118510, mar. 2022. ISSN 0167-7322.

MACOSKO, C. *Rheology: Principles, Measurements, and Applications*. [S.l.]: VCH, 1994. (Advances in interfacial engineering series). ISBN 9781560815792.

MAFFI, J. M.; MEIRA, G. R.; ESTENOZ, D. A. Mechanisms and conditions that affect phase inversion processes: A review. *The Canadian Journal of Chemical Engineering*, Wiley, v. 99, n. 1, p. 178–208, out. 2020. ISSN 1939-019X.

MAMDANI, E.; ASSILIAN, S. An experiment in linguistic synthesis with a fuzzy logic controller. *International Journal of Man-Machine Studies*, Elsevier BV, v. 7, n. 1, p. 1–13, jan. 1975. ISSN 0020-7373.

Prediction of Dispersion Viscosity of Oil/Water Mixture Flow in Horizontal Pipes, All Days de *SPE Annual Technical Conference and Exhibition*, (SPE Annual Technical Conference and Exhibition, All Days). SPE-18221-MS p.

MCCLEMENTS, D. J. Critical review of techniques and methodologies for characterization of emulsion stability. *Critical Reviews in Food Science and Nutrition*, Informa UK Limited, v. 47, n. 7, p. 611–649, set. 2007. ISSN 1549-7852.

NGAN, K. H. *Phase Inversion in dispersed liquid-liquid pipe flow*. Tese (PhD thesis) — University College London, London, UK, October 2010.

NIKOLOV M. RANDIE, C. S. S. A. D.; WASAN, D. T. Chemical demulsification of oil-in-water emulsion using air-flotation: The importance of film thickness stability. *Chemical Engineering Communications*, Taylor & Francis, v. 152-153, n. 1, p. 337–350, 1996.

NORATO, M. A.; TAVLARIDES, L. L.; TSOURIS, C. Phase inversion studies in liquid-liquid dispersions. *The Canadian Journal of Chemical Engineering*, v. 76, n. 3, p. 486–494, 1998.

NORISUYE, T. Structures and dynamics of microparticles in suspension studied using ultrasound scattering techniques. *Polymer International*, v. 66, n. 2, p. 175–186, 2017.

NOUR, A. H. Emulsion types, stability mechanisms and rheology: A review. *SRPN: Oil (Topic)*, 2018.

NäDLER, M.; MEWES, D. Flow induced emulsification in the flow of two immiscible liquids in horizontal pipes. *International Journal of Multiphase Flow*, v. 23, n. 1, p. 55–68, 1997. ISSN 0301-9322.

OKAZAWA, T.; BRON, J. On thermodynamically stable emulsions. *Journal of Colloid and Interface Science*, Elsevier BV, v. 69, n. 1, p. 86–96, mar. 1979. ISSN 0021-9797. Disponível em: <http://dx.doi.org/10.1016/0021-9797(79)90083-3>.

PAL, R. Effect of droplet size on the rheology of emulsions. *AIChE Journal*, v. 42, n. 11, p. 3181–3190, 1996.

PENA, A. A.; HIRASAKI, G. J.; MILLER, C. A. Chemically induced destabilization of water-in-crude oil emulsions. *Industrial & Engineering Chemistry Research*, American Chemical Society (ACS), v. 44, n. 5, p. 1139–1149, set. 2004. ISSN 1520-5045.

PENG, Y.; LIU, T.; GONG, H.; ZHANG, X. Review of the dynamics of coalescence and demulsification by high-voltage pulsed electric fields. *International Journal of Chemical Engineering*, Hindawi Limited, v. 2016, p. 1–8, 2016. ISSN 1687-8078.

PERAZZO, A.; PREZIOSI, V.; GUIDO, S. Phase inversion emulsification: Current understanding and applications. *Advances in Colloid and Interface Science*, Elsevier BV, v. 222, p. 581–599, ago. 2015. ISSN 0001-8686.

PIELA, K.; DELFOS, R.; OOMS, G.; WESTERWEEL, J.; OLIEMANS, R.; MUDDE, R. Experimental investigation of phase inversion in an oil-water flow through a horizontal pipe loop. *International Journal of Multiphase Flow*, v. 32, n. 9, p. 1087–1099, 2006. ISSN 0301-9322.

PLASENCIA, J.; PETTERSEN, B.; NYDAL, O. J. Pipe flow of water-in-crude oil emulsions: Effective viscosity, inversion point and droplet size distribution. *Journal of Petroleum Science and Engineering*, v. 101, p. 35 – 43, 2013.

PLASENCIA J., I. N.; NYDAL, O. Research on the viscosity of stabilized emulsions in different pipe diameters using pressure drop and phase inversion. *Exp. Comput. Multiph. Flow*, v. 4, p. 241–263, 2022.

POVEY, M. J. Ultrasound particle sizing: A review. *Particuology*, v. 11, n. 2, p. 135 – 147, 2013. ISSN 1674-2001. Measurement Technology for Particulate System.

PRIETO, L.; PINILLA, A.; BECERRA, D.; PICO, P.; VALDéS, J. P.; PEREYRA, E.; RATKOVICH, N. Phase inversion correlations analysis for oil-water flow in horizontal pipes. *Industrial & Engineering Chemistry Research*, v. 58, n. 31, p. 14436–14445, 2019.

RAJAK, V. K.; SINGH, I.; KUMAR, A.; MANDAL, A. Optimization of separation of oil from oil-in-water emulsion by demulsification using different demulsifiers. *Petroleum Science and Technology*, Informa UK Limited, v. 34, n. 11-12, p. 1026–1032, jun. 2016. ISSN 1532-2459.

RAYA, S. A.; SAAID, I. M.; AHMED, A. A.; UMAR, A. A. A critical review of development and demulsification mechanisms of crude oil emulsion in the petroleum industry. *Journal of Petroleum Exploration and Production Technology*, Springer Science and Business Media LLC, v. 10, n. 4, p. 1711–1728, jan. 2020. ISSN 2190-0566.

RAYNEL, G.; SALOMON, M. D.; AL-KHABAZ, S.; AL-THABET, M.; OSHINOWO, L. A new method to select demulsifiers and optimize dosage at wet crude oil separation facilities. *Oil Gas Sci. Technol. - Rev. IFP Energies nouvelles*, v. 76, p. 19, 2021.

RICHARDSON, E. G. The flow of emulsions. ii. *Journal of Colloid Science*, v. 8, n. 3, p. 367 – 373, 1953. ISSN 0095-8522.

Correlations for predicting Viscosity of W/O-Emulsions based on North Sea Crude Oils, All Days de *SPE International Conference on Oilfield Chemistry*, (SPE International Conference on Oilfield Chemistry, All Days). SPE-28968-MS p.

SAIKI, Y.; PRESTIDGE, C. Droplet deformability and emulsion rheology: Steady and dynamic behavior. *Journal December Korea-Australia Rheology Journal*, v. 17, p. 191–198, 12 2005.

SARAIVA, S. V.; BONETTI, D.; SILVA, C. A. M. da; PEREIRA, L. O. V.; CUNHA, R. L. da; FILETI, A. M. F.; SILVA, F. V. da. Identification of the catastrophic phase inversion point of water-in-oil emulsion using ultrasonic measurements. *Industrial & Engineering Chemistry Research*, v. 63, n. 8, p. 3711–3726, 2024.

SARAIVA, S. V.; SILVA, C. A.; BONETTI, D.; FILETI, A. M.; SILVA e F. V. Coupling of support vector machine and acoustic models to characterize the droplet size distribution of emulsions using ultrasonic techniques. In: KOKOSSIS, A. C.; GEORGIADIS, M. C.; PISTIKOPOULOS, E. (Ed.). *33rd European Symposium on Computer Aided Process Engineering*. [S.l.]: Elsevier, 2023, (Computer Aided Chemical Engineering, v. 52). p. 1745–1752.

SELKER, A. H.; JR., C. A. S. Factors affecting which phase will disperse when immiscible liquids are stirred together. *The Canadian Journal of Chemical Engineering*, v. 43, n. 6, p. 298–301, 1965.

SHI, S.; WANG, Y.; LIU, Y.; WANG, L. A new method for calculating the viscosity of w/o and o/w emulsion. *Journal of Petroleum Science and Engineering*, v. 171, p. 928–937, 2018. ISSN 0920-4105.

SILVA, C. A.; SARAIVA, S. V.; BONETTI, D.; HIGUTI, R. T.; CUNHA, R. L.; PEREIRA, L. O.; SILVA, F. V.; FILETI, A. M. Application of acoustic models for polydisperse emulsion characterization using ultrasonic spectroscopy in the long wavelength regime. *Colloids and Surfaces A: Physicochemical and Engineering Aspects*, v. 602, p. 125062, 2020. ISSN 0927-7757.

SILVA, F. L. M. C.; TAVARES, F. W.; CARDOSO, M. J. E. M. Thermodynamic stability of water-in-oil emulsions. *Brazilian Journal of Petroleum and Gas*, Brazilian Journal of Petroleum and Gas, v. 7, n. 1, p. 1–13, abr. 2013. ISSN 1982-0593.

SILVA, F. V. D.; FILETI, A. M. F.; PEREIRA, L. O. V.; SILVA, C. A. M. D.; SARAIVA, S. V. *Ultrasound Attenuation Spectroscopy Analisys - UASA*. 2023. Disponível em: <BR5120230018902>.

SULLIVAN, A. P.; KILPATRICK, P. K. The effects of inorganic solid particles on water and crude oil emulsion stability. *Industrial & Engineering Chemistry Research*, American Chemical Society (ACS), v. 41, n. 14, p. 3389–3404, jun. 2002. ISSN 1520-5045.

SUN, N. N.; JIANG, H. Y.; WANG, Y. L.; QI, A. J. A comparative research of microwave, conventional-heating, and microwave/chemical demulsification of tahe heavy-oil-in-water emulsion. *SPE Production & Operations*, Society of Petroleum Engineers (SPE), v. 33, n. 02, p. 371–381, ago. 2017. ISSN 1930-1863.

TAN, J.; LUO, P.; VAHAJI, S.; JING, J.; HU, H.; YU, B.; TU, J. Experimental investigation on phase inversion point and flow characteristics of heavy crude oil-water flow. *Applied Thermal Engineering*, v. 180, p. 115777, 2020. ISSN 1359-4311.

TAYLOR, G. I. The viscosity of a fluid containing small drops of another fluid. *Proceedings of the Royal Society of London. Series A, Containing Papers of a Mathematical and Physical Character*, v. 138, n. 834, p. 41–48, 1932.

TIAN, Y.; ZHOU, J.; HE, C.; HE, L.; LI, X.; SUI, H. The formation, stabilization and separation of oil-water emulsions: A review. *Processes*, MDPI AG, v. 10, n. 4, p. 738, abr. 2022. ISSN 2227-9717.

TRALLERO, J. L.; SARICA, C.; BRILL, J. P. A Study of Oil/Water Flow Patterns in Horizontal Pipes. *SPE Production & Facilities*, v. 12, n. 03, p. 165–172, 08 1997.

UMAR, A. A.; SAAID, I. B. M.; SULAIMON, A. A.; PILUS, R. B. M. P. A review of petroleum emulsions and recent progress on water-in-crude oil emulsions stabilized by natural surfactants and solids. *Journal of Petroleum Science and Engineering*, v. 165, p. 673 – 690, 2018.

VAN, V. Viscosity of solutions and suspensions; theory. *Phys Colloid Chem.*, v. 52, n. 2, p. 277–299, 1948.

VANKOVA, N.; TCHOLAKOVA, S.; DENKOV, N. D.; IVANOV, I. B.; VULCHEV, V. D.; DANNER, T. Emulsification in turbulent flow: 1. mean and maximum drop diameters in inertial and viscous regimes. *Journal of Colloid and Interface Science*, v. 312, n. 2, p. 363–380, 2007. ISSN 0021-9797.

VANKOVA, N.; TCHOLAKOVA, S.; DENKOV, N. D.; VULCHEV, V. D.; DANNER, T. Emulsification in turbulent flow: 2. breakage rate constants. *Journal of Colloid and Interface Science*, v. 313, n. 2, p. 612–629, 2007. ISSN 0021-9797.

VENKATARAMANI, D.; AICHELE, C. P. Concentrated emulsion characterization in flowing conditions. *Energy & Fuels*, American Chemical Society (ACS), v. 29, n. 5, p. 2801–2807, jan. 2015. ISSN 1520-5029.

VERMEULEN, T.; WILLIAMS, G. M.; LANGLOIS, G. E. Interfacial area in liquid-liquid and gas-liquid agitation. *Chem. Eng. Prog.*, v. 51, p. 85, 1955.

WANG, D.; YANG, D.; HUANG, C.; HUANG, Y.; YANG, D.; ZHANG, H.; LIU, Q.; TANG, T.; Gamal El-Din, M.; KEMPPI, T.; PERDICAKIS, B.; ZENG, H. Stabilization mechanism and chemical demulsification of water-in-oil and oil-in-water emulsions in petroleum industry: A review. *Fuel*, v. 286, p. 119390, 2021. ISSN 0016-2361.

YEH, G. C.; JR., F. H. H.; MOSES, R. A. Phase-volume relationship at the point of phase inversion in liquid dispersions. *AIChE Journal*, v. 10, n. 2, p. 260–265, 1964.

YONGUEP, E.; KAPIAMBA, K. F.; KABAMBA, K. J.; CHOWDHURY, M. Formation, stabilization and chemical demulsification of crude oil-in-water emulsions: A review. *Petroleum Research*, v. 7, n. 4, p. 459–472, 2022. ISSN 2096-2495.

ZADEH, L. Fuzzy sets. *Information and Control*, Elsevier BV, v. 8, n. 3, p. 338–353, jun. 1965. ISSN 0019-9958.

ZHANG, H.; YU, K.; CAYRE, O. J.; HARBOTTLE, D. Interfacial particle dynamics: One and two step yielding in colloidal glass. *Langmuir*, American Chemical Society (ACS), v. 32, n. 50, p. 13472–13481, dez. 2016. ISSN 1520-5827.

Appendix A

Supplementary material

A.1 Ultrasound sensor

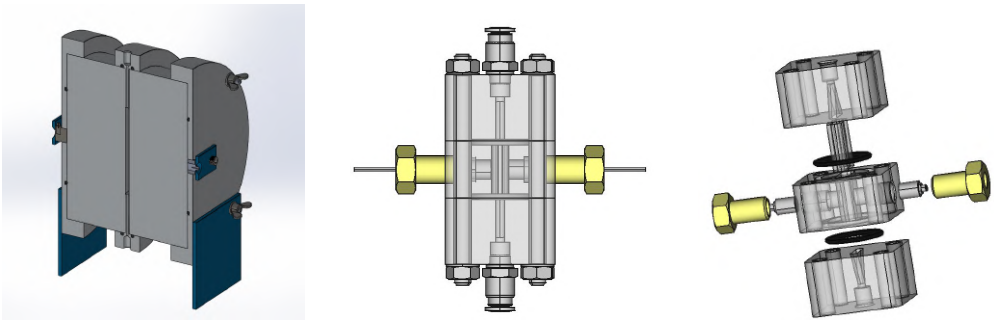

(a) Previous sensor (b) Actual sensor (c) Actual sensor - parts

Figure A.1: Ultrasonic sensor developed in previous work (a) and in the present work (b,c).

The new sensor developed for application in the analyzes carried out in this work was based on previous studies carried out by the research group (SILVA *et al.*, 2020). In these works, we built a duralumin cell that slightly attenuated the signal (Figure A.1a). However, the need for an update to the sensor already developed was observed due to some points observed.

- The sensor had a large chamber in which the sample could be stored, creating preferential paths for flow.
- The reflection coefficient was very high, i.e., most of the signal did not propagate through the sample but was reflected at the interface (wall/sample).

The new sensor was machined to eliminate the effect of preferential paths so that there were no places in the internal chamber where the fluid could stagnate. The internal chamber

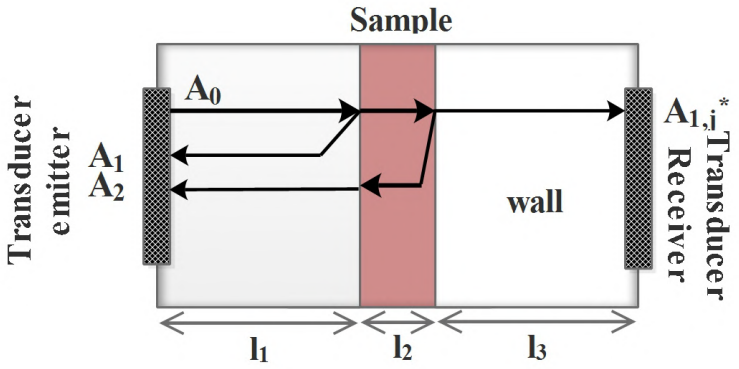

Figure A.2: Illustration of the ultrasonic cell and its operation to extract the echoes of interest.

is related to the cuvette in which the fluid passes (Figure A.1c). This cuvette is attached to the sensor body and pressed by the transducers in parallel with its internal walls. Screws fix the entire sensor and an oring is used to guarantee sealing.

A.1.1 Acoustic modeling of plane wave propagation in media

The sensor illustrated in the Figure A.2 refers to the transmission-reception analysis mode in which two transducers are used to analyze the sample. A transducer emits a signal A_0 that propagates through the material until it reaches the interface between the wall and the sample. Depending on the difference in impedance, part of the sound energy is reflected, and the other is transmitted. The various reflections and transmissions in the apparatus are captured by transducers and digitized. The echoes of interest for analyzing the sample in this work are A_1, A_2, and A_1^*. The equations that model these echoes are described below.

$$A_1 = A_0 R_{12} e^{-2\alpha_1 l_1} 2D_1 \tag{A.1}$$

$$A_2 = A_0 T_{12} R_{23} T_{21} e^{-2\alpha_1 l_1} e^{-2\alpha_2 l_2} 2D_1 2D_2 \tag{A.2}$$

$$A_1^* = A_0 T_{12} T_{23} e^{-\alpha_1 l_1} e^{-\alpha_2 l_2} e^{-\alpha_3 l_3} D_1 D_2 D_3 \tag{A.3}$$

The variables T_{ij}, D_i, R_{ij}, α_i, and l_i represent the transmission coefficient, correction factor for sound diffraction in the medium, reflection coefficient, acoustic attenuation, and

propagation path length, respectively. In the context of these variables, subscripts 1 and 3 denote the delay line, while 2 corresponds to the sample line.

The reflection coefficient signifies the proportion of sound energy incident on an interface that gets reflected back. It is determined by the difference in acoustic impedance (Z_i and Z_j) of the media sharing the interface. Acoustic impedance, the product of the speed of sound c_i and specific mass ρ_i, characterizes a medium's ability to impede sound propagation (Eq. A.4). A higher reflection coefficient implies a greater amount of energy reflected. Conversely, the transmission coefficient quantifies the energy that passes through the interface. These coefficients are interrelated according to Equations A.5 and A.6. The parameter α represents the rate of exponential decay in sound wave amplitude due to energy dissipation while traversing a medium. This dissipation is inherently influenced by factors such as viscosity, temperature, specific mass, and others (CHALLIS *et al.*, 2005).

$$R_{12} = \frac{Z_i - Z_j}{Z_i + Z_j} = \frac{\rho_i c_i - \rho_j c_j}{\rho_i c_i + \rho_j c_j} \tag{A.4}$$

$$R_{ij} = -R_{ji} \tag{A.5}$$

$$T_{ij} = 1 + R_{ij} \tag{A.6}$$

When sound energy traverses the delay line and sample lines, some of it undergoes diffraction and scattering. This diffraction distorts the calculated values of acoustic variables. To address this, a diffraction correction coefficient D_i is employed, which adjusts the amplitude of the modeled signal to account for the diffraction effect of the sound (KUSHIBIKI; ARAKAWA, 2000).

A.1.2 Simulation of ultrasonic signals

A series of simulations was conducted to choose the best material to build the sensor. In these simulations, the equations developed in the supplementary material A.1.1 were used. The Figure A.3 shows these simulations of echo propagation in cells. Note that the echo of the most significant interest (A_1^*) in acrylic has the greatest amplitude despite being the most attenuation material. This material was chosen to build the cells, the technical details of which are presented in the appendix A.1.1. In the simulation shown in the Figure A.3, the acoustic

properties of naphthenic oil were used. Details related to the technical drawing are present in the appendix B.1.

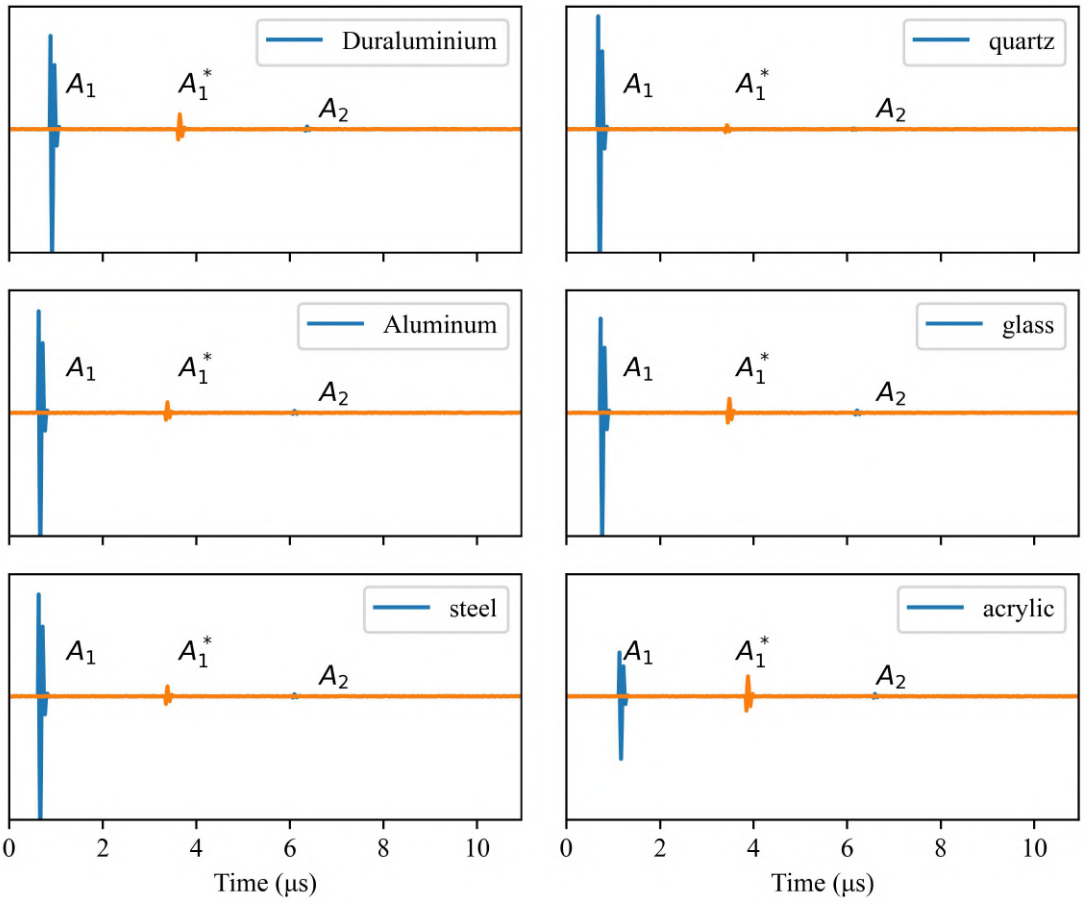

Figure A.3: Sensor simulations with different materials with a highly attenuating oil sample.

Details of the developed software applied to process ultrasonic signals are present in the user manual. The software was deposited at INPI (Brazilian Intellectual Property Institute) (SILVA *et al.*, 2023).

A.1.3 Software manual

Table A.1: List of equipment.

Items	Description
TK-101	Stainless steel tank (1 L)
P-101	Masterflex peristaltic pump model 7014-52 (Cole-Parmer Instrument Company, USA) adapted for flow rates from 0.1 to 3 ml/min.
P-102	Masterflex L/S peristaltic pump (Cole-Parmer Instrument Company, USA) 0.2 to 1000 mL/min.
P-103	Gear pump (RZR 500, BRA) 6 to 15 L/min.
TT101, TT102, TT103	Platinum resistance temperature sensors (Pt-100, 3-wire).
PT101	Absolute pressure gauge (Cole Parmer, USA).
PDT102	Differential pressure transducer LD301 (Smar tech. the company, BR).
PDT103	Differential pressure transducer (Rosemount, Emerson, USA).
PDT101, PDT104	Differential pressure transmitter (Zurich, BRA)
HE-101	One-pass heat exchanger

A.2 Emulsion Flow Plant Prototype: Items and Photography

Table A.1 describes the technical specification of each circuit item.

The photography of the prototype used in the analysis is show below.

A.3 Oil properties

The tables present the oil's physical properties as a temperature function. Viscosity was measured using a capillary viscometer, and density was measured using the Anton Paar DMA 4500M densimeter. The Federal University of Rio de Janeiro School of Chemistry made the experimental values available in the name of professors Krishnaswamy Rajagopal and Rafael Mengotti Charin.

The equations above represents the adjustment of the oil properties with the data.

$$\mu_o \|_{m^2/s} = \rho_o * e^{-0.0595171252*T} * 0.000001 \tag{A.7}$$

Table A.2: Viscosity of Naftenic oil at different temperatures

Temperature (°C)	Viscosity (mm^2/s)
30,00	261,683
45,00	95,904
60,00	43,887

Table A.3: Density of Naftenic oil at different temperatures

Temperature (°C)	Density (g/cm^3)
15,02	0,91317
19,98	0,91001
24,98	0,90687
29,98	0,90373
34,98	0,90057
39,98	0,89741
44,98	0,89425
49,98	0,8911
54,98	0,88796
59,98	0,88483

$$\rho_o\|_{kg/m^3} = (-0.0006304081 * T + 0.9226202158) * 1000 \tag{A.8}$$

Manual do UASA - Spectroscopy sound attenuation analysis

Autores:

Samuel Vitor Saraiva, Carlos Adriano Moreira da Silva, Ana Maria Frattini Fileti, Flavio Vasconcelos da Silva e Luiz Octavio Vieira Pereira.

Responsável:

Samuel Vitor Saraiva

26 de Julho de 2022

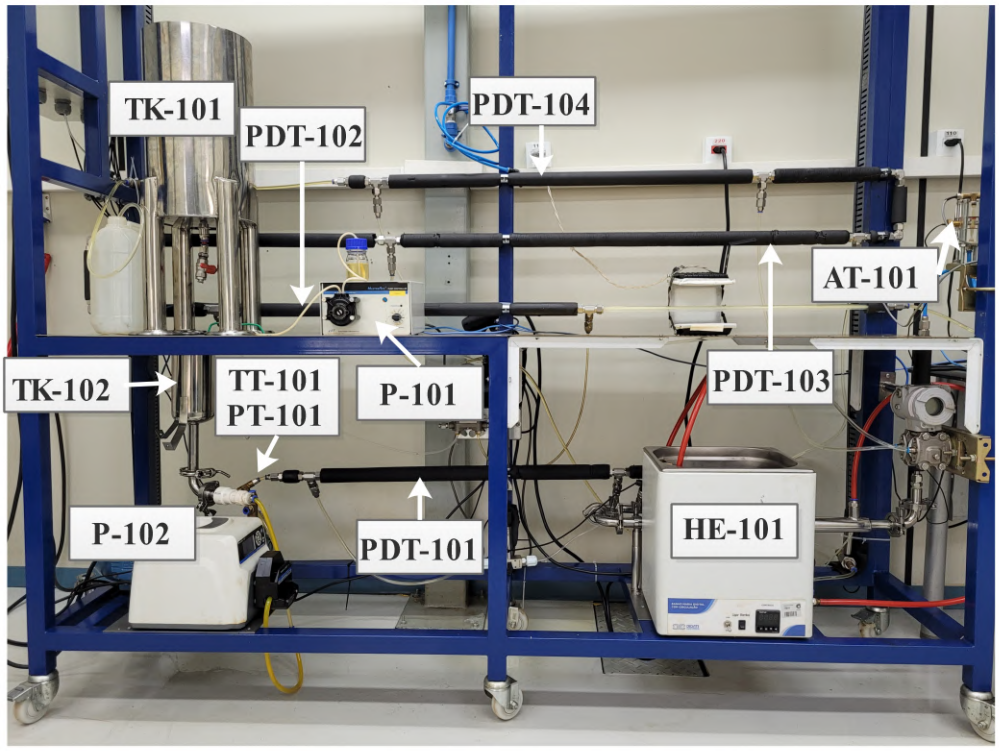
TK-101
PDT-102
PDT-104
AT-101
TK-102
TT-101
PT-101
P-101
PDT-103
P-102
PDT-101
HE-101

Appendix B

Primeiro Apêndice

B.1 Non-intrusive ultrasonic cell - Technical drawing

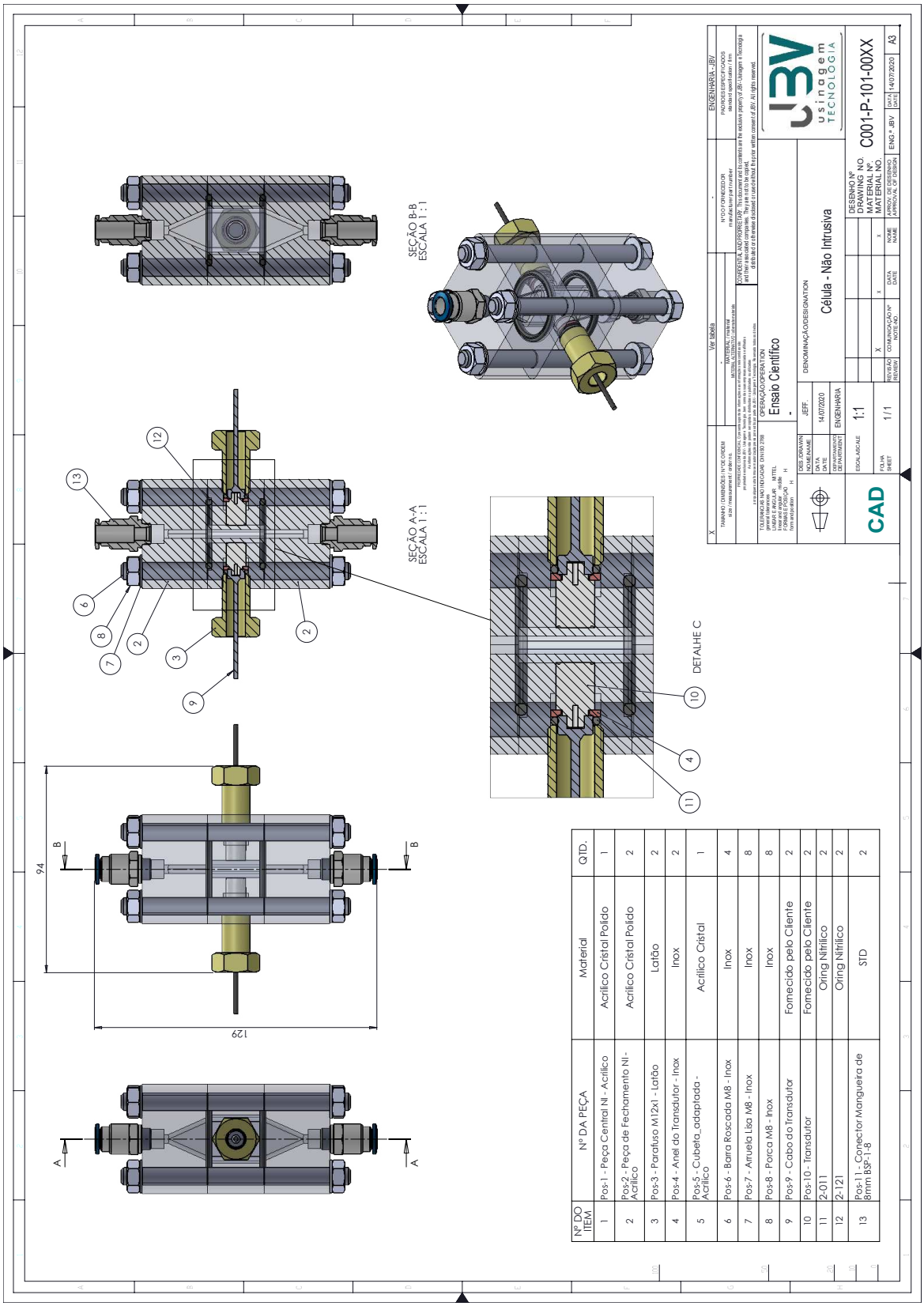

Nº DO ITEM	Nº DA PEÇA	Material	QTD.
1	Pos-1 - Peça Central NI - Acrilico	Acrilico Cristal Polido	1
2	Pos-2 - Peça de Fechamento NI - Acrilico	Acrilico Cristal Polido	2
3	Pos-3 - Parafuso M12x1 - Latão	Latão	2
4	Pos-4 - Anel do Transdutor - Inox	Inox	2
5	Pos-5 - Cubeta_adaptada - Acrilico	Acrilico Cristal	1
6	Pos-6 - Barra Roscada M8 - Inox	Inox	4
7	Pos-7 - Arruela Lisa M8 - Inox	Inox	8
8	Pos-8 - Porca M8 - Inox	Inox	8
9	Pos-9 - Cabo do Transdutor	Fornecido pelo Cliente	2
10	Pos-10 - Transdutor	Fornecido pelo Cliente	2
11	2-011	Oring Nitrílico	2
12	2-121	Oring Nitrílico	2
13	Pos-11 - Conector Mangueira de 8mm BSP-1-8	STD	2